# Quantum Optics with Molecules

## Quantenoptik mit Molekülen

Der Naturwissenschaflichen Fakultät
der Friedrich-Alexander-Universität
Erlangen-Nürnberg
zur
Erlangung des Doktorgrades

Dr. rer. nat.

vorgelegt von

Michael Reitz

aus Schweinfurt

Als Dissertation genehmigt
von der Naturwissenschaflichen Fakultät
der Friedrich-Alexander-Universität Erlangen-Nürnberg

| | |
|---|---|
| Tag der mündlichen Prüfung: | 06. Juli 2022 |
| Vorsitzender des Promotionsorgans: | Prof. Dr. Wolfgang Achtziger |
| Gutachter: | Dr. Claudiu Genes |
| | Prof. Dr. Philipp Hansmann |
| | Prof. Dr. Felipe Herrera |

©2022 – Michael Reitz
all rights reserved.

# Abstract

Molecules constitute compact hybrid quantum optical systems that can efficiently interface mechanical degrees of freedom with optical or infrared transitions. However, the coupling of molecules to the environment typically limits their coherence times which hampers their wider use in quantum optical applications. The aim of this thesis is to understand the properties of light-coupled molecules interacting with their environment and with each other and to investigate platforms where molecular degrees of freedom can be harnessed and collective effects can be observed.

To this end, for the description of molecules interacting with light, we develop an open system approach based on quantum Langevin equations. The method considers the time evolution of a polaron operator, i.e., a vibrationally-dressed electronic dipole operator and can account for all coherent and incoherent interactions. In a first step, we apply the method to Floquet engineering of infrared-active molecules and show how one can make use of strong driving of molecular vibrations to control the amplitude and coherence of vibronic sidebands. In a next step, we investigate molecules encased in crystalline host environments and coupled to optical cavities and illustrate how the coupling to the phonons of the host matrix imprints itself onto the molecular absorption and the transmission spectrum of the cavity. We also discuss the vibrationally-induced cross-talk between upper and lower polaritonic states and derive rate equations for the population transfer. We then move on to regularly spaced ensembles of dipole-dipole coupled molecules, especially in ring configurations, and discuss how the vibronic coupling affects the dispersion relation and cooperative radiative properties of the ring. In particular, by moving to a collective basis, we show molecular vibrations can be used to address collective subradiant states of the ensemble. Finally, for mesoscopic disordered ensembles of molecules strongly coupled to optical cavites, we quantitatively describe the loss mechanism from polaritonic states into the dark state manifold, providing an analytical scaling of the vacuum Rabi splitting on frequency disorder.

# Zusammenfassung

Moleküle stellen kompakte hybride quantenoptische Systeme dar, die eine effiziente Schnittstelle zwischen mechanischen Freiheitsgraden und optischen sowie infraroten Übergängen bilden können. Jedoch limitiert die Kopplung von Molekülen an ihre Umgebung typischerweise die Kohärenzzeiten, was ihre weitere Verbreitung in quantenoptischen Anwendungen erschwert. Ziel dieser Arbeit ist es, die Eigenschaften von lichtgekoppelten Molekülen, die mit ihrer Umgebung und miteinander wechselwirken zu verstehen sowie Plattformen zu untersuchen, bei denen molekulare Freiheitsgrade ausgenutzt werden können und kollektive Effekte beobachtet werden können.

Zur Beschreibung mit Licht wechselwirkender Moleküle entwickeln wir einen Ansatz basierend auf Quanten-Langevin-Gleichungen für offene Systeme. Die Methode betrachtet die Zeitentwicklung eines Polaronoperators, also eines schwingungsbekleideten elektronischen Dipoloperators, und erlaubt es, alle kohärenten und inkohärenten Wechselwirkungen mit einzubeziehen. In einem ersten Schritt wenden wir die Methode auf Floquet-Engineering von infrarot-aktiven Molekülen an und zeigen, wie man durch starkes Antreiben der Molekülschwingungen Amplitude und Kohärenz der vibronischen Seitenbänder kontrollieren kann. In einem nächsten Schritt wenden wir die Methode auf Moleküle, die in kristallinen Gastumgebungen eingebettet und an optische Resonatoren gekoppelt sind an und illustrieren, wie die Kopplung an die Phononen der Gastmatrix die Absorption sowie das Transmissionsspektrum des Resonators beeinflusst. Wir diskutieren auch die schwingungsinduzierte Wechselwirkung zwischen dem oberen und unteren polaritonischen Zustand und leiten Ratengleichungen für den Besetzungstransfer her. Wir betrachten dann regulär angeordnete Ensembles von dipol-dipol gekoppelten Molekülen, hauptsächlich in Ringkonfigurationen, und diskutieren wie die vibronische Kopplung die Dispersionsrelation und kooperativen Strahlungseigenschaften des Rings beeinflusst. Im Besonderen zeigen wir in der kollektiven Basis des Systems, dass Molekülschwingungen ausgenutzt werden können, um subradiante Zustände des Ensembles zu adressieren. Schließlich, für mesoskopische, ungeordnete Ensembles von Molekülen, die im Kollektiv stark an optische Resonatoren gekoppelt sind, beschreiben wir quantitativ den Zerfallsmechanismus von polaritonischen Zuständen in die Menge an Dunkelzuständen und leiten ein analytisches Gesetz für die Abhängigkeit des Vacuum Rabi Splittings von der Frequenzunordnung her.

# Contents


Publications xi

1 Introduction 1

2 Background and methods 5
- 2.1 The quantized electromagnetic field . . . 5
- 2.2 Fundamentals of light-matter interaction . . . 6
- 2.3 Fundamentals of molecular physics . . . 8
  - 2.3.a Born-Oppenheimer approximation . . . 9
  - 2.3.b Holstein Hamiltonian . . . 10
- 2.4 Open quantum system dynamics . . . 14
  - 2.4.a Master equation . . . 15
  - 2.4.b Master equation for collective spontaneous emission . . . 16
  - 2.4.c Quantum Langevin equations . . . 18
  - 2.4.d Quantum Brownian motion . . . 19
- 2.5 Super- and subradiance . . . 21
  - 2.5.a Two coupled emitters . . . 22
  - 2.5.b Quantum emitter rings and chains . . . 23
- 2.6 Vibronic dimer model . . . 25
- 2.7 Fundamentals of cavity QED . . . 27
  - 2.7.a Single emitter . . . 29
  - 2.7.b Many emitters . . . 31
  - 2.7.c Holstein-Tavis-Cummings Hamiltonian . . . 31

3 Polaron Langevin Equation 35
- 3.1 Derivation of the PLE . . . 35
- 3.2 Emission and absorption . . . 39
- 3.3 Thermal effects . . . 40
- 3.4 Förster resonance energy transfer . . . 41
- 3.5 Remarks . . . 43

4 Infrared-dressed molecules 45
- 4.1 Model . . . 46
- 4.2 Floquet states and transition strengths . . . 46
- 4.3 Langevin equations of motion . . . 48
- 4.4 Sideband control via Floquet engineering . . . 50
- 4.5 Purcell-induced suppression of sidebands . . . 52

5 Molecules in phononic host environments 55
5.1 Model and Hamiltonian formulation . . . 56
5.2 Vibrational relaxation . . . 58
5.3 Collective vibrational relaxation . . . 61
5.4 Phonon wing . . . 63
5.5 Dephasing . . . 65
5.6 Cavity-molecule spectroscopy . . . 66
5.7 Polariton cross-talk and transfer . . . 68

6 Molecular nanorings 71
6.1 Collective effects under vibronic coupling . . . 72
6.2 Dispersion relation . . . 74
6.3 Subradiant state preparation . . . 76

7 Cavity QED with mesoscopic disordered molecular ensembles 81
7.1 Cavity transmission . . . 81
7.2 Dark-bright state dynamics . . . 83
7.3 Elimination of dark reservoir . . . 85

8 Discussion and Outlook 91

Appendix A Dipole-dipole coupling functions 93

Appendix B Derivation of FRET rate 95

Appendix C Optical response of infrared-dressed molecule 97

Appendix D Derivation of molecule-host coupling 101

Appendix E Non-Markovian loss into the dark state reservoir 107

References 109

# Acknowledgments

First and foremost, my gratitude goes to my supervisor Claudiu Genes for giving me the opportunity to pursue a PhD as well as his mentorship and guidance along the way. In particular, I want to thank him for always trying to keep work fun, his open door and helping me to develop as a scientist (or actually turning me into one, in the first place). My many-times paper collaborator and Covid time lunch companion Christian Sommer deserves special thanks. It is fair to say that Christian knows (almost) everything and he contributed a great deal to all our common projects. I want to thank him for his support, the rushes of insanity when trying to finish papers and beat deadlines, and wish him all the best for his new job in Austria. Thanks to Francesca Mineo and Nico Baßler as well as all other current and past members of the group for valuable discussions, coffee breaks, four o'clock chocolate and occasional nights out. I also enjoyed working with other people outside the group from which I greatly benefited and would like to thank my collaborators Burak Gürlek, Raphael Holzinger, Diego Martín-Cano and David Plankensteiner as well as Helmut Ritsch and Vahid Sandoghdar. Thanks to Ahmed Jaber, Avinash Singh and Jean-Michel Ménard for hosting me in Ottawa in December 2021 and making my stay enjoyable, I am excited to see what will come out of the metasurface project. I am grateful for the funding and training which I received through the International Max Planck Research School and would like to thank the current and past coordinators Heike Schwender, Dorothea Mayer, Peter Banzer and Nicolas Joly for putting effort into the organization. Thanks to all the friendly people at MPL for making me feel welcome over the past years.
Der größte Dank gebührt meiner Familie, insbesondere meinen Eltern, die mich in allem unterstützen und denen ich alles zu verdanken habe.

# Publications

The contents of this thesis have been published in the following Refs. [1–4]. In particular, chapters 3, 4, 5 and 7 follow Refs. [1], [2], [3] and [4], respectively, with partial textual overlap. Chapter 6 closely follows Ref. [5] which has been recently submitted and is currently under review. Some of the notations and definitions from the publications have been modified to ensure consistency within the thesis. Further publications of the author are Refs. [6, 7] which mainly lie outside the scope of this thesis. However, some parts of the background chapter 2 have been adapted from the tutorial article Ref. [7].

### Articles related to thesis content


[1] M. Reitz, C. Sommer, C. Genes, Langevin approach to quantum optics with molecules, *Phys. Rev. Lett. 122, 203602 (2019)*

[2] M. Reitz, C. Genes, Floquet engineering of molecular dynamics via infrared coupling, *J. Chem. Phys. 153, 234305 (2020)*

[3] M. Reitz, C. Sommer, B. Gurlek, V. Sandoghdar, D. Martin-Cano, C. Genes, Molecule-photon interactions in phononic environments, *Phys. Rev. Research 2, 033270 (2020)*

[4] C. Sommer, M. Reitz, F. Mineo, C. Genes, Molecular polaritonics in dense mesoscopic disordered ensembles, *Phys. Rev. Research 3, 033141 (2021)*


### Submitted articles


[5] R. Holzinger, S. A. Oh, M. Reitz, H. Ritsch, C. Genes, Cooperative subwavelength molecular quantum emitter arrays, *arXiv:2203.04998 (2022)*


### Further publications


[6] D. Plankensteiner, C. Sommer, M. Reitz, H. Ritsch, C. Genes, Enhanced collective Purcell effect of coupled quantum emitter systems, *Phys. Rev. A 99, 043843 (2019)*

[7] M. Reitz, C. Sommer C. Genes, Cooperative quantum phenomena in light-matter platforms, *PRX Quantum 3 (Tutorial), 010201 (2022)*

# List of Acronyms

List of acronyms used in the main text in alphabetical order.

**DBT** Dibenzoterrylene

**FRET** Förster resonance energy transfer

**HTC** Holstein-Tavis-Cummings

**PAH** Polycyclic aromatic hydrocarbon

**PLE** Polaron Langevin equation

**QED** Quantum electrodynamics

**QLE** Quantum Langevin equation

**RWA** Rotating wave approximation

**TC** Tavis-Cummings

**VRS** Vacuum Rabi splitting

**ZPL** Zero-phonon line

# 1 Introduction

Molecules are natural quantum mechanical platforms where several atoms are interlinked via electronic bonds. They can possess a wide range of electronic and mechanical degrees of freedom which couple to each other and which can moreover be accessed and manipulated by light. In particular organic molecules have emerged over recent years as tunable and efficient light-matter interfaces due to their relatively large transition dipole moments and wide range of transition frequencies, typically lying between 200 and 800 nm [8]. As such, single organic molecules trapped in solid-state environments hold promise as single-photon sources [9–11], nonlinear optical elements at the single- or few-photon level [12, 13] and sensors, allowing for example for the readout of local material properties such as strain or electromagnetic fields [14–16]. Of particular relevance are so-called polycyclic aromatic hydrocarbons (PAHs) such as perylene, terrylene and dibenzoterrylene (DBT) [see chemical structures in Fig. 1.1(a)] as they feature a high branching ratio on the desired zero-phonon line transition and furthermore their linewidth is typically drastically reduced at cryogenic temperatures ($T \leq 4\,\mathrm{K}$) and becomes close to the natural linewidth limit ($\sim 10\,\mathrm{MHz}$), resulting in a high degree of electronic coherence. To further enhance the light-matter interaction, single molecules are interfaced with confined optical modes such as provided by Fabry-Pérot cavities [17, 18], waveguides and ring resonators [19–21] or plasmonic nanocavities [22, 23]. For example, an experiment has shown that the branching ratio of a molecule can be modified by the coupling to a resonant cavity [18]. Here, the cavity enhances the decay on the desired zero-phonon line transition whereby other decay paths are effectively suppressed, thus turning the molecule into an almost perfect two-level quantum system. As experiments now have unprecedented control over single organic molecules, the goal in the next years will be to construct more and more complex networks of molecular emitters interacting via common electromagnetic modes and to observe cooperative collective effects [7, 8].

While the excitation of molecular vibrational degrees of freedom is widely used for spectroscopic techniques such as Raman scattering and infrared spectroscopy [24], their possible application for quantum optical techniques has been less considered since the coupling to molecular vibrations in the solid state is typically associated with decoherence. However, molecules can exhibit a strong inherent optomechanical photon-vibration coupling mediated by resonant or off-resonant electronic transitions.

Moreover, molecular vibrations typically lie at high terahertz frequencies and are therefore typically in the ground state even at elevated temperatures, thus circumventing additional cooling requirements typically required for standard optomechanics. Current research is therefore trying to exploit the coupling to molecular vibrations for the realization of optomechanical effects at the single-molecule level, leading to the emergence of the field of molecular optomechanics [25–28].

As opposed to the previous paragraphs which mainly refer to experiments with single or few molecules, often under well-controlled, cryogenic conditions, a different interdisciplinary research community arose over the last 10 years which is located at the intersection between quantum optics, material science, chemistry and condensed matter physics. Here, mesoscopic ensembles of organic molecules or molecular materials are collectively coupled to cavities, often under room temperature conditions, with the aim to investigate the modification of material properties under strong light-matter hybridization. Despite the cavities typically being very lossy, the strong coupling regime is reached by the formation of a large collective molecular dipole and effective coupling strength scaling approximately proportional to the square root of the number of molecules in the mode volume of the resonator [see Fig. 1.1(b)]. While strong coupling of an organic semiconductor material in a microcavity was first demonstrated in 1998 [29], in 2012 an experiment reported modification of a photoizomerization reaction under collective strong coupling [30]. Since then, experimental and theoretical endeavors have investigated fascinating enhanced properties of molecular materials under strong coupling which besides chemical reactivity [30–34] includes modifications of charge and energy transfer [35–39], tuning of the work function [40], manipulation of triplet state dynamics [41, 42] and superconductivity [43]. Alongside strong coupling to optical transitions, more recently the collective strong coupling to molecular vibrational modes at infrared frequencies (*vibropolaritonics*) got into the focus of research [44] as it e.g. enables manipulation of chemical reactions in the ground state [45, 46] or alterations

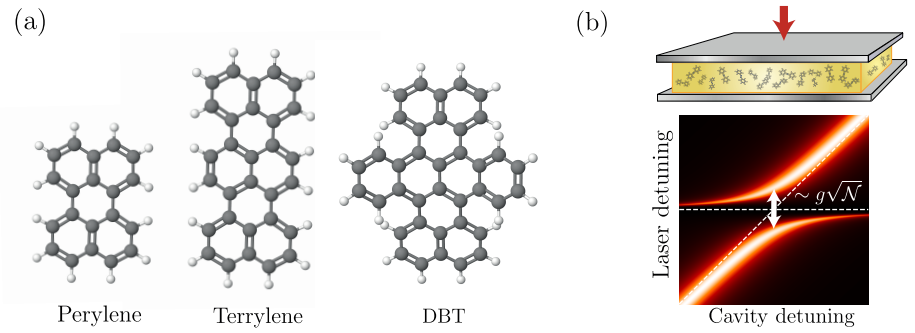


Figure 1.1: *Experimental platforms.* (a) Chemical structures of some of the relevant PAH molecules used for single-molecule experiments. (b) Typical setup in molecular polaritonics with organic microcavities: A coplanar cavity is filled with a mesoscopic ensemble of molecules and is probed by a laser. In the strong coupling regime, the output field shows an avoided crossing roughly proportional to the square root of the number of molecules when scanning both laser and cavity frequency around the common resonance.

of Raman scattering [47, 48]. The general idea behind both strong coupling to electronic and vibrational transitions is, to modify the potential energy landscape of the material in such a way that processes can happen which are impossible for materials in free space. Regarding strong coupling with molecular ensembles, theoretical efforts aimed at providing an understanding of vibrationally-dressed polaritons [49–51], the role of vibronic dark states [52, 53], the cavity-induced polariton asymmetry [54], the modification of potential energy surfaces under strong coupling and the development of ab-initio theories [55–58] or deriving relevant simplified models for large scale numerics in the mesoscopic limit [59, 60]. Recent theory reviews on the field of molecular polaritonics and polaritonic chemistry can be found in Refs. [61–66] while Refs. [67–69] provide overviews of the field from an experimental perspective.
All of the previous motivates us to study the properties of molecules coupled to light and interacting with each other.

This thesis is structured as follows: The necessary background and methods are laid out in chapter 2. In chapter 3 we introduce our main theoretical method for the description of molecular dynamics which consists in deriving a *polaron Langevin equation* (PLE), i.e., a differential equation for a vibrationally-dressed electronic dipole operator. Langevin equations are stochastic equations which describe the dynamics of open quantum systems in the Heisenberg picture of quantum mechanics. If the evolution is linear, a formal integration allows for the derivation of correlation functions and therefore the calculation of spectroscopic quantities. In a first step, we illustrate how the method accounts for molecular emission and absorption and use it for the description of the dipole-mediated Förster resonance energy transfer between two near-field coupled molecules.

In chapter 4 we then make use of the PLE method to describe Floquet engineering of molecular dynamics. We consider strong driving of infrared-active molecular vibrational modes, either directly or indirectly via a cavity mode, in combination with a weak optical probe of the electronic transition. We derive correlation functions and stationary quantities such as the absorption spectrum and show how driving of the vibrations leads to a strongly-modified optical response of the infrared-dressed molecules. In particular, we illustrate how the infrared field modifies the standard paths of emission and absorption and gives rise to a control over the amplitude as well as coherence of vibronic sidebands.

In chapter 5 we then apply the PLE method to describe the impurity problem of molecules embedded in solid state host environments and additionally coupled to cavity modes. We derive a first-principle model to account for the intricate many-body dynamics between electronic transitions, localized vibrational modes and delocalized phonons of the host environment. We start by analyzing how the molecular vibrations deposit their energy into the phonons of the host matrix and identify regimes of Markovian vs. non-Markovian vibrational relaxation. For two guest molecules immersed in the same

phonon bath we show how elimination of the phonons leads to collective vibron-vibron dynamics which leads to the possibility of decoupling intramolecular vibrations from the phononic bath. We then discuss the spectra under the influence of thermal effects and discuss sources of optical dephasing. For cavity-coupled molecules, we illustrate the imprint of phononic and vibrational signatures onto the cavity output field and show how the coupling to vibrations induces a dissipative cross-talk between the polaritonic states, resulting in an asymmetric transmission profile.

Chapters 6 and 7 will then deal with collective effects at the level of many molecules. In chapter 6 we discuss regularly spaced ensembles of molecules and analyze the cooperative radiative properties of molecular rings. in particular, we show how the dispersion relation and super-/subradiance properties are affected by the vibronic coupling. While coupling to vibrations is typically considered as detrimental for the realization of quantum coherent effects, we show how molecular vibrations can be used for the preparation of robust entangled subradiant states aided by vibrational relaxation. In chapter 7, we move to the mesoscopic limit of $\mathcal{N} \to \infty$ molecules coupled to a common cavity mode. We discuss the interplay between collective bright and dark superposition states and show how elimination of the dark reservoir leads to a generally non-Markovian decay of polaritonic states. In the Markovian limit, we then derive simple scaling laws for the decay rates into the dark state manifold. In both chapters 6 and 7, a transformation into a collective basis for electronic and/or vibrational operators helps to provide insight into the relevant processes. Finally, in chapter 8 we draw a conclusion and give an outlook on possible future research directions.

# 2

# Background and methods

This chapter gives an introduction into the concepts and methods necessary for the understanding of the results presented in the following chapters. We start by briefly reviewing the fundamentals of quantum optics and light-matter interaction in sections 2.1 and 2.2, leading to a dipolar coupling between light and matter under certain assumptions. We then introduce the fundamentals of molecular physics such as the adiabatic representation and the Born-Oppenheimer approximation in section 2.3 and derive the Holstein Hamiltonian which is a simple model to describe the vibronic coupling in molecules. Since molecular systems are, like most quantum systems, inherently open, we discuss the dynamics of open quantum systems in section 2.4 by introducing two alternative approaches for systems coupled to external reservoirs: quantum master equations and quantum Langevin equations. Using the quantum master equation formalism, we derive the open system formulation for a system of $\mathcal{N}$ emitters commonly coupled to the electromagnetic vacuum. The resulting phenomena of super-and subradiance are discussed for chain and ring geometries in section 2.5. While this section deals with electronic transitions only, we discuss the vibronic dimer as a prototypical model to study the interplay between vibrational effects and electronic interactions for near-field coupled molecules in section 2.6. Finally, in section 2.7, we introduce fundamental concepts of cavity quantum electrodynamics (cavity QED) such as strong coupling and the Purcell regime for a single and many emitters and introduce the Holstein-Tavis-Cummings Hamiltonian as a simple model to study molecules coupled to confined light modes.

## 2.1 The quantized electromagnetic field

Let us imagine a fictitious, perfectly reflecting box of volume $\mathcal{V} = \ell^3$ and assume periodic boundary conditions for the electromagnetic field inside the box. The explicit choice of boundary conditions is however not important as we will later consider the limit $\ell \to \infty$. After solving the wave equation, one follows a standard quantization procedure for the electromagnetic field [70–76]. The resulting electric field operator is obtained as the time derivative of the vector potential operator in the Heisen-

berg picture $\hat{\mathbf{E}}(\mathbf{R},t) = -\partial_t \hat{\mathbf{A}}(\mathbf{R},t)$[1] and is given as a sum over plane waves

$$\hat{\mathbf{E}}(\mathbf{R},t) = \sum_{\mathbf{k}} \mathcal{E}_k \left( a_{\mathbf{k}} e^{i\mathbf{k}\cdot\mathbf{R}} e^{-i\omega_k t} + a_{\mathbf{k}}^\dagger e^{-i\mathbf{k}\cdot\mathbf{R}} e^{i\omega_k t} \right) \mathbf{e}_{\mathbf{k}}, \tag{2.1}$$

where the allowed $\mathbf{k}$ vectors are multiples of $2\pi/\ell$ on each Cartesian direction and the index $\mathbf{k}$ runs over all possible $\mathbf{k}$ vectors and implicitly also over the two orthogonal polarizations associated with the unit vector $\mathbf{e}_{\mathbf{k}}$ for each $\mathbf{k}$ mode. The bosonic field operators $a_{\mathbf{k}}$ and $a_{\mathbf{k}}^\dagger$ follow the commutation $[a_{\mathbf{k}}, a_{\mathbf{k}'}^\dagger] = \delta_{\mathbf{k}\mathbf{k}'}$ and their action is to create and destroy excitations (photons) in a given field mode

$$a_{\mathbf{k}} |n_{\mathbf{k}}\rangle = \sqrt{n_{\mathbf{k}}}\, |n_{\mathbf{k}} - 1\rangle\,, \qquad a_{\mathbf{k}}^\dagger |n_{\mathbf{k}}\rangle = \sqrt{n_{\mathbf{k}} + 1}\, |n_{\mathbf{k}} + 1\rangle\,. \tag{2.2}$$

The zero-point electric field amplitude for a given mode with frequency $\omega_k = ck$ is defined as $\mathcal{E}_k = \sqrt{\omega_k/(2\varepsilon_0 \mathcal{V})}$, where $c$ is the speed of light and $\varepsilon_0$ is the vacuum permittivity. The Hamiltonian of the electromagnetic field inside the fictitious box can then be written in the time-independent Schrödinger picture as a sum over an infinite number of harmonic oscillators

$$\mathcal{H}_{\text{vac}} = \frac{1}{2} \int_{\mathcal{V}} \mathrm{d}\mathbf{R} \left( \varepsilon_0 \hat{\mathbf{E}}(\mathbf{R})^2 + \frac{1}{\mu_0} \hat{\mathbf{B}}(\mathbf{R})^2 \right) = \sum_{\mathbf{k}} \hbar\omega_k \left( a_{\mathbf{k}}^\dagger a_{\mathbf{k}} + \frac{1}{2} \right), \tag{2.3}$$

where the magnetic field is given as the curl of the vector potential $\hat{\mathbf{B}}(\mathbf{R}) = \nabla \times \hat{\mathbf{A}}(\mathbf{R})$ and $\mu_0$ is the vacuum permeability. The resulting Hamiltonian depends now only on the operator $a_{\mathbf{k}}^\dagger a_{\mathbf{k}}$ which counts the number of excitations in a given field mode with frequency $\omega_k$.

## 2.2 Fundamentals of light-matter interaction

Let us now assume that we place a generic matter system (atom, molecule, etc.) with center of mass located at position $\mathbf{R}_0$ inside the box. Let us assume that the matter system is comprised of $N$ point charges $q_j$ of mass $m_j$ located at positions $\mathbf{r}_j$ ($j = 1, \ldots, N$), interacting with the quantized electromagnetic field. The charges are described by standard position $\hat{\mathbf{r}}_j$ and momentum $\hat{\mathbf{p}}_j = -i\hbar\nabla_j$ operators. The coupling between light and matter occurs within the formalism of the minimal coupling Hamiltonian in the Coulomb gauge ($\nabla \cdot \hat{\mathbf{A}} = 0$) [70–76]

$$\mathcal{H} = \sum_{j=1}^{N} \frac{[\hat{\mathbf{p}}_j - q_j \hat{\mathbf{A}}(\hat{\mathbf{r}}_j)]^2}{2m_j} + \mathcal{H}_{\text{vac}} + \hat{V}_{\text{coul}}, \tag{2.4}$$

where the three terms describe the kinetic energy of the charged particles, the energy of the free electromagnetic field and the Coulomb interaction among the charges, respectively. The effect of the interaction is to shift the canonical momentum of the particles to $\hat{\mathbf{p}}_j = m_j \dot{\hat{\mathbf{r}}}_j + q_j \hat{\mathbf{A}}(\hat{\mathbf{r}}_j)$. It is convenient to decompose the minimal coupling Hamiltonian into matter, interaction and field part as

[1] Remarks on the notation: Operators are indicated by hats only when we want to stress that the respective quantity is an operator. Vectors and matrices are both indicated by bold symbols.

$\mathcal{H} = \mathcal{H}_0 + \mathcal{H}_{\text{int}} + \mathcal{H}_{\text{vac}}$ with

$$\mathcal{H}_0 = \sum_j \frac{\hat{\mathbf{p}}_j^2}{2m_j} + \hat{V}_{\text{coul}}, \tag{2.5a}$$

$$\mathcal{H}_{\text{int}} = -\sum_j \frac{q_j}{m_j}\hat{\mathbf{p}}_j \cdot \hat{\mathbf{A}}(\hat{\mathbf{r}}_j) + \sum_j \frac{q_j^2}{2m_j}\hat{\mathbf{A}}^2(\hat{\mathbf{r}}_j), \tag{2.5b}$$

where we used the fact that $\hat{\mathbf{p}}$ and $\hat{\mathbf{A}}$ commute in the Coulomb gauge. While the above is valid for any set of charges, for atoms or molecules, the extension of the electronic orbitals is typically much smaller than the wavelength $\lambda_0 = 2\pi c/\omega_0$ associated with the optical transition between two electronic orbitals, i.e., $|\mathbf{k}\cdot\mathbf{r}_j| \ll 1$. This allows for the so-called *dipole approximation* where the vector potential is evaluated at the center of mass of the system: $\hat{\mathbf{A}}(\hat{\mathbf{r}}_j) \approx \hat{\mathbf{A}}(\mathbf{R}_0)$. The term proportional to $\hat{\mathbf{A}}^2$ in Eq. (2.5b) is typically small and can be neglected as long as the electric field is small as compared to intra-atomic or intra-molecular field strengths ($E_{\text{at}} \sim 10^{10}\,\text{Vm}^{-1}$ [74]). However, this term can also be eliminated exactly by a proper choice of transformation. For example, the dipole approximation allows one to perform a so-called length gauge transformation $\tilde{\mathcal{H}} = \mathcal{U}_L \mathcal{H} \mathcal{U}_L^\dagger$, where

$$\mathcal{U}_L = e^{-\frac{i}{\hbar}\hat{\mathbf{d}}\cdot\hat{\mathbf{A}}(\mathbf{R}_0)}, \tag{2.6}$$

with the total dipole operator $\hat{\mathbf{d}} = -\sum_j q_j(\hat{\mathbf{r}}_j - \mathbf{R}_0)$. After some algebra, one obtains a direct coupling between the dipole moment and the electric field[2]

$$\tilde{\mathcal{H}} = \mathcal{H}_0 + \hat{\mathbf{d}} \cdot \hat{\mathbf{E}}(\mathbf{R}_0) + \mathcal{H}_{\text{vac}}. \tag{2.7}$$

Additionally, the length gauge transformation leads to a dipole self-energy term which we have discarded as it is not relevant for the simplified phenomenological approach taken by us in the following.[3] Generally, the coupling to the electromagnetic field in Eq. (2.7) allows for transitions between a large set of eigenstates of the matter Hamiltonian $\mathcal{H}_0$. However, for instance for atomic systems one typically assumes that all of the physics only involves transitions between the ground state $|g\rangle$ and a single excited state $|e\rangle$ at energy $\omega_0$ (from now on we set $\hbar = 1$). The unity of the matter Hilbert space is then a sum of the two projectors $\mathbf{1}_0 = |g\rangle\langle g| + |e\rangle\langle e|$. To describe transitions between the two levels, one introduces the Pauli raising and lowering operators

$$\sigma = |g\rangle\langle e|, \qquad \sigma^\dagger = |e\rangle\langle g|. \tag{2.8}$$

Their commutator $[\sigma^\dagger, \sigma] = \sigma_z$ is the population difference operator and the matter Hamiltonian

[2] A full derivation can e.g. be found in Complement $A_{IV}$ of Ref. [77] (pp. 304 – 311).

[3] However, this term is generally important and its relevance is is e.g. discussed in Ref. [78].

can be written as $\mathcal{H}_0 = \omega_0 \sigma^\dagger \sigma$ or alternatively as $\mathcal{H}_0 = \omega_0 \sigma_z/2$ (up to a constant energy shift). Under the two-level assumption, the dipole operator is then written as $\hat{\mathbf{d}} = \mathbf{d}_{\mathrm{eg}} \sigma + \mathrm{h.c.}$, where the transition dipole moment is computed between the two states $\mathbf{d}_{\mathrm{eg}} = \langle g | \hat{\mathbf{d}} | e \rangle$ and the diagonal terms vanish. Moreover, one performs an additional *rotating-wave approximation* (RWA) where fast oscillating terms $\sigma a_{\mathbf{k}}$ and $\sigma^\dagger a_{\mathbf{k}}^\dagger$ (oscillating under free evolution with $e^{i(\omega_0+\omega_k)t}$) are neglected. Under these approximations, the light-matter interaction part of the Hamiltonian can be written as

$$\mathcal{H}_{\mathrm{int}} = \sum_{\mathbf{k}} \left( g_{\mathbf{k}} \sigma^\dagger a_{\mathbf{k}} e^{i\mathbf{k}\cdot\mathbf{R}_0} + g_{\mathbf{k}}^* a_{\mathbf{k}}^\dagger \sigma e^{-i\mathbf{k}\cdot\mathbf{R}_0} \right), \tag{2.9}$$

describing photon-matter energy exchanges at rates $g_{\mathbf{k}} = \mathcal{E}_k \mathbf{e}_{\mathbf{k}} \cdot \mathbf{d}_{\mathrm{eg}}$ and conserving the number of excitations in the system. For an ensemble of $\mathcal{N}$ two-level systems located at different positions $\mathbf{R}_j$ ($j = 1, \ldots, \mathcal{N}$) such that the electronic orbitals of the different emitters do not overlap, this can interaction can be straightforwardly generalized to read

$$\mathcal{H}_{\mathrm{int}} = \sum_{j=1}^{\mathcal{N}} \sum_{\mathbf{k}} \left( g_{\mathbf{k}}^{(j)} \sigma^\dagger a_{\mathbf{k}} e^{i\mathbf{k}\cdot\mathbf{R}_j} + g_{\mathbf{k}}^{*,(j)} a_{\mathbf{k}}^\dagger \sigma e^{-i\mathbf{k}\cdot\mathbf{R}_j} \right), \tag{2.10}$$

with $g_{\mathbf{k}}^{(j)} = \mathcal{E}_k \mathbf{e}_{\mathbf{k}} \cdot \mathbf{d}_{\mathrm{eg}}^j$ and dipole moment of the $j$th emitter $\mathbf{d}_{\mathrm{eg}}^j = \langle g_j | \hat{\mathbf{d}}_j | e_j \rangle$, describing now the common coupling of an ensemble of $\mathcal{N}$ two-level systems to the electromagnetic vacuum field.

## 2.3 Fundamentals of molecular physics

For molecules, the matter part of the Hamiltonian is generally much more complicated than for atoms. The molecular Hamiltonian $\mathcal{H}_0 \equiv \mathcal{H}_{\mathrm{mol}}$ governing the system of $N_{\mathrm{e}}$ electrons and $N_{\mathrm{n}}$ nuclei can be represented by the sums of kinetic and potential energies

$$\mathcal{H}_{\mathrm{mol}} = \hat{T}_{\mathrm{e}} + \hat{T}_{\mathrm{n}} + \hat{V}_{\mathrm{coul}}(\hat{\mathbf{r}}, \hat{\mathbf{R}}) = -\sum_{j=1}^{N_{\mathrm{e}}} \frac{\nabla_j^2}{2m_{\mathrm{e}}} - \sum_{\alpha=1}^{N_{\mathrm{n}}} \frac{\nabla_\alpha^2}{2M_\alpha} + \hat{V}_{\mathrm{coul}}(\hat{\mathbf{r}}, \hat{\mathbf{R}}), \tag{2.11}$$

where the potential depends on all electronic $\hat{\mathbf{r}} = \{\hat{\mathbf{r}}_1, \ldots, \hat{\mathbf{r}}_{N_{\mathrm{e}}}\}$ and nuclear $\hat{\mathbf{R}} = \{\hat{\mathbf{R}}_1, \ldots, \hat{\mathbf{R}}_{N_{\mathrm{n}}}\}$ coordinates. We index electronic quantities by Roman letters and nuclear quantities by Greek letters. The Coulomb interaction is given by

$$\hat{V}_{\mathrm{coul}}(\mathbf{r}, \mathbf{R}) = \frac{e^2}{4\pi\varepsilon_0} \left[ \sum_{i=1}^{N_{\mathrm{e}}} \sum_{j>i}^{N_{\mathrm{e}}} \frac{1}{|\hat{\mathbf{r}}_i - \hat{\mathbf{r}}_j|} + \sum_{\alpha=1}^{N_{\mathrm{n}}} \sum_{\beta>\alpha}^{N_{\mathrm{n}}} \frac{Z_\alpha Z_\beta}{|\hat{\mathbf{R}}_\alpha - \hat{\mathbf{R}}_\beta|} - \sum_{i=1}^{N_{\mathrm{e}}} \sum_{\alpha=1}^{N_{\mathrm{n}}} \frac{Z_\alpha}{|\hat{\mathbf{r}}_i - \hat{\mathbf{R}}_\alpha|} \right], \tag{2.12}$$

with $Z_\alpha$ the charge of the nucleus. The general goal is to find solutions to the Schrödinger equation

$$\mathcal{H}_{\text{mol}}\Psi(\mathbf{r},\mathbf{R}) = E\Psi(\mathbf{r},\mathbf{R}), \tag{2.13}$$

which is an intractable many-body problem except for the most simple cases (e.g., $H_2^+$ molecule). Ab-initio approaches which can provide approximate solutions include, among others, density functional theory [79] and Hartree-Fock theory [80]. In the following we introduce the Born-Oppenheimer approximation which is probably the most important concept in molecular physics as it allows for a great simplification of the problem.

### 2.3.a Born-Oppenheimer approximation

The Born-Oppenheimer approximation is based on the observation that the nuclei are much heavier than the electrons ($\sim 10^4 : 1$) and are therefore moving much slower [81]. By considering the nuclei as clamped and separating the molecular Hamiltonian into the kinetic energy of the nuclei and the electronic part $\mathcal{H}_{\text{mol}} = \hat{T}_{\text{n}} + \hat{\mathcal{H}}_{\text{e}}$, one solves the electronic part of the Schrödinger equation for a given nuclear configuration $\mathbf{R}$ [82]

$$\hat{\mathcal{H}}_{\text{e}}(\hat{\mathbf{r}},\mathbf{R})\varphi_\ell(\mathbf{r},\mathbf{R}) = \mathcal{V}_\ell(\mathbf{R})\varphi_\ell(\mathbf{r},\mathbf{R}). \tag{2.14}$$

The eigenfunctions of the above equation are the so-called adiabatic electronic wavefunctions. The eigenenergies $\mathcal{V}_\ell$ with quantum number $\ell$ are the potential energy surfaces (PESs) which have a parametric dependence on $\mathbf{R}$. Since the adiabatic electronic wavefunctions form a complete orthonormal set, one may expand the total molecular wavefunction in terms of this basis

$$\Psi(\mathbf{r},\mathbf{R}) = \sum_{\ell=1}^{\infty} \chi_\ell(\mathbf{R})\varphi_\ell(\mathbf{r},\mathbf{R}), \tag{2.15}$$

where the expansion coefficients $\chi_\ell(\mathbf{R})$ describe the nuclear wavefunctions. This is also known as the Born-Huang ansatz which at this level is still exact [83] (for electronic wave functions depending parametrically on nuclear coordinates). Substituting this into the Schrödinger equation (2.13), using the product rule for the spatial derivatives and projecting onto the electronic eigenfunction $\langle\varphi_m|$, one arrives at a system of coupled equations for the nuclear wave functions

$$E\chi_m(\mathbf{R}) = (\hat{T}_{\text{n}} + \mathcal{V}_m(\mathbf{R}))\chi_m(\mathbf{R}) - \sum_{\ell,\alpha} \frac{1}{M_\alpha}\left(T^{(1)}_{m\ell,\alpha}\nabla_\alpha + \frac{1}{2}T^{(2)}_{m\ell,\alpha}\right)\chi_\ell(\mathbf{R}), \tag{2.16}$$

with the *non-adiabatic* first and second-order coupling elements

$$T^{(1)}_{m\ell,\alpha} = \langle \varphi_m | \nabla_\alpha | \varphi_\ell \rangle \,, \tag{2.17a}$$

$$T^{(2)}_{m\ell,\alpha} = \langle \varphi_m | \nabla^2_\alpha | \varphi_\ell \rangle \,. \tag{2.17b}$$

The Born-Oppenheimer approximation in the narrow sense then consists in neglecting the non-adiabatic couplings:[4]

$$E\chi_m(\mathbf{R}) = (\hat{T}_\mathrm{n} + \mathcal{V}_m(\mathbf{R}))\chi_m(\mathbf{R}). \tag{2.18}$$

In the Born-Oppenheimer approximation, the motion of the nuclear wave function is therefore restricted to a single potential energy surface and electronic and nuclear degrees of freedom are separated, i.e., the electronic cloud adjusts instantaneously to the nuclear motion. While generally this is a good approximation, one can show that the non-adiabatic couplings scale with the inverse energy difference between electronic states. Therefore, they become highly relevant if two potential energy surfaces become close or degenerate, which leads e.g. to the formation of conical intersections [84].

### 2.3.b Holstein Hamiltonian

We now derive the Holstein Hamiltonian, which is a simple, second-quantized Hamiltonian to describe the electron-vibration (vibronic) coupling within the Born-Oppenheimer approximation. Generally, the potential energy surfaces of molecules introduced in the previous section are complex multidimensional objects. For a molecule comprised of $N_\mathrm{n}$ atoms, the PES will depend on $3N_\mathrm{n} - 6$[5] generalized nuclear coordinates, since displacements of the center of mass and rotations do not change the potential energy.

Along a given nuclear coordinate, the PES may possess no minimum, a single minimum or many minima, corresponding to unbound or bound states of nuclear motion. A single nuclear coordinate may be imagined as the relative motion of a diatomic molecule with nuclei made of mass $m$ and relative motion with reduced mass $\mu = m/2$. Assuming that bound states exist in both ground and excited state, we assume that along the nuclear coordinate, the equilibrium positions for ground (coordinate $R_\mathrm{g}$, electronic state vector $|g\rangle$) and excited (coordinate $R_\mathrm{e}$, electronic state vector $|e\rangle$) electronic orbitals are slightly shifted with respect to each other (as illustrated in Fig. 2.1). We can generally express the total molecular Hamiltonian $\mathcal{H}_\mathrm{mol} = \mathcal{H}_\mathrm{el} \otimes \mathcal{H}_\mathrm{vib}$ in terms of the potential energy surfaces of ground and excited state $\mathcal{V}_{g/e}(\hat{R})$ as

[4] To be precise, the second-order diagonal couplings give rise to a correction of the PESs which is however typically very small since the coupling terms scale with the inverse mass of the nuclei [82].

[5] $3N_\mathrm{n} - 5$, for linear molecules.

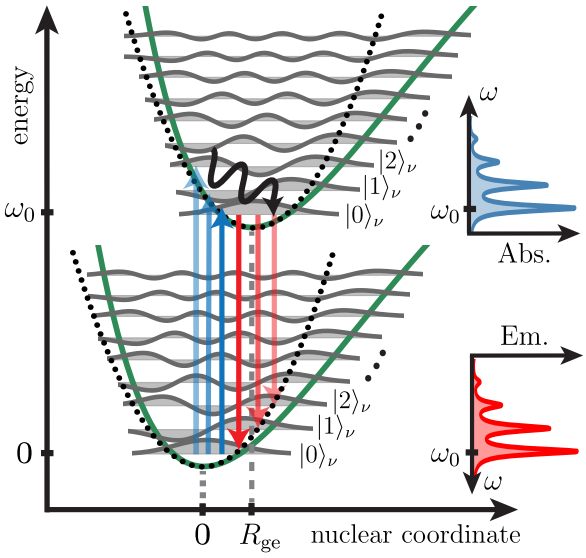


Figure 2.1: *Franck-Condon physics.* Displaced oscillator model used to derive the Holstein Hamiltonian. The Morse potential energy landscapes (green curves) of electronic ground and excited state with eigenstates shown in grey are approximated as harmonic oscillators (black dotted curves). The position mismatch between ground and excited state potential energy surfaces $R_{ge}$ gives rise to vibronic coupling leading to a mismatch between absorption (blue) and emission (red). Emission and absorption typically occur from the ground state due to quick vibrational relaxation. The insets show typical absorption/emission profiles following a Poissonian distribution with zero-phonon line at frequency $\omega_0$.

$$\mathcal{H}_{\text{mol}} = \frac{\hat{P}^2}{2\mu} \otimes \mathbf{1}_{\text{el}} + \mathcal{V}_g(\hat{R}) \otimes \sigma\sigma^\dagger + \mathcal{V}_e(\hat{R}) \otimes \sigma^\dagger\sigma, \tag{2.19}$$

with the quantized position and momentum operator satisfying $[\hat{R}, \hat{P}] = i$. The dynamics takes place now in an infinite-dimensional Hilbert space: in the electronic subspace the algebra is that of a spin 1/2 and is described by projectors $\sigma^\dagger\sigma$ (onto the excited state) and $\sigma\sigma^\dagger$ (onto the ground state) while in the motional subspace the dynamics is generally best described by an anharmonic Morse potential [85]. A great simplification can be obtained by performing a harmonic expansion of the potential surfaces around their respective minima

$$\mathcal{V}_g(\hat{R}) = \frac{1}{2}\mu\nu^2\left(\hat{R} - R_g\right)^2, \qquad \mathcal{V}_e(\hat{R}) = \omega_0 + \frac{1}{2}\mu\nu^2\left(\hat{R} - R_e\right)^2, \tag{2.20}$$

where we have assumed identical vibrational frequencies in ground and excited state. While the harmonic approximation is often not suffient for e.g. for small diatomic molecules which become anharmonic already at the level of a few vibrational quanta, this is often a good approximation for larger molecules where the vibrational modes correspond to large reduced masses [82]. Introducing

$\hat{Q} = \hat{R} - R_g$ and subsequently $\hat{R} - R_e = \hat{Q} + R_g - R_e =: \hat{Q} - R_{ge}$, this leads to

$$\mathcal{H}_{mol} = \left(\omega_0 + \frac{1}{2}\mu\nu^2 R_{ge}^2\right) \otimes \sigma^\dagger\sigma + \left(\frac{\hat{P}^2}{2\mu} + \frac{1}{2}\mu\nu^2\hat{Q}^2\right) \otimes \mathbf{1}_{el} - \mu\nu^2 R_{ge}\hat{Q} \otimes \sigma^\dagger\sigma. \tag{2.21}$$

We can now rewrite the momentum and position operators in terms of bosonic operators

$$\hat{Q} = r_{zpm}(b^\dagger + b), \qquad \hat{P} = ip_{zpm}(b^\dagger - b), \tag{2.22}$$

with the zero-point motion $r_{zpm} = 1/\sqrt{2\mu\nu}$ and $p_{zpm} = \sqrt{\mu\nu/2}$. Reexpressing the terms above via the factor $\lambda = \mu\nu R_{ge} r_{zpm}$ ($\lambda^2$ is called the Huang-Rhys factor) yields the Holstein-Hamiltonian for a single nuclear coordinate [86]

$$\mathcal{H}_{mol} = (\omega_0 + \lambda^2\nu)\sigma^\dagger\sigma + \nu b^\dagger b - \lambda\nu(b^\dagger + b)\sigma^\dagger\sigma, \tag{2.23}$$

where the coupling to the vibrations leads to a shift of $\lambda^2\nu$ of the bare electronic transition (sometimes referred to as reorganization energy) as well as to a displacement of the electronic excited state.
One can bring this Hamiltonian into diagonal form via the canonical polaron transformation (also called Lang-Firsov transformation [87])

$$\mathcal{U}_{pol}^\dagger = (\mathcal{D}^\dagger)^{\sigma^\dagger\sigma} = |g\rangle\langle g| + \mathcal{D}^\dagger |e\rangle\langle e|, \tag{2.24}$$

where the displacement operator is defined as

$$\mathcal{D} = \exp(-i\sqrt{2}\lambda p) = \exp[\lambda(b^\dagger - b)], \tag{2.25}$$

with the dimensionless momentum quadrature $p = i(b^\dagger - b)/\sqrt{2}$ as generator. The position quadrature is defined analogously as $q = (b^\dagger + b)/\sqrt{2}$. The displacement operator creates a coherent state with amplitude $\lambda$ when applied to the vibrational ground state $\mathcal{D}|0\rangle_\nu = |\lambda\rangle_\nu$. The vibrational creation and annihilation operators are shifted in the polaron picture dependent on the electronic state[6]

$$\mathcal{U}_{pol}^\dagger b \mathcal{U}_{pol} = b + \lambda\sigma^\dagger\sigma, \tag{2.26a}$$

$$\mathcal{U}_{pol}^\dagger b^\dagger \mathcal{U}_{pol} = b^\dagger + \lambda\sigma^\dagger\sigma, \tag{2.26b}$$

and furthermore the following commutation relations are fulfilled

$$[p, \mathcal{D}^\dagger] = 0, \qquad [q, \mathcal{D}^\dagger] = -\sqrt{2}\lambda\mathcal{D}^\dagger. \tag{2.27}$$

[6] Using that $e^A B e^{-A} = B + [A, B]$ if all higher order commutators vanish.

The Hamiltonian in the diagonal basis then becomes $\tilde{\mathcal{H}}_{\rm mol} = \omega_0\sigma^\dagger\sigma + \nu b^\dagger b$ and has eigenvectors $\{|g,n\rangle, |e,n\rangle\}$ while the eigenvectors in the original basis can be obtained by an inverse polaron transform and are given by $\{|g,n\rangle, \mathcal{D}|e,n\rangle\}$.

*Franck-Condon physics.* Let us now ask what the optical response of the molecule is to a weak laser excitation modeled via $\mathcal{H}_\ell = i\eta(\sigma^\dagger e^{-i\omega_\ell t} - \sigma e^{i\omega_\ell t})$. In an interaction picture, reached after performing a rotating frame transformation of the Hamiltonian with $\mathcal{U}_{\rm rf} = e^{i\omega_\ell\sigma^\dagger\sigma t}$, one has

$$\tilde{\mathcal{H}} = (\omega_0 - \omega_\ell)\sigma^\dagger\sigma + \nu b^\dagger b + i\eta\left(\sigma^\dagger\mathcal{D}^\dagger - \sigma\mathcal{D}\right). \tag{2.28}$$

Starting with the molecule in the absolute ground state $|g,0\rangle$, the result of the drive is to excite the electron to state $|e\rangle$ while exciting motion on the nuclear coordinate to a coherent motional state. One can immediately compute the probability of absorption

$$P_{\rm abs} = |\langle e,n|\tilde{\mathcal{H}}|g,0\rangle|^2 = \langle e,n|\sigma^\dagger\mathcal{D}^\dagger|g,0\rangle|^2 = s_\lambda^n, \tag{2.29}$$

showing a Poissonian distribution $s_\lambda^n = e^{-\lambda^2}\lambda^{2n}/n!$ of the occupancies of vibrational number states $|n\rangle_\nu$ with coefficients known as Franck-Condon factor (see Fig. 2.1 for typical profiles). In particular, the so-called zero-phonon line (ZPL, transition corresponding to $n = 0$) is reduced by a factor $e^{-\lambda^2}$ at zero temperature as compared to a pure two-level system. The Huang-Rhys factor $\lambda^2$ should be interpreted as the average number of vibrational quanta created upon excitation or deexciation of the molecule. The probability of the emission process is similarly computed between $|e,0\rangle$ and final states $|g,n\rangle$ and yields the same Poissonian distribution in $n$ which means that under these assumptions emission and absorption spectra are mirror images of each other.

*Many vibrational modes.* The Holstein Hamiltonian in Eq. (2.23) can be generalized to a more complex molecular system involving $n_\nu = 3N_{\rm n} - 6(5)$ independent nuclear coordinates with frequencies $\nu_k$ and coupling strengths $\lambda_k$. The total Hamiltonian is then expressed as

$$\mathcal{H}_{\rm mol} = \bar{\omega}_0\sigma^\dagger\sigma + \sum_{k=1}^{n_\nu}\nu_k b_k^\dagger b_k - \sum_{k=1}^{n_\nu}\lambda_k\nu_k(b_k^\dagger + b_k)\sigma^\dagger\sigma, \tag{2.30}$$

where the accumulated frequency shift of the excited state is given by $\bar{\omega}_0 = \omega_0 + \sum_{k=1}^{n_\nu}\lambda_k^2\nu_k$. This generalization is made under the assumption that the normal modes in the ground state are the same as in the excited state which is not always true and is referred to as Duschinsky mixing [88] which is however typically small for planar molecules such as PAHs [89]. Diagonalization of the Hamiltonian in (2.30) is straightforward as it involves a collective displacement for all nuclear coordinates

$$\mathcal{U}_{\rm pol}^\dagger = \left(\prod_k \mathcal{D}_k^\dagger\right)^{\sigma^\dagger\sigma} = |g\rangle\langle g| + \prod_k \mathcal{D}_k^\dagger |e\rangle\langle e|, \tag{2.31}$$

with $\mathcal{D}_k = \exp(-i\sqrt{2}\lambda_k p_k)$. The expectation value of the displacement operator $\langle \mathcal{D}_k \rangle = \langle \mathcal{D}_k^\dagger \rangle = e^{-\lambda_k^2 \langle p_k^2 \rangle}$ (assuming the vibrational mode to be in a thermal state[7]) expresses as $\langle \mathcal{D}_k \rangle = e^{-\lambda_k^2(\bar{n}_k+1/2)}$ where the average thermal occupancy at temperature $T$ is given by

$$\bar{n}_k = \frac{1}{\exp[\hbar\nu_k/(k_B T)] - 1}, \tag{2.32}$$

with $k_B$ the Boltzmann constant.

*Quadratic electron-vibration coupling.* In the previous derivation, we have assumed identical curvatures for the potential energy surfaces in electronic ground and excited state which is typically a good approximation for the relevant molecules [89]. However, assuming different curvatures for the vibrational frequencies for the potentials in ground ($\nu_g$) and excited ($\nu_e$) state, the molecular Hamiltonian becomes (for a single vibrational mode)

$$\mathcal{H}_{\text{mol}} = \bar{\omega}_0 \sigma^\dagger \sigma + \nu_g b^\dagger b - \lambda \nu_e (b + b^\dagger)\sigma^\dagger \sigma + \beta_{\text{quad}} (b + b^\dagger)^2 \sigma^\dagger \sigma, \tag{2.33}$$

with the frequency of the electronic excited state $\bar{\omega}_0 = \omega_0 + \mu \nu_e^2 R_{\text{ge}}^2/2$, the linear coupling constant $\lambda = R_{\text{ge}} \nu_e \sqrt{\mu/(2\nu_g)}$ and the additional quadratic coupling constant $\beta_{\text{quad}} = \nu_{ge}^2/(2\nu_g)$ which depends on the parameter $\nu_{ge}^2 = (\nu_e^2 - \nu_g^2)/2$ quantifying the difference in vibrational frequency between electronic ground and excited state. We remark that this Hamiltonian be diagonalized by a polaron transformation followed by a squeezing transformation $\mathcal{U}_{\mathcal{S}} = \mathcal{S}^{\sigma^\dagger \sigma}$ where $\mathcal{S}$ is the standard quantum optical squeezing operator $\mathcal{S} = e^{\frac{r}{2}[b^2 - (b^\dagger)^2]}$ and the explicit choice of $r$ depends on $\lambda$ and $\beta_{\text{quad}}$ [90].

## 2.4 Open quantum system dynamics

The free space light-matter interaction Hamiltonian for a system of $\mathcal{N}$ emitters Eq. (2.10) governs unitary evolution in an infinitely large Hilbert space owing to the infinite number of electromagnetic field modes. While in principle, one could write a Schrödinger equation or equivalently a von-Neumann equation for the density operator total system, this is an extremely complex task even for small-size systems. One typically reduces the complexity by proceeding with one of two competing, but interconnected approaches: one at the level of the density operator time evolution (the *master equation* [70–76]) and the other one following the time dynamics of system operators (*quantum Langevin equations* [73]). We detail the two approaches in the following and illustrate how the master equation approach deals with collective spontaneous emission of a quantum emitter ensemble in section 2.4.b, resulting in coherent dipole-dipole interactions and incoherent collective radiative emission. We fur-

[7] To see this, one can expand the displacement operator in an exponential series and make use of the fact that thermal, i.e., Gaussian states are fully characterized by their second-order moments.

thermore discuss quantum Brownian motion as a particular case of quantum Langevin equations in section 2.4.d.

### 2.4.a Master equation

Let us consider a system $S$ which is weakly coupled to a bath (or reservoir) $B$. The Hamiltonian of the total system is given by [70]

$$\mathcal{H} = \mathcal{H}_0 + \mathcal{H}_{\text{int}} = \mathcal{H}_S \otimes \mathbf{1}_B + \mathbf{1}_S \otimes \mathcal{H}_B + \mathcal{H}_{\text{int}}, \tag{2.34}$$

where $\mathcal{H}_S$ and $\mathcal{H}_B$ denote the free Hamiltonians of the system and bath, respectively, and $\mathcal{H}_{\text{int}}$ accounts for the interaction between the two. The symbols $\mathbf{1}_B$ and $\mathbf{1}_S$ represent the unity in the $B$ and $S$ Hilbert spaces. In the Schrödinger picture, the density operator satisfies $\dot{\rho} = -i[\mathcal{H}, \rho]$. We remove the free Hamiltonian by going into an interaction picture with a unitary transformation $\rho_I(t) = \mathcal{U}_0^\dagger(t)\rho(t)\mathcal{U}_0$ where $\mathcal{U}_0(t) = e^{-i\mathcal{H}_0 t}$. The von Neumann equation in the interaction picture then takes the form

$$\frac{\mathrm{d}}{\mathrm{d}t}\rho(t) = -i[\mathcal{H}_{\text{int}}(t), \rho(t)], \tag{2.35}$$

where the interaction Hamiltonian is now time-dependent $\mathcal{H}_{\text{int}}(t) = \mathcal{U}_0^\dagger(t)\mathcal{H}_{\text{int}}\mathcal{U}_0(t)$ and we omitted the index $I$ indicating the interaction picture. The formal solution of this is given by

$$\rho(t) = \rho(0) - i\int_0^t \mathrm{d}s\,[\mathcal{H}_{\text{int}}(s), \rho(s)]. \tag{2.36}$$

Inserting this back into Eq. (2.35) and taking the trace over the bath $\rho_S = \mathrm{Tr}_B[\rho]$, one finds

$$\frac{\mathrm{d}}{\mathrm{d}t}\rho_S(t) = -\int_0^t \mathrm{d}s\,\mathrm{Tr}_B[\mathcal{H}_{\text{int}}(t), [\mathcal{H}_{\text{int}}(s), \rho(s)]], \tag{2.37}$$

with $\mathrm{Tr}_B[\mathcal{H}_{\text{int}}, \rho(0)] = 0$. The above expression still contains the density operator of the total system on its right-hand side. The density matrix of the total system should show deviations on the order of $\mathcal{H}_{\text{int}}$ from an uncorrelated state $\rho(t) = \rho_S(t) \otimes \rho_B + \mathcal{O}(\mathcal{H}_{\text{int}})$. Assuming the coupling between system and bath to be weak (Born approximation),[8] one can neglect terms higher than second order in $\mathcal{H}_{\text{int}}$ and obtain an integro-differential equation for the reduced system operator

$$\frac{\mathrm{d}}{\mathrm{d}t}\rho_S(t) = -\int_0^t \mathrm{d}s\,\mathrm{Tr}_B[\mathcal{H}_{\text{int}}(t), [\mathcal{H}_{\text{int}}(s), \rho_S(s) \otimes \rho_B]]. \tag{2.38}$$

[8] A detailed discussion of the Born approximation can be found in Ref. [91].

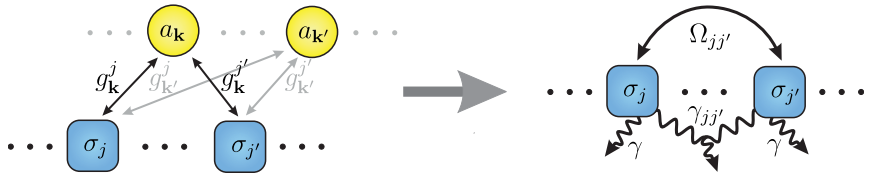


Figure 2.2: *Elimination of the electromagnetic vacuum.* Schematics of the procedure followed to obtain the open system dynamics formulation for a system of $\mathcal{N}$ quantum emitters (denoted by $\sigma_j$ and $\sigma_{j'}$) subject to the quantum electromagnetic vacuum. For a pair of emitters, coupling to the *common reservoir modes* (denoted by $a_{\mathbf{k}}$ and $a_{\mathbf{k}'}$) gives rise to separation-dependent dipole-dipole interactions at rate $\Omega_{jj'}$ as well as to collective decay rates $\gamma_{jj'}$.

This equation of motion can be brought in time-local form by replacing $\rho_S(s)$ with $\rho_S(t)$ which is then called the Redfield equation. Finally, to obtain a Markovian master equation, one first performs a change of variables $s \to t - s$. Under the assumption that the bath correlations decay quickly as compared to the time scale over which the state of the system varies (as induced by the bath), one may replace the upper bound of the integral by infinity and obtain

$$\frac{\mathrm{d}}{\mathrm{d}t}\rho_S(t) = -\int_0^\infty \mathrm{d}s\, \mathrm{Tr}_B[\mathcal{H}_{\mathrm{int}}(t), [\mathcal{H}_{\mathrm{int}}(t-s), \rho_S(t)\otimes\rho_B]]. \tag{2.39}$$

Under some conditions, this gives rise to a master equation in so-called Lindblad form as we will illustrate on the process of spontaneous emission in the next section.

### 2.4.b Master equation for collective spontaneous emission

As an example to illustrate the master equation, let us now apply Eq. (2.39) to the specific case of $\mathcal{N}$ identical emitters located at positions $\mathbf{R}_j$ (relative distance $R_{jj'} = |\mathbf{R}_j - \mathbf{R}_{j'}|$) mutually coupled to the electromagnetic vacuum described by the interaction Eq. (2.10). This procedure is schematically illustrated in Fig. 2.2 and results in an effective dynamics for the reduced matter system only. In the interaction picture, we can rewrite the Hamiltonian as $\mathcal{H}_{\mathrm{int}} = \sum_j(\sigma_j^\dagger \mathcal{F}_j(t) + \mathcal{F}_j^\dagger(t)\sigma_j)$ with $\mathcal{F}_j(t) = \sum_{\mathbf{k}} g_{\mathbf{k}} a_{\mathbf{k}} e^{i\mathbf{k}\mathbf{R}_j} e^{-i(\omega_k-\omega_0)t}$, where we assume equal orientation of all transition dipoles $\mathbf{d}^j_{\mathrm{eg}} = \mathbf{d}_{\mathrm{eg}}$ in the following. Using the cyclic property of the trace, the master equation takes the form [92]

$$\dot{\rho}(t) = \sum_{j,j'=1}^{\mathcal{N}} \int_0^\infty \mathrm{d}s \left\{ \sigma_j \rho(t) \sigma_{j'}^\dagger \left(\mathcal{C}_{j'j}(s) + \mathcal{C}^*_{jj'}(s)\right) - \sigma_j^\dagger \sigma_{j'} \rho(t) \mathcal{C}_{jj'}(s) - \rho(t)\sigma_j^\dagger \sigma_{j'} \mathcal{C}^*_{j'j}(s) \right\}, \tag{2.40}$$

where we denoted the relevant correlations as

$$\mathcal{C}_{jj'}(s) = \langle \mathcal{F}_j(t)\mathcal{F}_{j'}^\dagger(t-s)\rangle = \sum_{\mathbf{k}} |g_{\mathbf{k}}|^2 e^{i\mathbf{k}(\mathbf{R}_j - \mathbf{R}_{j'})} e^{i(\omega_0-\omega_k)s}, \tag{2.41}$$

and used furthermore that $\langle \mathcal{F}_j(t)\mathcal{F}_{j'}^\dagger(t-s)\rangle = \langle \mathcal{F}_{j'}(t-s)\mathcal{F}_j^\dagger(t)\rangle^*$. Identifying the minimal volume in $k$ space which is occupied by two modes of orthogonal polarization and same $\mathbf{k}$ vector as $(2\pi/\ell)^2$, we can replace the sum over $k$ vectors by an integral and go intro spherical coordinates

$$\frac{1}{\mathcal{V}}\sum_{\mathbf{k}} \to \int \frac{\mathrm{d}^3k}{(2\pi)^3} = \frac{1}{(2\pi c)^3}\int_0^\infty \mathrm{d}\omega_k\, \omega_k^2 \int \mathrm{d}\Omega_k. \tag{2.42}$$

Additionally, one has to account for the sum over the two orthogonal polarizations which can be performed as $\sum_\lambda (\mathbf{e}_{\mathbf{k}}^{(\lambda)}\cdot\mathbf{d}_{\mathrm{eg}})^2 = d_{\mathrm{eg}}^2 - (\mathbf{k}\cdot\mathbf{d}_{\mathrm{eg}})^2/k^2$. The correlation function can then be written as

$$\langle \mathcal{F}_j(t)\mathcal{F}_{j'}^\dagger(t-s)\rangle = \frac{d_{\mathrm{eg}}^2}{4\pi^2c^3\varepsilon_0}\int \mathrm{d}\omega_k\, \omega_k^3 F(kR_{jj'})e^{i(\omega_0-\omega_k)s}, \tag{2.43}$$

where the function $F(kR)$ is defined as the solid angle integral $F(kR) = 1/(4\pi)\int \mathrm{d}\Omega_k(1-(\mathbf{d}_{\mathrm{eg}}\cdot\mathbf{k})^2)/(d_{\mathrm{eg}}^2k^2)\cdot e^{i\mathbf{k}\mathbf{R}}$. This integral can be evaluated as

$$F(kR) = \frac{1}{4\pi}\left(1+\frac{(\mathbf{e}_{\mathbf{d}}\cdot\nabla_{\mathbf{R}})^2}{k^2}\right)\int_0^\pi \mathrm{d}\theta_k\, e^{ikR\cos\theta_k}\int_0^{2\pi}\mathrm{d}\varphi_k = \left[1+\frac{(\mathbf{e}_{\mathbf{d}}\cdot\nabla_{\mathbf{R}})^2}{k^2}\right]\frac{\sin(kR)}{kR}. \tag{2.44}$$

The integral over $s$ can be resolved by means of the Sokhotski-Plemelj theorem and results in

$$\int_0^\infty \mathrm{d}s\,\langle \mathcal{F}_j(t)\mathcal{F}_{j'}^\dagger(t-s)\rangle = \frac{3\gamma}{2}F(k_0R_{jj'}) - i\frac{3\gamma}{2}G(k_0R_{jj'}) =: \gamma_{jj'} + i\Omega_{jj'}, \tag{2.45}$$

where we introduced the spontaneous emission rate of a single emitter as $\gamma = \omega_0^3 d_{\mathrm{eg}}^2/(6\pi c^3\varepsilon_0)$ and

$$G(k_0R) = \frac{1}{\pi\omega_0^3}\mathcal{P}\int \mathrm{d}\omega_k\, \frac{\omega_k^3}{\omega_k-\omega_0}F(kR). \tag{2.46}$$

Here, $\mathcal{P}$ denotes the Cauchy principal value. Putting everthing together, one arrives at the master equation for an ensemble of $\mathcal{N}$ quantum emitters

$$\dot{\rho}(t) = i\,[\rho(t), \mathcal{H}_0 + \mathcal{H}_{\mathrm{dd}}] + \mathcal{L}_{\mathrm{e}}[\rho]. \tag{2.47}$$

The second term in the above equation is the Lindblad term for collective spontaneous emission

$$\mathcal{L}_{\mathrm{e}}[\rho] = \sum_{j,j'=1}^{\mathcal{N}}\gamma_{jj'}\left[2\sigma_j\rho(t)\sigma_{j'}^\dagger - \sigma_j^\dagger\sigma_{j'}\rho(t) - \rho(t)\sigma_j^\dagger\sigma_{j'}\right], \tag{2.48}$$

describing collective loss of excitation via radiative emission at rates $\gamma_{jj'} = (3\gamma/2)F(k_0 R_{jj'})$ where the diagonal terms $\gamma_{jj} = \gamma$ give the independent decay of the individual emitters. This is not in diagonal Lindblad form which for a single decay channel with collapse operator $c$ and rate $\gamma_c$ would be defined as

$$\mathcal{L}_c[\rho] = \gamma_c \left[ 2c\rho(t)c^\dagger - c^\dagger c\rho(t) - \rho(t)c^\dagger c \right]. \tag{2.49}$$

The coherent term $\mathcal{H}_{\mathrm{dd}}$ in Eq. (2.47) describes a dipole-dipole interaction characterized by a virtual exchange of excitation without loss of photons.

$$\mathcal{H}_{\mathrm{dd}} = \sum_{j,j':j\neq j'} \Omega_{jj'} \sigma_j^\dagger \sigma_{j'}, \tag{2.50}$$

with dipole-dipole exchange rate $\Omega_{jj'} = -(3\gamma/2)G(k_0 R_{jj'})$. The explicit functional dependence of $F(kR)$ and $G(kR)$ on distance is detailed in Appendix A. We discuss the master equation above in more detail for the simplest case of a two-emitter system as well as for chain and ring geometries in section 2.5.

### 2.4.c Quantum Langevin equations

The master equation formalism introduced previously is based on discarding the state of the environment and focusing on the dynamics of the reduced density operator of the much smaller system of interest. An alternative approach are quantum Langevin equations (QLEs, also called Heisenberg-Langevin equations) [73, 93] which follow the evolution at the level of system operators instead of system states, i.e., the density matrix. In essence, the formalism consists in supplementing the standard Heisenberg equations of motion with the proper dissipation and fluctuation terms. The fluctuation (or noise) terms contain information about the correlations of the environment and are crucial as they preserve the fundamental commutation relations for the respective operators.

For the $\mathcal{N}$ emitter system, one could proceed in a similar way as in the previous section by writing the Heisenberg equation for a generic emitter operator $\mathcal{O}$ and total Hamiltonian Eq. (2.10). After some computations, one arrives at [6, 73]

$$\begin{aligned} \dot{\mathcal{O}} = i[\mathcal{H}_0 + \mathcal{H}_{\mathrm{dd}}, \mathcal{O}] &- \sum_{j,j'} [\mathcal{O}, \sigma_j^\dagger](\delta_{jj'}\sqrt{2\gamma}\sigma_{\mathrm{in},j}(t) + \gamma_{jj'}\sigma_{j'}) \\ &+ \sum_{j,j'} (\delta_{jj'}\sqrt{2\gamma}\sigma_{\mathrm{in},j}^\dagger(t) + \gamma_{jj'}\sigma_{j'}^\dagger)[\mathcal{O}, \sigma_j], \end{aligned} \tag{2.51}$$

where $\sigma_{\mathrm{in},j}(t)$ is the noise affecting the electronic transition of the $j$th emitter and is defined as a sum

over all bath modes

$$\sigma_{\mathrm{in},j}(t) = \frac{i}{\sqrt{2\gamma}} \sum_{\mathbf{k}} g_{\mathbf{k}}^{(j)} a_{\mathbf{k}}(0) e^{-i\omega_k t} e^{i\mathbf{k}\cdot\mathbf{R}_j}, \tag{2.52}$$

with non-vanishing correlations $\langle \sigma_{\mathrm{in},j}(t)\sigma_{\mathrm{in},j}^{\dagger}(t')\rangle = (\gamma_{jj'}/\gamma)\delta(t-t')$ indicating the correlations of the noise between different emitters.

For open-system dynamics described by loss in standard, diagonal Lindblad form [Eq. (2.49)], a direct transformation between the master equation and the QLE formulation exists that reads [73]

$$\dot{\mathcal{O}} = i[\mathcal{H},\mathcal{O}] - [\mathcal{O},c^{\dagger}]\left\{\gamma_{\mathrm{c}} c + \sqrt{2\gamma_{\mathrm{c}}} c_{\mathrm{in}}\right\} + \left\{\gamma_{\mathrm{c}} c^{\dagger} + \sqrt{2\gamma_{\mathrm{c}}} c_{\mathrm{in}}^{\dagger}\right\}[\mathcal{O},c]. \tag{2.53}$$

For a system operator $\mathcal{O}$, the equation above is applied to each individual Lindblad collapse operator $c$ acting at rate $\gamma_{\mathrm{c}}$ and with associated input noise $c_{\mathrm{in}}$. The input noise $c_{\mathrm{in}}$ is zero averaged $\langle c_{\mathrm{in}}\rangle = 0$, delta-correlated in time $\langle c_{\mathrm{in}}(t)c_{\mathrm{in}}^{\dagger}(t')\rangle = \delta(t-t')$ (all other correlations vanish) and satisfies the commutation relation $[c_{\mathrm{in}}(t), c_{\mathrm{in}}^{\dagger}(t')] = \delta(t-t')$. For linear evolution, such an equation can be formally integrated and expectation values of correlations containing any number of operators can be obtained. For instance, for a single two-level system $\mathcal{H}_0 = \omega_0\sigma^{\dagger}\sigma$ undergoing spontaneous emission, the QLE for the dipole operator $\sigma$ simply reads

$$\dot{\sigma} = -(\gamma + i\omega_0)\sigma + \sqrt{2\gamma}\sigma_{\mathrm{in}}. \tag{2.54}$$

We will extend the standard QLEs for two-level sytems in chapter 3 to include vibronic coupling and to describe the properties of molecules interacting with light. Supplementing the QLEs with the corresponding input-output relations also allows for the readout of intracavity light-matter interactions which we exemplify for a cavity containing a single molecule in chapter 5 and for mesoscopic disordered ensembles in chapter 7.

### 2.4.d Quantum Brownian motion

A frequently encountered case of dissipation arises in the case of a quantum harmonic oscillator with free energy $\mathcal{H}_{\mathrm{HO}} = \nu(q^2+p^2)/2$ interacting with a heat bath of (mutually independent) harmonic oscillators. This case will become relevant in the following chapters as we need to describe the incoherent relaxation of the molecular vibrational modes into a thermal phononic environment. The dynamics is encompassed in the following equations of motion for the dimensionless quadratures $q$

and $p$

$$\dot{q}(t) = \nu p, \tag{2.55a}$$

$$\dot{p}(t) = -\nu q - 2\Gamma p + \xi(t), \tag{2.55b}$$

where the decay $\Gamma$ and corresponding stochastic input noise $\xi$ are only affecting the momentum quadrature. This model arises from the displacement-displacement interactions between the oscillator and the infinite surrounding bath $\mathcal{H}_{\text{int}} = -q\sum_k \alpha_k Q_k$ with coupling coefficients $\alpha_k$ [71]. The correlations of the input noise $\xi$ at a given bath temperature in the time domain read [94]

$$\langle \xi(t)\xi(t')\rangle = \int_{-\infty}^{\infty} \frac{\mathrm{d}\omega}{2\pi}\, e^{-i\omega(t-t')} S_{\text{th}}(\omega). \tag{2.56}$$

where we defined the thermal noise spectrum $S_{\text{th}}(\omega)$

$$S_{\text{th}}(\omega) = \frac{2\Gamma\omega}{\nu}\left[\coth\left(\frac{\hbar\omega}{2k_{\text{B}}T}\right) + 1\right]. \tag{2.57}$$

While generally, the noise is not delta-correlated, one can approximate Eq. (2.56) in the limit of large temperatures $k_B T/(\hbar\nu) \gg 1$ as [9]

$$\langle \xi(t)\xi(t')\rangle \approx 2\Gamma(1+2\bar{n})\delta(t-t') + i\frac{2\Gamma}{\nu}\delta'(t-t'), \tag{2.58}$$

where $\delta'(t-t')$ is the derivative of the delta function. From the spectrum evaluated at $\pm\nu$ one can obtain the cooling and heating contributions: $S_{\text{th}}(\nu) = 4\Gamma(\bar{n}+1)$ and $S_{\text{th}}(-\nu) = 4\Gamma\bar{n}$. Generally, from these properties one can always estimate the damping rate and the equilibrium thermal occupancy as

$$2\Gamma = \frac{1}{2}(S_{\text{th}}(\nu) - S_{\text{th}}(-\nu)), \qquad \bar{n} = \frac{S_{\text{th}}(-\nu)}{S_{\text{th}}(\nu) + S_{\text{th}}(-\nu)}. \tag{2.59}$$

In the case of small temperatures $k_B T/(\hbar\nu) \ll 1$, the thermal spectrum becomes very asymmetric $S_{\text{th}}(\omega) = [4\omega\Gamma/\nu]\,\theta(\omega)$ as it vanishes for negative frequencies (we introduced the Heaviside function $\theta(\omega)$). One can proceed with a Fourier domain analysis of Eqs. (2.55) which leads to $p(\omega) = \chi_m(\omega)\xi(\omega)$ and $q(\omega) = i\nu p(\omega)/\omega$ with the mechanical susceptibility describing the Lorentzian response of the phonon bath to the input noise

$$\chi_m(\omega) = \frac{i\omega}{\omega^2 - \nu^2 + 2i\Gamma\omega}. \tag{2.60}$$

Further more, one can also make use of the fact that the noise is always delta-correlated in Fourier domain as one can easily show that $\langle \xi(\omega)\xi(\omega')\rangle = S_{\text{th}}(\omega)\delta(\omega+\omega')$. One can then proceed by

[9] Using that in this limit $\bar{n} + 1/2 \approx k_B T/(\hbar\nu)$ and $\coth(x) \approx 1/x$ for $x \ll 1$.

computing the time-domain correlations [using that $\chi_m(-\omega) = \chi_m^*(\omega)$]:

$$\langle p(t)p(t')\rangle = \frac{1}{2\pi}\int_{-\infty}^{\infty} \mathrm{d}\omega\, e^{-i\omega(t-t')}|\chi_m(\omega)|^2 S_{\mathrm{th}}(\omega), \tag{2.61a}$$

$$\langle q(t)q(t')\rangle = \frac{1}{2\pi}\int_{-\infty}^{\infty} \mathrm{d}\omega\, e^{-i\omega(t-t')}\frac{\nu}{\omega}|\chi_m(\omega)|^2 S_{\mathrm{th}}(\omega). \tag{2.61b}$$

These expressions can be solved by a contour integral in the complex plane. We note that the integral of the momentum correlation function diverges and generally requires the introduction of a cutoff frequency $\Lambda > \nu$ to keep it finite.[10] However, one can notice that for $\Gamma \ll \nu$, the expression for $|\chi_m(\omega)|^2 S_{\mathrm{th}}(\omega)$ is sharply peaked around $\pm\nu$. In this case, one may expand around the poles $\omega = \nu + \delta$ and $\omega = -\nu + \delta$ with $|\delta| \ll |\nu|$ and only keep leading order terms in $\delta$. The integrals in Eq. (2.61) can then be approximated as the Fourier transforms of Lorentzian lineshapes which is much simpler to solve and results in (for $t > t'$)

$$\langle p(t)p(t')\rangle = \left[\left(\bar{n} + \frac{1}{2}\right)\cos(\nu\tau) - \frac{i}{2}\sin(\nu\tau)\right] e^{-\Gamma|\tau|}, \tag{2.62}$$

with $\tau = t - t'$ and similarly for $\langle q(t)q(t')\rangle$. Wen note here that, in principle, Brownian motion can also be expressed in terms of a master equation (the so-called Caldeira-Leggett model) which however cannot be expressed in Lindblad form and is cumbersome to solve analytically [95–97].

## 2.5 Super- and subradiance

Let us discuss now more in detail the master equation (2.47) for an ensemble of dipole-dipole coupled emitters. The Lindblad term describes nontrivial mutual decay characterized by the decay matrix $\mathbf{G}$ made up by the elements $\gamma_{jj'}$. However, this term is not in diagonal form as it is not comprised of $\mathcal{N}$ independent decay channels. One can perform a basis transformation with a matrix $\mathbf{T}$ (such that $\mathbf{T}^{-1} = \mathbf{T}^{\top}$) which diagonalizes $\mathbf{G}$ such that $\mathrm{diag}\,(\tilde{\gamma}_1, ..., \tilde{\gamma}_{\mathcal{N}}) = \mathbf{T}^{\top}\mathbf{G}\mathbf{T}$ where $\tilde{\gamma}_k$ is the $k$th eigenvalue of the decay matrix. In order to achieve diagonal Lindblad form one can then define a set of collapse operators $\Pi_k = \sum_j T_{jk}\sigma_j$ such that

$$\mathcal{L}_e[\rho] = \sum_{k=1}^{\mathcal{N}} \tilde{\gamma}_k \left(2\Pi_k\rho\Pi_k^{\dagger} - \Pi_k^{\dagger}\Pi_k\rho - \rho\Pi_k^{\dagger}\Pi_k\right), \tag{2.63}$$

now describes $\mathcal{N}$ independent decay channels each with an associated collapse operator $\Pi_k$ and associated loss rate $\tilde{\gamma}_k$. Notice that the preparation of a collective quantum superposition that decays at one of the rates $\tilde{\gamma}_k$ would require the application of the Hermitian conjugate of the corresponding collapse

[10] The cutoff is nothing artificial but arises naturally in many cases, e.g. from the dispersion of the surrounding phonon bath as discussed in chapter 5.

operator $\Pi_k^\dagger$ to the collective ground state $|G\rangle = |g\rangle_1 \otimes |g\rangle_2 \otimes ... \otimes |g\rangle_\mathcal{N}$ of the system, which is not a straightforward task since the eigenstates of the Lindblad term are generally not identical to the eigenstates of the Hamiltonian. In the so-called Dicke limit ($d \to 0$) where all the decay rates become equal and maximal $\gamma_{jj'} = \gamma$, the above Lindblad term gives rise to the famous model of *Dicke superradiance* where a single symmetric decay channel with rate $\mathcal{N}\gamma$ emerges while all other decay channels are vanishing [98].

### 2.5.a Two coupled emitters

Let us consider the simplest example of two quantum emitters separated by distance $a$. Diagonalization of the decay matrix $\mathbf{G}$ then leads to superradiant/subradiant decay channels characterized by $\gamma_\pm = \gamma \pm \gamma_{12}(a)$ and at the same time renders the Hamiltonian in diagonal form with eigenenergies $\omega_\pm = \omega_0 \pm \Omega(a)$. The eigenstates are symmetric/antisymmetric superpositions

$$|\pm\rangle = (|e\rangle_1 \otimes |g\rangle_2 \pm |g\rangle_1 \otimes |e\rangle_2)/\sqrt{2}. \tag{2.64}$$

This is illustrated in Fig. 2.3(a) in the collective basis where the other two states are the fully excited one $|E\rangle = |e\rangle_1 \otimes |e\rangle_2$ and the ground state $|G\rangle = |g\rangle_1 \otimes |g\rangle_2$. The splitting between the two levels in the collective basis $2\Omega = 2\Omega_{12}(a)$ as well as the magnitude and the sign of the mutual decay rate depend strongly on the particular choice of dipole orientations as well as on separation (as illustrated in Fig. 2.3(b)). For emitters separated by much more than $\lambda_0$, the decay becomes purely diagonal ($\gamma_{12} \to 0$) as expected for independent emitters while for short distances the mutual decay rate goes towards the independent decay rate $\gamma$. One can understand the connection between state symmetry

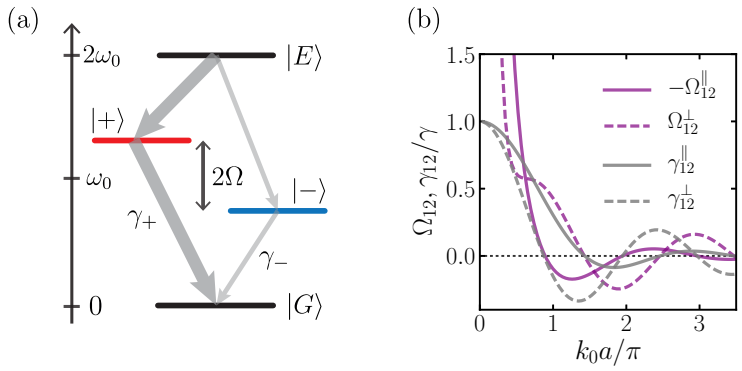


Figure 2.3: *Collective two-emitter system.* (a) Decay and eigenstates in the collective two-emitter basis. Superradiant and subradiant decay channels emerge through the formation of symmetric and antisymmetric superposition states. (b) Dipole-dipole coupling $\Omega_{12}$ and collective decay rate $\gamma_{12}$ scaling with normalized inter-emitter distance $k_0 a$ for parallel ($\parallel$) and perpendicular ($\perp$) orientation of dipoles (with respect to the connection vector $\mathbf{R}_{12}$).

and radiative properties in terms of an destructive (constructive) interference of radiative paths. For distances $a \ll \lambda_0$, the dipole-dipole interaction scales as $a^{-3}$ which leads to a divergence at extremely small separations. This is however only an artifact of our initial assumption that the dipole-dipole interaction is valid at any separation which is not true as for extremely small separations the overlap of electronic orbitals has to be taken into account.

### 2.5.B Quantum emitter rings and chains

While the simultaneous diagonalization of the Lindblad term and the Hamiltonian is generally not possible for $\mathcal{N} > 2$, one can still get some intuition in the nature of cooperative decay in the particular case of $\mathcal{N}$ equally spaced quantum emitters in a 1D configuration. Let us first inspect the Hamiltonian in the analytically solvable case where a nearest-neighbor (NN) approximation is performed. This is justified as the dipole-dipole interactions scales as $R_{jj'}^{-3}$ for distances smaller than a wavelength and thus the nearest neighbor coupling is almost an order of magnitude larger than that of the next to nearest neighbor one. The resulting Hamiltonian is then has the form

$$\mathcal{H}_{\mathrm{NN}} = \omega_0 \sum_j \sigma_j^\dagger \sigma_j + \sum_j \Omega(\sigma_j^\dagger \sigma_{j+1} + \sigma_{j+1}^\dagger \sigma_j), \tag{2.65}$$

where $\Omega$ is the coupling between two neighbors. We will just consider a single excitation hopping along the chain which is characterized by the particle basis $|j\rangle = \sigma_j^\dagger |G\rangle$ with $j = 1, \ldots, \mathcal{N}$ and the

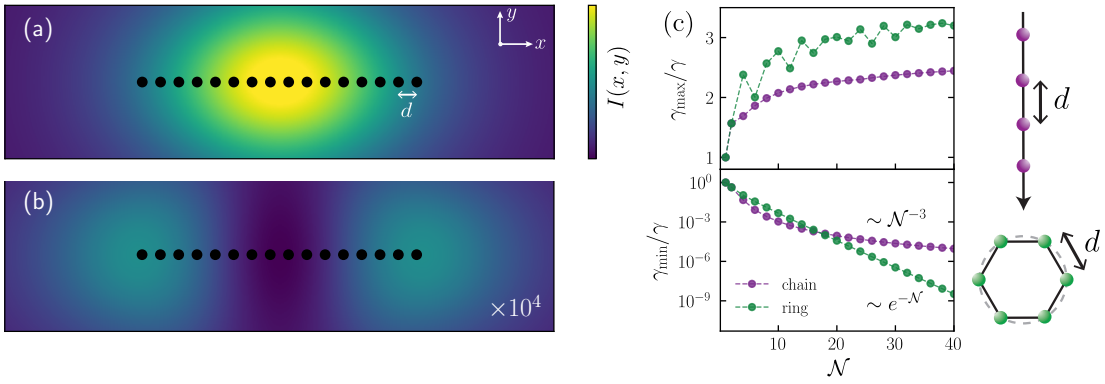


Figure 2.4: *Super- and subradiance of chains and rings.* Intensity distribution in the $x$-$y$ plane (in arbitrary units) of field emitted by a chain of 16 emitters in the (a) most superradiant state $|k = 1\rangle$ and (b) the most subradiant state $|k = \mathcal{N}\rangle$ for separations $d = 0.05\lambda_0$. The dipole orientation is chosen perpendicular to the chain and the field is observed at a transverse distance $z = 0.5\lambda_0$. Note that the intensity of the subradiant state was rescaled by a factor $10^4$ since it is orders of magnitude smaller than the intensity of the superradiant state. (c) Decay rate of most superradiant state $\gamma_{\mathrm{max}}$ and most subradiant state $\gamma_{\mathrm{min}}$ of chain and ring configurations as a function of the number of emitters for $d = 0.25\lambda_0$. While for ring configurations, the subradiant state shows an exponential scaling with $\mathcal{N}$, for chains the scaling is proportional to $\mathcal{N}^{-3}$.

collective ground state $|G\rangle$. The resulting Hamiltonian is a trigonal Toeplitz matrix with eigenvalues

$$\omega_k = \omega_0 + 2\Omega \cos\left[\frac{\pi k}{\mathcal{N}+1}\right], \tag{2.66}$$

for an index $k$ running from 1 to $\mathcal{N}$ (and the trivial energy of the ground state is 0). The corresponding eigenstates of the Hamiltonian are then described in the collective excitation basis

$$|\tilde{k}\rangle = \sum_j \sqrt{\frac{2}{\mathcal{N}+1}} \sin\left(\frac{\pi k j}{\mathcal{N}+1}\right) |j\rangle = \sum_j f_{jk} |j\rangle . \tag{2.67}$$

To compute the decay rates of the Hamiltonian eigenstates, we use the master equation to derive the equation of motion for the population component $\rho_{kk} = \langle\tilde{k}| \rho |\tilde{k}\rangle$. One arrives

$$\dot{\rho}_{kk} = -\sum_{k'} \left\{ \sum_{jj'} \gamma_{jj'} f_{jk} f_{j'k'} \right\} (\rho_{kk'} + \rho_{k'k}), \tag{2.68}$$

which shows that the eigenstates of the Hamiltonian couple within the first excitation manifold in addition to the decay to the ground state. The diagonal elements can then be estimated by setting $k = k'$ to derive $\tilde{\gamma}_k = \sum_{jj'} \gamma_{jj'} f_{jk} f_{j'k}$ and more explicitly

$$\tilde{\gamma}_k = \frac{2}{\mathcal{N}+1} \sum_{jj'} \gamma_{jj'} \sin\left(\frac{\pi k j}{\mathcal{N}+1}\right) \sin\left(\frac{\pi k j'}{\mathcal{N}+1}\right). \tag{2.69}$$

From this expression, one can derive a scaling of subradiant states with roughly $\mathcal{N}^{-3}$ for 1D chains (see lower panel of Fig. 2.4c for the scaling of the most subradiant state). Also superradiance emergence which starts to increase linearly with $\mathcal{N}$ and saturates against a constant value for large $\mathcal{N}$. Fig. 2.4(a) shows the emission profile of the most superradiant state $|k = 1\rangle$ with a large intensity due to constructive interference in the middle of the chain while for the subradiant state $|k = \mathcal{N}\rangle$ the intensity in the middle of the chain is close to zero due to destructive interference and one only has residual emission from the ends of the chain.

An interesting special case arises if one considers rings of emitters such as illustrated in Fig. 2.4(c) with ring radius $r$ and interparticle separation $d = 2r\sin(\pi/\mathcal{N})$. As opposed to finite chains, rings exhibit periodic boundary conditions, resulting in interesting optical properties such as highly subradiant states [99, 100]. Another motivation to study rings stems from the resemblance to the structure of certain light-harvesting complexes appearing in the photosynthetic complexes of bacteria and plants where energy is transfered with exteremly high efficiency [101–103]. In the case of a ring, the Hamiltonian and Lindblad term can be diagonalized simultaneously beyond the NN approximation due to the periodic boundary conditions by introducing the symmetric spin operator $\mathcal{S} = \sum_j \sigma_j/\sqrt{\mathcal{N}}$ as

well as $\mathcal{N}-1$ antisymmetric combinations orthogonal to the symmetric mode

$$\mathcal{A}_k = \frac{1}{\sqrt{\mathcal{N}}}\sum_{j=1}^{\mathcal{N}} \sigma_j e^{2\pi i j k/\mathcal{N}}, \quad \text{for} \quad k \in \{1,...,\mathcal{N}-1\}. \tag{2.70}$$

The ring Hamiltonian in terms of these collective operators then expresses as $\tilde{\mathcal{H}}_{\text{ring}} = \omega_{\mathcal{S}}\mathcal{S}^\dagger\mathcal{S} + \sum_{k=1}^{\mathcal{N}-1}\omega_k\mathcal{A}_k^\dagger\mathcal{A}_k$. This is based on the cyclic symmetry of the ring allowing to write sums as

$$\sum_{j'\neq j} e^{2\pi i k(j'-j)/\mathcal{N}}\Omega_{jj'} = \sum_{j'=2}^{\mathcal{N}} e^{2\pi i k(j'-1)/\mathcal{N}}\Omega_{1j'}. \tag{2.71}$$

The modified eigenenergies are given by $\omega_{\mathcal{S}} = \omega_0 + \sum_{j=2}^{\mathcal{N}}\Omega_{1j}$ for the symmetric mode while the antisymmetric combinations are shifted to $\omega_k = \omega_0 + \sum_{j=2}^{\mathcal{N}}\Omega_{1j}e^{2\pi i(j-1)k/\mathcal{N}}$. Also the Lindblad term can be split into a contribution from symmetric as well as antisymmetric modes in the collective basis

$$\mathcal{L}_e^{\text{ring}}[\rho] = \tilde{\gamma}_{\mathcal{S}}(2\mathcal{S}\rho\mathcal{S}^\dagger - \{\mathcal{S}^\dagger\mathcal{S},\rho\}) + \sum_{k=1}^{\mathcal{N}-1}\tilde{\gamma}_k(2\mathcal{A}_k\rho\mathcal{A}_k^\dagger - \{\mathcal{A}_k^\dagger\mathcal{A}_k,\rho\}), \tag{2.72}$$

with the decay rate of the symmetric, superradiant mode $\tilde{\gamma}_{\mathcal{S}} = \sum_{j=1}^{\mathcal{N}}\gamma_{1j}$ as well as the decay rates of the antisymmetric modes $\tilde{\gamma}_{\mathcal{A}} = \sum_{j=1}^{\mathcal{N}}\gamma_{1j}e^{i2\pi(j-1)k/\mathcal{N}}$. In Fig. 2.4(c) the decay rates of the ring are compared with the chain, revealing an exponential scaling $\sim \exp(-\mathcal{N})$ for the most subradiant modes of the ring which becomes beneficial especially for large emitter numbers. In chapter 6 this formalism will be extended to include the influence of vibronic coupling onto the superradiance and subradiance properties.

## 2.6 Vibronic dimer model

The vibronic dimer is a simple model to describe the interplay between electronic and vibrational interactions in molecular aggregates (i.e., arrays of molecules) which has been studied both theoretically [104–106] and experimentally [107, 108]. In contrast to the purely electronic dimer discussed in section 2.5.a, the model features a more complicated energy landscape with states containing both electronic and vibrational character. The model consists of two identical molecules (indexed here by 1 and 2), each coupled to a single harmonic nuclear coordinate $q_{1/2}$ with Huang-Rhys factor $\lambda^2$. The molecules are coupled to each other via dipole-dipole interaction with strength $\Omega$ (see Fig. 2.5(a)). Assuming that the excited state energies of the two molecules are identical and restricting to the single-excitation subspace spanned by states $|e\rangle_1 \otimes |g\rangle_2$ and $|g\rangle_1 \otimes |e\rangle_2$, the Hamiltonian of the dimer can

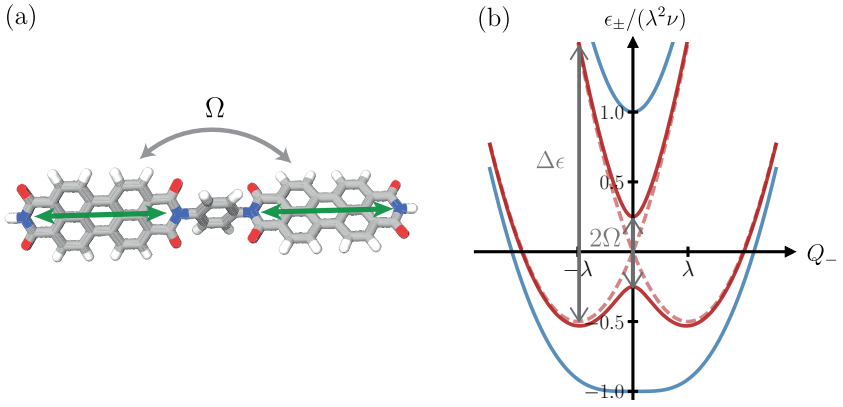


Figure 2.5: *Vibronic dimer*. (a) Two identical chromphores are connected with nanometer separation by an insulating bridge and are coupled via dipole-dipole interactions. The green arrows represent the orientation of the transition dipoles [107]. (b) Potential energy surfaces $\varepsilon_\pm$ of the excited state manifold of the vibronic dimer model as a function of the dimensionless relative motion coordinate $Q_-$ for $\Omega = 0$ (red dashed), $2\Omega = \Delta\varepsilon/4$ (red solid) and $2\Omega = \Delta\varepsilon$ (blue.)

be represented by

$$\mathcal{H}_{\text{dim}} = \begin{pmatrix} -\sqrt{2}\lambda\nu q_1 & \Omega \\ \Omega & -\sqrt{2}\lambda\nu q_2 \end{pmatrix} + \frac{\nu}{2}\sum_{i=1,2}\left(p_i^2 + q_i^2\right)\mathbf{1}_{2\times 2}, \tag{2.73}$$

where $\mathbf{1}_{2\times 2}$ is the $2\times 2$ unity matrix. Introducing both symmetrized coordinates $Q_\pm = (q_1 \pm q_2)/\sqrt{2}$ as well as symmetrized electronic operators $(\sigma_1 \pm \sigma_2)/\sqrt{2}$, the Hamiltonian transforms to

$$\tilde{\mathcal{H}}_{\text{dim}} = \begin{pmatrix} \Omega - \lambda\nu Q_+ & -\lambda\nu Q_- \\ -\lambda\nu Q_- & -\Omega - \lambda\nu Q_+ \end{pmatrix} + \frac{\nu}{2}\sum_{k=\pm}\left(Q_k^2 + P_k^2\right)\mathbf{1}_{2\times 2}, \tag{2.74}$$

from which one can see that only the relative motion coordinate $Q_-$ couples between electronic states in the collective basis. The coordinate $Q_+$ instead leads to a constant shift and can eventually be eliminated by a proper transformation.[11] The Hamiltonian in Eq. (2.74) can be easily diagonalized leading to the eigenvalues for the excited state potential energy surfaces

$$\varepsilon_\pm = \frac{\nu}{2}\left(Q_+^2 + Q_-^2\right) - \lambda\nu Q_+ \pm \sqrt{\lambda^2\nu^2 Q_-^2 + \Omega^2}. \tag{2.75}$$

The potential energy surfaces are plotted in Fig. 2.5(b) as a function of $Q_-$ for various coupling strengths $\Omega$. One can see that the coupling lifts the degeneracy of the potential surfaces at $Q_- = 0$ and leads to a splitting of $2\Omega$. Depending on the magnitude of $\Omega$, the lower energy surface either possesses two minima or just a single minimum. An important quantity is the reorganization energy $\Delta\varepsilon = 2\lambda^2\nu$ defined as the vertical energy separation between the potential curves at each minimum

[11] Namely, a polaron transformation in the collective basis with $P_+$ as generator, see chapter 6.

for zero coupling $\Omega = 0$ [as illustrated in Fig. 2.5(b)]. One finds that a double minimum of the lower energy surface located at $Q_{-}^{\pm} = \pm\sqrt{\lambda^2\nu[1-(\Omega/\lambda^2\nu)^2]}$ exists when the level splitting $2\Omega$ is smaller than the reorganisation energy $|2\Omega| < \Delta\varepsilon$.
We will revisit vibronic dimers in chapter 3 when we discuss the Förster resonance energy transfer between two chromophores. In chapter 6, we will generalize the model to more complicated geometries such as vibronic rings and will investigate the model in the presence of collective radiative emission and vibrational relaxation.

## 2.7 Fundamentals of cavity QED

Light-matter interactions can be greatly enhanced by using optical elements which confine electromagnetic fields in small volumes. This is obvious from the scaling of the zero-point electric field amplitude $\mathcal{E}_k = \sqrt{\omega_k/(2\varepsilon_0\mathcal{V})}$ which indicates that stronger field amplitudes per photon mode are achieved for smaller mode volumes. This led to the development of cavity QED as a subfield of quantum optics specializing in the description of coherent light-matter interactions in cavities [109–112]. This section introduces fundamental concepts and of cavity QED with a single and many emitters which are mainly used for the description of single molecules coupled to light in chapter 5 as well as for the description of disordered mesoscopic ensembles in chapter 7.

The simplest example of an optical cavity is the coplanar design known as a Fabry-Pérot cavity comprised of two highly reflective parallel mirrors. For a distance $L$ between the mirrors and assuming at first perfect reflectivity, such a setup defines resonances conditioned by $L = n\lambda/2$. The fundamental mode has, therefore, a wavelength of $2L$ with frequency $\pi c/L$ and higher harmonics are multiples of this mode. The quantity $\omega_{\mathrm{FSR}} = \pi c/L$ is known as the free spectral range and gives the frequency difference between consecutive optical resonances of the structure. Assuming two mirrors positioned at $z = 0$ and $z = L$ and a transverse area $\mathcal{S}$ of the supported optical resonances, one can proceed in quantizing the field inside the optical resonator by associating bosonic operators $a_n$ to all resonances and writing the total Hamiltonian as $\mathcal{H}_c = \sum_n \omega_n a_n^\dagger a_n$. The electric field operator can then be decomposed as

$$\hat{\mathbf{E}}(z) = \sum_n \mathcal{E}_n \left(a_n + a_n^\dagger\right) \sin(k_n z)\mathbf{e}_n, \tag{2.76}$$

where the sum runs over all allowed wave vectors $k_n = n\pi/L$ and the zero-point electric field amplitude $\mathcal{E}_n = \sqrt{\omega_n/(\varepsilon_0 L\mathcal{S})}$ and all polarizations $\mathbf{e}_n$ are assumed orthogonal to the $z$ direction. For all situations we will consider in the following, a single cavity mode suffices. We denote the mode by the operator $a$ at frequency $\omega_c$ such that the free Hamiltonian of the cavity becomes $\mathcal{H}_c = \omega_c a^\dagger a$.

Perfect mirrors define infinitely sharp resonances and would not allow light to enter or exit the cav-

ity. In order to allow the in-coupling of light into the optical resonator side mirrors with slightly less than unit reflectivity are used. For a double-sided optical resonator, the localized resonances can then couple to the infinite number of modes to the left and right of the cavity, leading to a loss of the intracavity photons. This loss can be described within the master equation formalism by following a phenomenological model where photons from mode $a$ can tunnel to the left and right continuum of free radiation modes via an excitation exchange Hamiltonian. The open-system dynamics approach detailed in section 2.4.a leads to a standard Lindblad form of the cavity photon decay

$$\mathcal{L}_\kappa[\rho] = \kappa \left[2a\rho a^\dagger - a^\dagger a\rho - \rho a^\dagger a\right], \tag{2.77}$$

where $\kappa = \kappa_R + \kappa_L$ encompasses total losses via both left and right mirror.
To allow for the driving of the cavity mode let us now assume a continuous-wave laser with power $\mathcal{P}$ entering the cavity from the left side. This can be included in the following Hamiltonian

$$\mathcal{H}_\ell = i\eta_c(a^\dagger e^{-i\omega_\ell t} - ae^{i\omega_\ell t}), \tag{2.78}$$

where the drive amplitude is $\eta_c = \sqrt{2\kappa_L \mathcal{P}/\omega_\ell}$. The equation of motion for the cavity operator can be derived from the Heisenberg-Langevin equation in a frame rotating at the laser frequency (with Hamiltonian $\mathcal{H}_c + \mathcal{H}_\ell$ and Lindblad term $\mathcal{L}_\kappa[\rho]$) leading to

$$\dot{a} = -\kappa a - i(\omega_c - \omega_\ell)a + \eta_c + \sqrt{2\kappa}a_{\text{in}}. \tag{2.79}$$

The steady state of the equation above, which is reached by requiring that $\langle \dot{a} \rangle = 0$, describes the expected Lorentzian response $\langle a \rangle_{\text{ss}} = \eta_c/(\kappa + i(\omega_c - \omega_\ell))$ of the cavity field exhibiting a linewidth $\kappa$ and resonance frequency $\omega_c$. In addition to the equation of motion for the cavity field operator, the full description of the optical cavity includes the input-output relation [73]

$$a_{\text{out}} + a_{\text{in}} = \sqrt{\kappa}a(t), \tag{2.80}$$

which allows to investigate experimentally observable quantities such as the transmission of the cavity. For example, the average shows that the cavity transmission can simply be written as

$$t_c = \frac{\langle a_{\text{out}} \rangle}{\eta_c} = \frac{\sqrt{\kappa}\,\langle a \rangle}{\eta_c}. \tag{2.81}$$

Let us consider now $\mathcal{N}$ identical quantum emitters placed inside the optical cavity around a single optical mode of interest. Assuming the field to be varying only along the cavity axis, for emitter $j$ positioned at $z_j$ within the cavity volume, the dipolar interaction is characterized by a position-dependent coupling strength $g_j = \mathcal{E} d_{\text{eg}} \sin(kz_j)$. The light-matter Hamiltonian describing excitation exchange

between the emitters and the cavity mode can then be cast in *Tavis-Cummings* [113] form

$$\mathcal{H}_{\mathrm{TC}} = \omega_0 \sum_{j=1}^{\mathcal{N}} \sigma_j^\dagger \sigma_j + \omega_c a^\dagger a + \sum_{j=1}^{\mathcal{N}} \left( g_j a \sigma_j^\dagger + g_j^* \sigma_j a^\dagger \right). \tag{2.82}$$

This interaction can be understood as a particular case of the free space interaction in Eq. (2.10) where the coupling to the cavity mode $a$ is enhanced while the coupling to all other modes is inhibited.

### 2.7.a Single emitter

Let us first describe a few properties of the interaction in Eq. (2.82) at the level of a single emitter $\mathcal{N} = 1$ where the interaction is known as the *Jaynes-Cummings Hamiltonian* and can be diagonalized exactly [113, 114]. However, the classical equations of motion in the weak excitation limit $\langle \sigma_z^j \rangle \approx -1$ for the cavity field amplitude $\alpha = \langle a \rangle$ and the dipole of the quantum emitter $\beta = \langle \sigma \rangle$ are sufficient to characterize the different regimes of interaction inside the optical cavity,

$$\dot{\alpha} = -\left(\kappa - i\Delta_c\right)\alpha - ig^*\beta + \eta_c, \tag{2.83a}$$

$$\dot{\beta} = -(\gamma - i\Delta_\ell)\beta - ig\alpha, \tag{2.83b}$$

where we introduced the detunings $\Delta_\ell = \omega_\ell - \omega_0$, $\Delta_c = \omega_\ell - \omega_c$. The diagonalization of the above equations (under resonance conditions, i.e., fixed $\Delta_c = \Delta_\ell = 0$) leads to the hybridized decay rates and frequencies,

$$\Gamma_\pm = \frac{\kappa + \gamma}{2} \pm \Re\left\{ \sqrt{\left(\frac{\kappa - \gamma}{2}\right)^2 - g^2} \right\}, \tag{2.84a}$$

$$\omega_\pm = \pm \Im\left\{ \sqrt{\left(\frac{\kappa - \gamma}{2}\right)^2 - g^2} \right\}. \tag{2.84b}$$

The threshold $g > |(\kappa - \gamma)/2|$ indicates the onset of the strong coupling regime where the two frequencies split into distinct polariton branches. Far above this threshold the polaritons are symmetrically displaced by $\pm g$ from the original energies [see Fig. 2.6(b)]. The decay rates show a different behavior as they already start hybridizing before the onset of strong coupling and ultimately reach the algebraic average $(\kappa + \gamma)/2$. In the weak coupling (or Purcell) regime [115], highlighted in grey in Figs. 2.6(a) and (b), a strong modification of the emitter bare decay rate by a factor $1 + C$ occurs for $\gamma \ll \kappa$, where $C$ is the cooperativity defined as $C = g^2/(\kappa\gamma)$. The cooperativity can be interpreted as the ratio between the emission into the cavity mode and the emission into the free space modes. Inserting the explicit definitions of $g$, $\gamma$ and defining the quality factor $\mathcal{Q} = \omega_c/\kappa$, the cooperativity

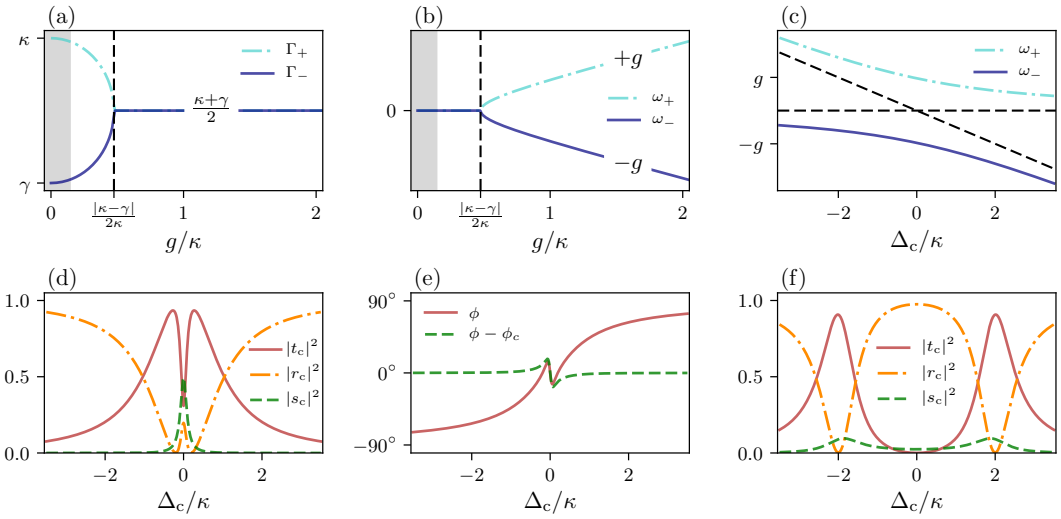


Figure 2.6: *Cavity mode hybridization of a single quantum emitter*. Plot of (a) hybrid cavity-emitter decay rates and (b) frequencies when sweeping the coupling $g$ past the strong coupling onset point of $g = |(\kappa - \gamma)/2|$ (in the resonant case). The grey region shows the weak-coupling but strong cooperativity regime where the Purcell effect shows up as a modification of the emitter's radiative rate. (c) Avoided crossing in the strong-coupling regime when the cavity detuning is scanned. (d) Intensity of transmitted, reflected and scattered fields of an emitter-cavity system in the Purcell regime (antiresonance regime) for a laser scan around the resonance. The parameters are $g = \kappa/5$, $\gamma = \kappa/20$. (e) Cavity phase shift and emitter-only induced phase shift in the same regime. (f) Cavity response in transmission and reflection as well as scattered field showing the signature of polaritons in the strong coupling regime ($g = 2\kappa$).

parameter can be recast as the original Purcell factor [115]

$$C = \frac{6\pi c^3 \mathcal{Q}}{\omega_0^3 \mathcal{V}}. \tag{2.85}$$

The complex transmission amplitude of the cavity can be expressed as

$$t_c = \frac{\kappa}{\kappa - i\Delta_\ell + g^2/(\gamma - i\Delta_\ell)}, \tag{2.86}$$

while the reflectivity is immediately derived as $r_c = -1 + t_c$. The cavity transmission is illustrated in the Purcell (antiresonance regime) in Fig. 2.6(d) and in the strong coupling regime in Fig. 2.6(f). In the strong coupling regime, the newly formed polaritons can be read in the cavity transmission as two well-separated peaks corresponding to the newly formed hybrid light-matter states

$$|\pm\rangle = \frac{1}{\sqrt{2}}(|g1\rangle \pm |e0\rangle). \tag{2.87}$$

The difference between the peaks $\omega_+ - \omega_-$ is known as the *vacuum Rabi splitting* (VRS). For the derivation of the scattered field, one can use the fact that the sum of all the intensities has to be conserved, namely $|r_c|^2 + |t_c|^2 + |s_c|^2 = 1$. This gives the scattered intensity $|s_c|^2 = 1 - |t_c - 1|^2 - |t_c|^2 =$

$2\left(\Re\{t_c\} - |t_c|^2\right)$. Moreover the phase shift of the field that passes through the cavity is given by the transmission coefficient as $\phi_c = \arctan(\Im\{t_c\}/\Re\{t_c\})$ (see Fig. 2.6(e)).

### 2.7.b Many emitters

While we will discuss disordered ensembles of $\mathcal{N}$ molecules coupled to a common cavity mode in more depth in chapter 7, let us analyze a few properties of the Tavis-Cummings Hamiltonian already here. In the simplified case that all transition frequencies are identical $\omega_j = \omega_0$ and also all couplings are identical $g_j = g$, an immediate observation is the cavity only couples to a symmetric superposition of all dipoles $\hat{B} = \sum_j \sigma_j/\sqrt{N}$ (the so-called *bright mode*) such that the interaction can be expressed as $\mathcal{H}_{\text{int}} = g_{\mathcal{N}}(a\hat{B}^\dagger + a^\dagger\hat{B})$ with the collective coupling strength $g_{\mathcal{N}} = g\sqrt{\mathcal{N}}$. The bright state is defined as $|B\rangle = \hat{B}^\dagger|0\rangle$ and the hybridized light-matter states in the single excitation subspace are given by

$$|\pm\rangle = \frac{1}{\sqrt{2}}(|g1\rangle \pm |B0\rangle). \tag{2.88}$$

In terms of the collective bright state, the discussion can now be lead largely analogous to the single emitter case as the strong coupling regime is entered when $g_{\mathcal{N}} > |(\kappa-\gamma)/2|$ and in the weak coupling regime one can define the $\mathcal{N}$-emitter cooperativity $C_{\mathcal{N}} = g_{\mathcal{N}}^2/(\kappa\gamma)$, scaling linearly with the number emitters.

If the coupling strength $g_j$ varies from emitter to emitter the definition of the collective bright mode can be generalized to

$$\hat{B} = \frac{1}{\sqrt{\sum_{j=1}^{\mathcal{N}} |g_j|^2}} \sum_{j=1}^{\mathcal{N}} g_j^* \sigma_j, \tag{2.89}$$

which leads to a collective coupling strength $\tilde{g}_{\mathcal{N}} = \sqrt{\sum_{j=1}^{\mathcal{N}} |g_j|^2}$.

### 2.7.c Holstein-Tavis-Cummings Hamiltonian

The combination of the Tavis-Cummings Hamiltonian and the Holstein Hamiltonian is known as Holstein-Tavis-Cummings (HTC) Hamiltonian which is the simplest model to study the influence of vibronic coupling onto the light-matter interaction in confined geometries [50, 52, 116]. In the simplest case, one considers a set of indentical molecules, each coupled to a single nuclear coordinate with Huang-Rhys factor $\lambda^2$ and coupled to a common cavity mode. The HTC Hamiltonian then

expresses as

$$\mathcal{H}_{\mathrm{HTC}} = \bar{\omega}_0 \sum_{j=1}^{\mathcal{N}} \sigma_j^\dagger \sigma_j + \omega_c a^\dagger a + \nu \sum_{j=1}^{\mathcal{N}} b_j^\dagger b_j + \sum_{j=1}^{\mathcal{N}} \left( g_j a \sigma_j^\dagger + g_j^* \sigma_j a^\dagger \right) - \lambda\nu \sum_{j=1}^{\mathcal{N}} (b_j^\dagger + b_j) \sigma_j^\dagger \sigma_j, \tag{2.90}$$

which generally gives rise to non-trivial eigenstates with mixed electronic-vibrational-photonic character (polaron-polaritons) [49]. The HTC model has been successfully invoked to explain the spectra of organic microcavities [52] and has been shown to lead to a decoupling between electronic and nuclear degrees of freedom at certain light-matter interaction strengths (the so-called polaron decoupling [32]). While in the bare basis, both analytical and numerical investigations are cumbersome, moving into a collective basis can shed insight onto the relevant processes and provide numerical simplification [52, 60]. In a first step, some intuition can be gained by considering the Hamiltonian in the single-excitation manifold (regarding the light-matter part) for just a single molecule $\mathcal{N} = 1$ [117]. The Hamiltonian can then be expressed in terms of the vibrational quadratures $q$ and $p$ as

$$\mathcal{H}_{\mathrm{HJC}} = \begin{pmatrix} \omega_c & g \\ g & \bar{\omega}_0 - \sqrt{2}\lambda\nu q \end{pmatrix} + \frac{\nu}{2}(q^2 + p^2)\mathbf{1}_{2\times 2}. \tag{2.91}$$

Similarly to the vibronic dimer model from section 2.6, for the calculation of the hybrid potential energy surfaces, one treats the vibrational operators simply as parameters. The resulting eigenenergies are illustrated in Fig. 2.7 for the resonant case $\omega_c = \omega_0$ where the color indicates the respective weight

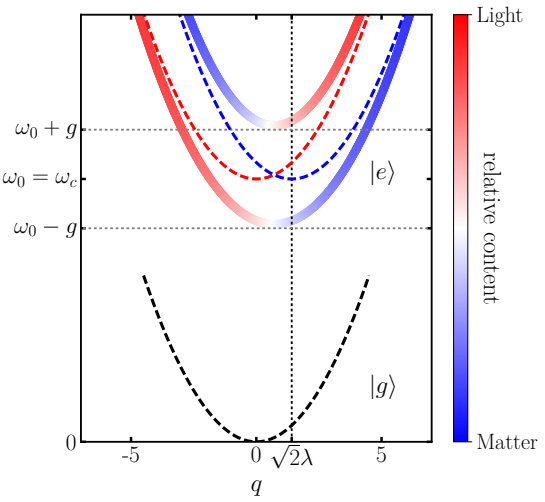


Figure 2.7: *Polaritonic potential energy surfaces.* Ground state (black dashed curve) as well as excited state potential energy curves (red-white-blue curves) of the Holstein-Jaynes-Cummings model where the color indicates the degree of light-matter hybridization for $g = 3\nu$, $\lambda = 1$. The bare excited-state potential energy curves of cavity/molecule are indicated by the red/blue dashed curves (corresponds to $g = 0$).

of photon/matter contributions obtained by projection of the corresponding eigenvectors $|m\rangle$ onto the single photon/matter excitation states $|\langle 1_{\mathrm{ph}}|m\rangle|^2$ and $|\langle e|m\rangle|^2$, respectively. One can see that the light-matter hybridization depends strongly on the nuclear coordinates and reaches its maximum at the intersection of the bare potential energy surfaces.

We will discuss cavity-coupled molecules in the presence of incoherent interactions with the environment in chapter 5.

# 3

# Polaron Langevin Equation

We now introduce our main theoretical method which consists in deriving a quantum Langevin equation for a *polaron operator* $\tilde{\sigma} = \sigma\mathcal{D}^\dagger$, i.e., a vibrationally-dressed electronic dipole operator) [1, 51, 118]. Here, the collective displacement operator $\mathcal{D}^\dagger$ can refer to a large set of molecular vibrational modes $\mathcal{D}^\dagger = \prod_{k=1}^{n_v} \mathcal{D}_k^\dagger$. The method has been used similarly previously for the description of optomechanical systems where resemblant interactions occur [119, 120]. Also, the method can be seen as the equivalent of other approaches developed for polaron physics at the level of quantum master equations [121–124]. The advantage of quantum Langevin equations is however that, since the time evolution of operators is known, it is relatively easy to obtain correlation functions between operators and therefore spectroscopic quantities. Furthermore, it is more straightforward to include colored noise and non-Markovian dynamics which is cumbersome with master equations. The drawback is that Langevin equations are difficult to implement numerically as one has to account for the stochastic quantum noise. For all numerical simulations presented in this thesis we therefore use quantum master equations [125, 126]. We show in this chapter that – as a proof of principle – the method can be used to calculate molecular emission and absorption spectra and illustrate it on the process of Förster resonance energy transfer (FRET) between two dipole-dipole coupled molecules. The polaron Langevin equation will be the starting point for the results presented in the following chapters, in particular chapters 4 and 5 where the method will be extended to coherently driven vibrational modes of infrared-active molecules, an infinite number of phonon modes of the surrounding host environment as well as cavity-coupled molecules.

## 3.1 Derivation of the PLE

Let us consider the simplest case of a single molecule which is (weakly) driven by a laser

$$\mathcal{H}_\ell = \eta_\ell(\sigma^\dagger e^{-i\omega_\ell t} + \text{h.c.}) \tag{3.1}$$

and described by the Holstein Hamiltonian Eq. (2.30)

$$\mathcal{H}_{\rm mol} = \sum_{k=1}^{n_\nu}(\omega_0 + \lambda_k^2\nu_k)\sigma^\dagger\sigma + \sum_{k=1}^{n_\nu}\nu_k b_k^\dagger b_k - \sum_{k=1}^{n_\nu}\lambda_k\nu_k(b_k^\dagger + b_k)\sigma^\dagger\sigma. \tag{3.2}$$

We will assume a Brownian noise dissipation model (see section 2.4.d for details) for the molecular vibrational modes. We will more specifically derive the Brownian noise model for a molecule embedded in a crystal in chapter 5. For the vibrational degrees of freedom, one can then derive the equations of motion

$$\dot{q}_k = \nu_k p_k, \tag{3.3a}$$

$$\dot{p}_k = -2\Gamma_k p_k - \nu_k q_k - \sqrt{2}\lambda_k\nu_k\sigma^\dagger\sigma + \xi_k. \tag{3.3b}$$

In addition to the environment-induced damping at rates $2\Gamma_k$ and associated thermal input noise $\xi_k$ (see section 2.4.d for noise properties), vibrations are driven by their coupling to the electronic degree of freedom. In the weak excitation limit $\langle\sigma^\dagger\sigma\rangle \ll 1$ this can however be neglected and the vibrations approximately undergo free evolution. We note that, in principle, one can also use a Lindblad model for vibrational relaxation with rates $\Gamma_k$ and collapse operator $b_k$ [1]. This is however only an approximated model, as some care has to be taken regarding the correct collapse operator since the vibronic coupling can be strong ($\lambda_k \sim 1$) and the vibrational relaxation is typically much faster than the spontaneous emission $\Gamma \gg \gamma$. It can be shown that in such a case, a local master equation is thermodynamically not consistent and a global master equation approach has to be taken with correct collapse operator given by $b_k - \lambda_k\sigma^\dagger\sigma$ [127–130]. For the electronic transition, the time evolution of the polaron operator can be computed from $\dot{\tilde{\sigma}} = \dot{\sigma}\mathcal{D}^\dagger + \sigma\dot{\mathcal{D}}^\dagger$ where the full Langevin equation for $\sigma$ is derived from the Holstein Hamiltonian and the radiative emission in Lindblad form with the transformation indicated by the relation in Eq. (2.53). The equation of motion for the displacement operator $\mathcal{D}_k^\dagger = e^{i\lambda_k\sqrt{2}p_k}$ is given by

$$\begin{aligned}\dot{\mathcal{D}}_k^\dagger &= i\sqrt{2}\lambda_k\mathcal{D}_k^\dagger\int_0^1 \mathrm{d}s\, e^{-is\sqrt{2}\lambda p_k}\dot{p}_k(t)e^{is\sqrt{2}\lambda_k p_k} \\ &= -2\sqrt{2}i\Gamma_k\lambda_k\mathcal{D}_k^\dagger p_k - i\sqrt{2}\lambda_k\nu_k\mathcal{D}_k^\dagger q_k + i\nu_k\lambda_k^2\mathcal{D}_k^\dagger + 2i\nu_k\lambda_k^2\mathcal{D}_k^\dagger\sigma^\dagger\sigma + \sqrt{2}i\lambda_k\mathcal{D}_k^\dagger\xi_k,\end{aligned} \tag{3.4}$$

where special attention has to be paid to the rules for taking the time derivative of an exponential operator $e^{A(t)}$ with $[\dot{A}(t), A(t)] \neq 0$ [131, 132]. We obtain in total

$$\dot{\tilde{\sigma}} = -\left[\gamma - i(\omega_\ell - \omega_0)\right]\tilde{\sigma} - 2i\sum_k\sqrt{2}\lambda_k\Gamma_k p_k\tilde{\sigma} + \eta_\ell\mathcal{D}^\dagger + \sqrt{2\gamma}\tilde{\sigma}_{\rm in} + i\sum_k\sqrt{2}\lambda_k\xi_k\tilde{\sigma}. \tag{3.5}$$

The equation is derived under the assumption of weak driving $\eta_\ell \ll \gamma$ and therefore small occupancy of the electronic excited state $\langle \sigma^\dagger \sigma \rangle \ll 1$. Moreover, the second and last term on the right hand side of the above equation do not contribute to the dynamics and effectively cancel out which can be seen by an average over the vibrations

$$-2i\sqrt{2}\Gamma_k \lambda_k \sigma \langle p_k \mathcal{D}_k^\dagger \rangle + i\sqrt{2}\lambda_k \sigma \langle \xi_k \mathcal{D}_k^\dagger \rangle = 0, \tag{3.6}$$

where we used that $\langle p_k \mathcal{D}_k^\dagger \rangle = \frac{1}{i\sqrt{2}} \frac{\mathrm{d}}{\mathrm{d}\lambda_k} \langle \mathcal{D}_k^\dagger \rangle$ and furthermore one obtains $\langle \xi_k \mathcal{D}_k^\dagger \rangle = i\sqrt{2}\Gamma_k \lambda_k e^{-\lambda_k^2/2}$ by application of the Isserlis' theorem and with relation $\langle \xi_k(t) p_k(t) \rangle = \Gamma_k$. An extremely simple equation for the polaron operator is now obtained

$$\dot{\tilde{\sigma}} = -[\gamma - i(\omega_\ell - \omega_0)]\tilde{\sigma} + \sqrt{2\gamma}\tilde{\Sigma}_{\mathrm{in}}. \tag{3.7}$$

Here we have combined the input fields affecting the electronic transition (drive plus noise) into the expression $\Sigma_{\mathrm{in}} = \eta_\ell/\sqrt{2\gamma} + \sigma_{\mathrm{in}}$ and the displaced input field is $\tilde{\Sigma}_{\mathrm{in}} = \Sigma_{\mathrm{in}} \mathcal{D}^\dagger$. A solution of the bare electronic dipole operator can then be obtained by a formal integration as a sum between transient and steady state solutions

$$\sigma(t) = \sigma(0)\mathcal{D}(t)\mathcal{D}^\dagger(0) e^{-(\gamma - i\Delta_\ell)t} + \sqrt{2\gamma} \int_0^t \mathrm{d}t' e^{-(\gamma - i\Delta_\ell)(t-t')} \Sigma_{\mathrm{in}}(t') \mathcal{D}(t) \mathcal{D}^\dagger(t'), \tag{3.8}$$

with the laser detuning $\Delta_\ell = \omega_\ell - \omega_0$. The above expression describes the time evolution of the transition dipole operator in the presence of vibrations. In principle, the expression allows for the derivation of any system property in the transient regime as well as in steady state. To derive the optical response of the electronic degree of freedom in the presence of its coupling to vibrations one then has to evaluate two-time correlation functions of the displacement operator. This is factorizable as we consider that all vibrational modes are independent from each other, i.e., $\langle \mathcal{D}(t)\mathcal{D}^\dagger(t') \rangle = \prod_k \langle \mathcal{D}_k(t) \mathcal{D}_k^\dagger(t') \rangle$. By expanding the displacement operators and applying the Isserlis' theorem (or Wick's probability theorem for multivariate normal distributions), one obtains

$$\langle \mathcal{D}_k(t) \mathcal{D}_k^\dagger(t') \rangle = \langle e^{-i\sqrt{2}\lambda_k p_k(t)} e^{i\sqrt{2}\lambda_k p_k(t')} \rangle = e^{-2\lambda_k^2 (\langle p_k^2 \rangle - \langle p_k(t) p_k(t') \rangle)}, \tag{3.9}$$

where we made use of the fact that the momentum variance is stationary, i.e., $\langle p_k^2 \rangle = \langle p_k(t)^2 \rangle$. This can be easily computed by using the properties for the Brownian noise model (see section 2.4.d)

$$\langle p_k(t) p_k(t') \rangle = \left[ \left( \bar{n}_k + \frac{1}{2} \right) \cos(\nu_k \tau) - \frac{i}{2} \sin(\nu_k \tau) \right] e^{-\Gamma_k \tau}, \tag{3.10}$$

with $\tau = t - t'$. While expressions can be derived for any temperature of the bath, in the following we will, for the sake of simplicity, focus on the zero temperature case for all vibrational modes. This is

typically a very good approximation as molecular vibrations lie in the range of THz frequencies and are therefore barely occupied as the condition $\hbar\nu_k \ll k_B T$ is typically fulfilled. The displacement correlation function in this case simplifies to

$$\langle \mathcal{D}_k(t)\mathcal{D}_k^\dagger(t')\rangle = e^{-\lambda_k^2} e^{\lambda_k^2 \exp[-(\Gamma_k + i\nu_k)\tau]}, \tag{3.11}$$

which we will make use of in section 3.2 to derive analytical expressions for absorption and emission lines and linewidths.

From the Holstein Hamiltonian, one can further more estimate the power spectrum of the force acting on the excited state electronic orbital by defining the Hermitian force $F = -\lambda\nu(b^\dagger + b)$

$$J(\omega) = 2\Re\left\{\int_0^\infty \mathrm{d}\tau\, e^{i\omega\tau}\,\langle F(\tau)F(0)\rangle\right\}. \tag{3.12}$$

Since the position correlations are given by (at zero temperature)

$$\langle q(t)q(t')\rangle = \frac{1}{2} e^{-(\Gamma + i\nu)(t-t')}, \tag{3.13}$$

this leads to a spectrum of the force acting on the excited electronic orbital

$$J(\omega) = 2\lambda^2\nu^2\Re\left\{\frac{1}{\Gamma + i(\omega-\nu)}\right\} = \frac{2\lambda^2\nu^2\Gamma}{\Gamma^2 + (\omega-\nu)^2}. \tag{3.14}$$

For many vibrational modes, the total power spectrum is then simply given as a sum over Lorentzians with coupling strengths $\lambda_k$ and decay rates $\Gamma_k$, positioned at frequencies $\nu_k$ (as illustrated in Fig. 3.1(a)).

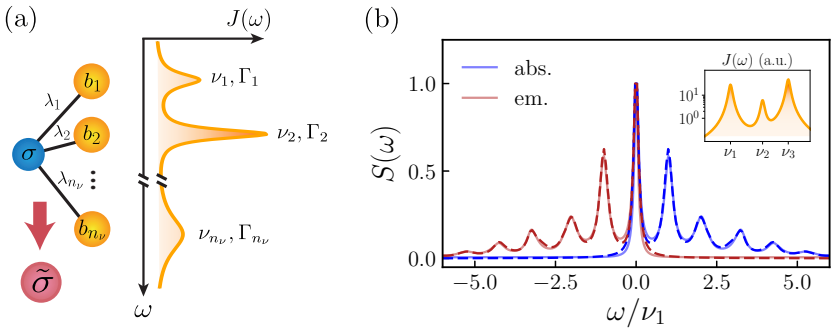


Figure 3.1: *Illustration of the method.* (a) A molecule is "constructed" by coupling of an electronic transition operator $\sigma$ to $n_\nu$ vibrations $b_k$ with frequencies, linewidths and strengths dictated by the spectral density function $J(\omega)$. The polaron operator $\tilde{\sigma}$ then contains all of the information about the system. (c) Absorption and emission spectrum (normalized) for a toy-model molecule with 3 vibrational modes (spectral density shown in inset) plotted in a frame rotating at the laser frequency. Solid lines show numerical master equation results, dashed lines are the analytical results. Parameters: $\{\lambda_1, \lambda_2, \lambda_3\} = \{1, 0.2, 0.4\}$, $\{\nu_1, \nu_2, \nu_3\} = \{1, 2.25, 3.25\} \cdot 10^3\gamma$ and $\Gamma = 70\gamma$ for all vibrational modes.

## 3.2 Emission and absorption

The absorption and emission spectra of a driven molecule can be readily obtained from Eq. (3.8). Considering large times $t \gg 1/\gamma$, the first term in Eq. (3.8) goes towards zero and the average dipole moment can be expressed as (taking the average over both electronic and vibrational degrees of freedom)

$$\langle \sigma(t) \rangle = \eta_\ell \int_0^t \mathrm{d}t' e^{-(\gamma - i\Delta_\ell)(t-t')} \langle \mathcal{D}(t)\mathcal{D}^\dagger(t') \rangle \,. \tag{3.15}$$

The population of the electronic excited state evolves according to

$$\frac{\mathrm{d}}{\mathrm{d}t} \langle \sigma^\dagger \sigma \rangle = -2\gamma \langle \sigma^\dagger \sigma \rangle + 2\eta_\ell \Re \langle \sigma(t) \rangle \,, \tag{3.16}$$

implying that the steady state absorption profile can be directly computed from the expectation value of the real part of the coherence $\langle \sigma(t) \rangle$. We define the excited state population $S_{\mathrm{abs}}(\Delta_\ell) := \langle \sigma^\dagger \sigma \rangle$ as the absorption profile for a varying laser frequency with expression

$$S_{\mathrm{abs}}(\Delta_\ell) = 2\eta_\ell \int_{-\infty}^t \mathrm{d}t' e^{-2\gamma(t-t')} \Re \langle \sigma(t') \rangle \,. \tag{3.17}$$

To evaluate this integral, we expand the displacement correlation function from Eq. (3.11) in a power series

$$\langle \mathcal{D}_k(t)\mathcal{D}_k^\dagger(t') \rangle = e^{-\lambda_k^2} \sum_{m_k=0}^{\infty} \frac{\lambda_k^{2m_k}}{m_k!} e^{-m_k(\Gamma_k + i\nu_k)(t-t')}. \tag{3.18}$$

The absorption spectrum can then be readily expressed as a sum over all indices $\{m_k\} = m_1, \ldots, m_{n_\nu}$ weighted by the Franck-Condon factors $s_{m_k}^{\lambda_k}$

$$S_{\mathrm{abs}}(\Delta_\ell) = \frac{\eta_\ell^2}{\gamma} \sum_{\{m_k\}=0}^{\infty} \frac{s_{\lambda_1}^{m_1} \ldots s_{\lambda_{n_\nu}}^{m_{n_\nu}} \left[\gamma + \Gamma_{\{m_k\}}\right]}{\left[\gamma + \Gamma_{\{m_k\}}\right]^2 + \left[\Delta_\ell - \nu_{\{m_k\}}\right]^2}, \tag{3.19}$$

where the denominator indicates a series of blue-shifted absorption sidebands with increased linewidths $\Gamma_{\{m_k\}} = \sum_{\{m_k\}} m_k \Gamma_k$ at positions $\omega_\ell = \omega_0 + \sum_k \nu_{\{m_k\}}$ with $\nu_{\{m_k\}} = \sum_{\{m_k\}} m_k \nu_k$. The two-level system limit is immediately recovered by setting all $\lambda_k = 0$ which gives the expected simple Lorentzian $S_{\mathrm{abs}}(\Delta_\ell) = \eta_\ell^2/(\gamma^2 + \Delta_\ell^2)$.

For the definition of the emission spectrum one can consider the transient dynamics of a molecule which is partially excited at time $t = 0$: $\langle \sigma^\dagger \sigma(0) \rangle = \mathcal{P}_0$. The emission spectrum is then defined as the Fourier transform [74]

$$S_{\mathrm{em}}(\omega) = 2\Re \int_0^\infty \mathrm{d}\tau \langle \mathcal{T}\{\sigma^\dagger(\tau)\sigma(0)\} \rangle \, e^{-i\omega\tau}, \tag{3.20}$$

where $\mathcal{T}$ denotes time ordering

$$\langle \mathcal{T}\{\sigma^\dagger(\tau)\sigma(0)\}\rangle = \mathcal{P}_0 \langle \mathcal{D}^\dagger(\tau)\mathcal{D}(0)\rangle e^{-(\gamma - i\omega_0)\tau} = \mathcal{P}_0 \prod_{k=1}^{n_\nu} \sum_{m_k} s_{\lambda_k}^{m_k} e^{-(\gamma + m_k\Gamma_k - i(\omega_0 - \nu_k))\tau}. \quad (3.21)$$

The emission spectrum then can be computed as (normalized by $\mathcal{P}_0$)

$$S_{\mathrm{em}}(\omega) = \sum_{\{m_k\}=0}^{\infty} \frac{2 s_{\lambda_1}^{m_1} \dots s_{\lambda_{n_\nu}}^{m_{n_\nu}} \left[\gamma + \Gamma_{\{m_k\}}\right]}{\left[\gamma + \Gamma_{\{m_k\}}\right]^2 + \left[\omega - \omega_0 + \nu_{\{m_k\}}\right]^2}. \quad (3.22)$$

The denominator indicates a series of red-shifted Stokes lines at frequencies $\omega = \omega_0 - \nu_{\{m_k\}}$. The branching ratio of the molecule, i.e., the ratio of the emission into the zero-phonon line $|e,0\rangle \to |g,0\rangle$ versus all other lines is given as the Franck-Condon factor $f_{\mathrm{FC}} = \langle \mathcal{D}^\dagger \rangle^2 = e^{-\sum_k \lambda_k^2}$. Fig. 3.1(b) shows an example of emission and absorption for a toy-model molecule with three vibrational modes. We note that generally, for driven molecules in steady state, the evaluation of the emission spectrum is more cumbersome as it involves the evaluation of four-point correlation functions [1].

## 3.3 Thermal effects

Let us briefly discuss how finite thermal occupation of the vibrational modes would affect the results derived previously. We will discuss this in more detail in chapter 5 where we consider coupling to a thermal bath of surrounding phonons. The displacement correlation function in a thermal state can be estimated by means of Eq. (3.10) (just considering a single vibrational mode)

$$\langle \mathcal{D}(t)\mathcal{D}^\dagger(t')\rangle_{\mathrm{th}} = f_{\mathrm{FC}} \cdot e^{\lambda^2[(2\bar{n}+1)\cos(\nu\tau) - i\sin(\nu\tau)]e^{-\Gamma\tau}}, \quad (3.23)$$

with the generalized Franck-Condon factor $f_{\mathrm{FC}} = \langle \mathcal{D} \rangle_{\mathrm{th}}^2 = e^{-\lambda^2(1+2\bar{n})}$. Evaluating the integral Eq. (3.15) yields the absorption spectrum

$$S_{\mathrm{abs}}(\Delta_\ell) = \frac{\eta_\ell^2}{\gamma} \sum_{n=0}^{\infty} \sum_{\ell=0}^{n} \frac{L(n)B(n,\ell)(\gamma + n\Gamma)}{(\gamma + n\Gamma)^2 + [\Delta_\ell - (n-2\ell)\nu]^2}, \quad (3.24)$$

where we defined $L(n) = f_{\mathrm{FC}}\lambda^{2n}/n!$ and $B(n,\ell) = \binom{n}{\ell}(\bar{n}+1)^{n-\ell}\bar{n}^\ell$. As one can see from the expression above, non-zero occupation additionally leads to red-shifted lines in absorption described by the index $\ell$ and weighted by the binomial distribution. In the limit $2\lambda^2\sqrt{\bar{n}(\bar{n}+1)} \ll 1$, the integral of the correlation function can be expressed in terms of *modified* Bessel functions of the first kind $I_n(x)$ (using that the generating function of the modified Bessel functions is given by $e^{\frac{1}{2}x(a+1/a)} =$

$\sum_{n=-\infty}^{\infty} I_n(x)a^n$). The absorption spectrum can then be expressed as a sum over just a single index

$$S(\Delta_\ell) = \frac{\eta_\ell^2}{\gamma} \sum_{n=-\infty}^{\infty} \frac{f_{\mathrm{FC}} \left(\frac{\bar{n}+1}{\bar{n}}\right)^{\frac{n}{2}} I_n(2\lambda^2\bar{N})(\gamma + |n|\Gamma)}{(\gamma + |n|\Gamma)^2 + (\Delta_\ell - n\nu)^2}, \tag{3.25}$$

with $\bar{N} = \sqrt{\bar{n}(\bar{n}+1)}$. The above result is similar to the result known from standard Huang-Rhys theory, however additionally includes vibrational relaxation [133].

## 3.4 Förster resonance energy transfer

Let us provide a first illustration of the usefulness of the PLE method by applying it to the process of Förster resonance energy transfer, i.e., dipole-dipole mediated energy transfer between two molecules. FRET is the main excitation transfer mechanism in photosynthetic light harvesting complexes, where energy is transfered with high efficiency from a light-harvesting antenna through a network of chromophores to a reaction centre [134, 135], and is also of great importance for many applications in biological and chemical technologies [136]. Generally speaking, the requirement for FRET is a spectral overlap between the emission profile of the donor molecule and the absorption profile of the acceptor, giving rise to a resonant transfer process typically accompanied by quick vibrational relaxation [137]. One distinguishes between the Förster regime, where the dipole-dipole coupling may be treated perturbatively and the Redfield regime where the coherent coupling dominates and population can oscillate many times between donor and acceptor.

Here we exemplify the application of the PLE method to derive a perturbative expression for the FRET rate between two dipole-coupled molecules $D$ and $A$ described by $\mathcal{H}_{\mathrm{dd}} = \Omega(\sigma_D^\dagger \sigma_A + \mathrm{h.c.})$ with an energy mismatch in the electronic transition frequencies $\Delta = \omega_D - \omega_A$, first by considering a simple configuration where each molecule has a single vibrational mode $b_D$ and $b_A$ (with corresponding vibrational frequencies $\nu_D$ and $\nu_A$ and Huang-Rhys factors $\lambda_D^2$ and $\lambda_A^2$). We will assume an initially excited donor molecule which can undergo a resonant exchange with the acceptor's excited state vibrational manifold. A unidirectional process emerges as the acceptor quickly relaxes to its vibrational ground state $\Gamma_D \gg \Omega$. We start with the QLEs for the polaron operators $\tilde{\sigma}_D = \sigma_D \mathcal{D}_D^\dagger$ and $\tilde{\sigma}_A = \sigma_A \mathcal{D}_A^\dagger$ with the displacement operators $\mathcal{D}_D = e^{\lambda_D(b_D^\dagger - b_D)}$ and $\mathcal{D}_A = e^{\lambda_A(b_A^\dagger - b_A)}$ which show coherent coupling induced by the dipole-dipole interaction

$$\dot{\tilde{\sigma}}_D = -(\gamma_D + i\omega_D)\,\tilde{\sigma}_D - i\Omega\tilde{\sigma}_A \mathcal{D}_A \mathcal{D}_D^\dagger + \sqrt{2\gamma}\tilde{\sigma}_{\mathrm{in},D}, \tag{3.26a}$$

$$\dot{\tilde{\sigma}}_A = -(\gamma_A + i\omega_A)\,\tilde{\sigma}_A - i\Omega\tilde{\sigma}_D \mathcal{D}_D \mathcal{D}_A^\dagger + \sqrt{2\gamma}\tilde{\sigma}_{\mathrm{in},A}. \tag{3.26b}$$

The above equations show that the coherent electronic coupling $\Omega$ is modified by the presence of the vibrations via the displacement operators. To derive a perturbative expression for the energy transfer rate, we consider a scenario with an initial full excitation of $D$ and no excitation of $A$. Then from above

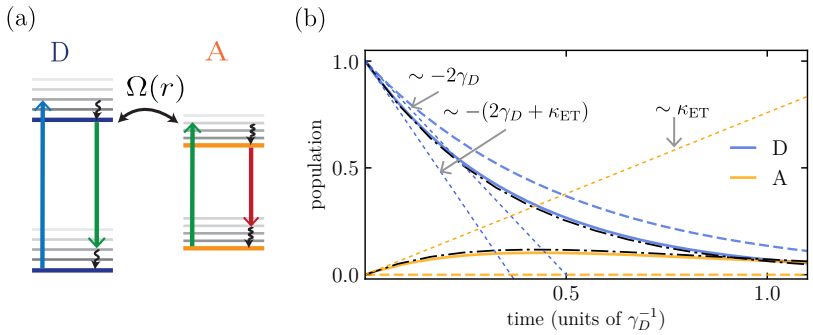


Figure 3.2: *FRET process.* (a) Unidirectional near-field FRET processes showing donor excitation (blue) followed by vibrational relaxation, resonant energy exchanges (green) and acceptor emission (red). (b) Solution of the rate equations for time dynamics of the D-A system with (full lines) and without dipole-dipole coupling (dashed lines) in a pump-probe scenario. The tangents (dotted lines) show that the independent radiative emission of the donor at rate $2\gamma_D$ is accelerated by the energy transfer rate $\kappa_{\mathrm{ET}}$ while the initial population increase of the acceptor is governed by the same quantity $\kappa_{\mathrm{ET}}$. Agreement with numerical simulations is indicated by the dashed-dotted curves with parameters $\gamma_A = \gamma_D = \gamma$, $\Omega(r) = 15\gamma$, $\Delta = 500\gamma$, $\nu_A = \nu_D = 250\gamma$, $\Gamma_A = \Gamma_D = 30\gamma$, $\lambda_D = 0.6$, $\lambda_A = 0.4$.

one can derive an equation of motion for the acceptor's population

$$\dot{\mathcal{P}}_A = -2\gamma_A \mathcal{P}_A + 2\Omega \Im \langle \sigma_A^\dagger \sigma_D \rangle + \sqrt{2\gamma_A} \langle \sigma_A^\dagger \sigma_{\mathrm{in},D} + \sigma_{\mathrm{in},A}^\dagger \sigma_A \rangle , \tag{3.27}$$

which shows how the imaginary part of the two-particle correlation $\langle \sigma_A^\dagger \sigma_D \rangle$ appears as a source terms for the acceptor population. The procedure to compute $2\Omega \Im \langle \sigma_A^\dagger \sigma_D \rangle$ involves then formal integration of the equation of motion for the acceptor polaron operator (as detailed in the Appendix B) under the assumption that $\Gamma_D, \Gamma_A \gg \gamma_D, \gamma_A$. Finally, one arrives at an expression for the energy transfer rate showing proportionality to the donor population $2\Omega \langle \sigma_A^\dagger \sigma_D \rangle = \kappa_{\mathrm{ET}} \mathcal{P}_D(t)$

$$\kappa_{\mathrm{ET}} = \sum_{n_D, n_A} \frac{2\Omega^2 s_{\lambda_D}^{n_D} s_{\lambda_A}^{n_A} (n_D \Gamma_D + n_A \Gamma_A)}{(n_D \Gamma_D + n_A \Gamma_A)^2 + [\Delta - n_D \nu_D - n_A \nu_A]^2} , \tag{3.28}$$

scaling with $\Omega(d)^2 \propto 1/d^6$. The denominator of the above expression asks that the resonance condition $\omega_D - n_D \nu_D = \omega_A + n_A \nu_A$ is fulfilled, i.e., fluorescence lines of the donor $|e_D, 0\rangle \to |g_D, n_D\rangle$ have to overlap with absorption lines of the acceptor $|g_A, 0\rangle \to |e_A, n_A\rangle$, both of which are weighted by the respective Franck-Condon factors. Agreement between the rate derived above and numerical simulations is shown in Fig. 3.2(b) which shows that the donor population decays at an accelerated rate due to the transfer process.

In the case of many vibrational modes $n_\nu$ for donor and acceptor, we can generalize the result by writing general displacements $\mathcal{D}_A = \prod_{k=1}^{n_\nu} \mathcal{D}_A^k$ and $\mathcal{D}_D = \prod_{k=1}^{n_\nu} \mathcal{D}_D^k$ for all vibrational modes. The rate is computed by assuming multiple paths of energy transfer between the two molecules involving all vibrational modes. We assume an initially electronically excited state with no vibrations present

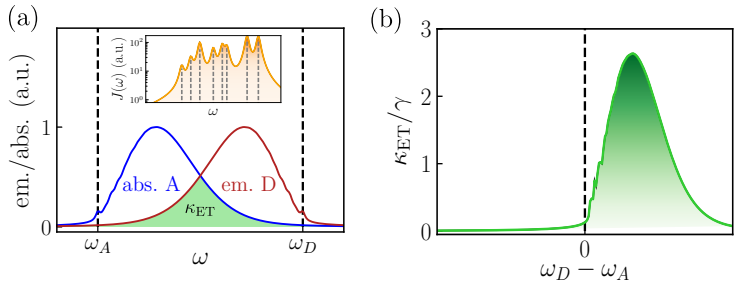


Figure 3.3: *FRET process for many vibrational modes.* (a) Absorption and emission spectra for donor-acceptor pair with 8 vibrational modes (power spectrum $J(\omega)$ shown in inset). The spectral overlap between D and A gives rise to an incoherent rate $\kappa_{\rm ET}$ from $D$ to $A$. (b) Plot of $\kappa_{\rm ET}$ as a function of frequency mismatch $\omega_D - \omega_A$ for the same spectral density as in (a) and $\Omega = 60\gamma$.

$|e_D; 0_1, 0_2 ... 0_{n_v}\rangle$ of molecule $D$ and ground state without vibrations $|g_A; 0_1, 0_2 ... 0_{n_v}\rangle$ for molecule $A$. The emission of molecule $D$ leads it into state $|g_D; m_1, ... m_k, ... m_{n_v}\rangle$ and resonant interactions can occur with state $|e_A; l_1, ... l_{k'}, ... l_{n_v}\rangle$ of molecule $A$. Summing over all these processes leads to an expression for $\kappa_{\rm ET}$ (listed in Appendix B) seen simply as a generalization of the energy transfer rate from above. This is illustrated in Fig. 3.3(a) for a donor-acceptor pair with 8 vibrational modes. In Fig. 3.3(b) we plot the corresponding energy transfer rate as a function of the detuning between donor and acceptor $\Delta = \omega_D - \omega_A$, revealing a unidirectional flow of energy from $D$ to $A$ dictated by the sign of the detuning.

## 3.5 Remarks

The polaron Langevin equation provides an intuitive description of the time evolution of a molecular system, namely as a vibrationally-dressed electronic dipole. We have shown in this chapter how the PLE accounts for molecular emission and absorption spectra and how it can be used to perturbatively describe the FRET process between two near-field coupled molecules. We will extend the method in the following two chapters to infrared-driven vibrational modes, molecules in phononic host environments and cavity-coupled molecules. We remark here that, in addition to displacement of the electronic excited state, the method can also be extended to account for different curvatures of the potential energy surfaces in ground and excited state as discussed in section 2.3.b in which case the electronic dipole operator would have to be augmented by both a displacement and a squeezing operator $\tilde{\sigma} = \sigma \mathcal{D}^\dagger \mathcal{S}^\dagger$. However, the method also has some limitations: For two or more molecules coupled to each other and each coupled to their own vibrational bath, the diagonalization of the resulting set of equations is generally not straightforward as it involves time-ordering of displacement operators which is cumbersome. This can be circumvented in two ways: either by tracing over the vibrational degrees of freedom in the polaron picture to obtain an effective, reduced description or by moving into a collective basis for both electronic and vibrational operators, as we will discuss in chapter 6.

# 4

# Infrared-dressed molecules

Over recent years Floquet engineering, i.e., the coherent manipulation of quantum systems by means of (strong) periodic driving has been used to enable controlled engineering of matter states, from the single to the many-body level [138, 139]. In particular, more recently, the coherent excitation of phononic modes has been shown as a possibility to modify the properties of materials by steering them into non-equilibrium states. This includes dynamical control of electron-phonon coupling [140, 141] and superconductivity [142–144], topological phase transitions [145], and the control of real or synthetic magnetic fields [146–149]. Some of the experimental techniques rely on the excitation of phonon modes through acoustic modulation. Alternatively, the coupling to infrared-active vibrational modes provides another way to drive and modulate vibrational degrees of freedom.

We consider here the case of *infrared-dressed* molecules, where the vibronic coupling is modified by periodic driving of vibrational modes, either directly or indirectly via a cavity mode. The immediate effect is the modification of the standard Franck-Condon physics as the transition matrix elements for optical absorption from electronic ground to excited state are largely impacted by the coherent infrared drive. The main mechanism is the competition between coherent processes, such as the simultaneous absorption of probe and drive photons and the standard path of direct optical photon absorption.

A remarkable result is the strong modification of vibronic sidebands which, under external infrared driving, can exhibit both enhanced amplitudes and reduced linewidths. The improved lifetime stems from a competition between vibrational relaxation and gain from coherent optical and vibrational processes even under weak vibrational excitation. The embedding within an infrared, cavity-confined electromagnetic mode brings an enhancement of the interaction by a factor proportional to the cavity finesse. Moreover, an infrared cooling effect can increase the vibrational relaxation in a wide bandwidth, thus effectively reducing undesired scattering. This can be understood as a cavity Purcell effect at the level of the vibrational relaxation damping rate.

We start this chapter by introducing the model of the infrared-dressed molecule in section 4.1. In section 4.2 we show, purely at the Hamiltonian level, how periodic driving of a vibrational mode modifies the absorption by generating new optical transitions – the so-called Floquet states. We then make use of the polaron Langevin equation method to compute the absorption spectrum of the infrared-

dressed molecule in section 4.3. Finally, we generalize the method to cavity-coupled, indirectly driven molecules in section 4.4.

## 4.1 Model

An external infrared field $\mathcal{E}(q,t)$ can couple to the molecular vibrations via a dipole operator depending on the nuclear displacement $d(q)$. In the dipole approximation $\mathcal{E}(q,t) \approx \mathcal{E}(t)$, the Hamiltonian describing the coupling is given by

$$\mathcal{H}_{\mathrm{IR}}(t) = -d(q) \cdot \mathcal{E}(t). \tag{4.1}$$

A first order Taylor expansion around the equilibrium positions of the nuclei (subscript "0"); $\langle d(q)\rangle = \langle d\rangle_0 + (\partial \langle d(q)\rangle / \partial q)_0 \, q$ then gives rise to a coupling between the nuclear displacement and the electric field. Commonly used experimental modes with large $(\partial \langle d\rangle / \partial q)_0$ are e.g. carbonyl (C=O) bonds with frequencies typically around 50 THz [150]. To engineer an *infrared-dressed* molecule, we consider a strong classical drive of the molecular vibrational mode with amplitude $\eta_d$ and frequency $\omega_d$ expressed in Hamiltonian form as

$$\mathcal{H}_d = \eta_d \cos(\omega_d t)(b^\dagger + b). \tag{4.2}$$

Simultaneously, we consider a weak optical field probing the electronic transition at some variable laser frequency $\omega_p$ and small amplitude $\eta_p$ modeled as a standard drive Hamiltonian $\mathcal{H}_p = i\eta_p(\sigma^\dagger e^{-i\omega_p t} - \sigma e^{i\omega_p t})$ such that the total Hamiltonian expresses as $\mathcal{H}_{\mathrm{mol}} + \mathcal{H}_d + \mathcal{H}_p$.
Additionally to the dissipative processes considered previously (spontaneous emission and vibrational relaxation), we also include pure dephasing of the electronic transition (i.e., decay of the electronic coherences) with rate $\gamma_\phi = \gamma_\phi(T)$. As we will discuss in some more detail in chapter 5, this is a term originating from quadratic electron-phonon coupling to the surrounding host and can be included by the Lindblad term $\mathcal{L}^{\gamma_\phi}_{\sigma^\dagger\sigma}[\rho]$ with collapse operator $\sigma^\dagger\sigma$. This is a strongly temperature-dependent term ($\propto T^2$ at low temperatures) which is close to zero at cryogenic temperatures ($T \leq 4\,\mathrm{K}$) [124, 151]. The coherent and dissipative processes are illustrated in Fig. 4.1(a).

## 4.2 Floquet states and transition strengths

To gain some intuition into how the periodic driving affects the optical transition, we first go into the polaron-displaced basis which diagonalizes the Holstein Hamiltonian and leads to a transformed probe Hamiltonian $\tilde{\mathcal{H}}_p = i\eta_p(\sigma^\dagger \mathcal{D}^\dagger e^{-i\omega_p t} - \sigma \mathcal{D} e^{i\omega_p t})$. The drive Hamiltonian in the polaron picture

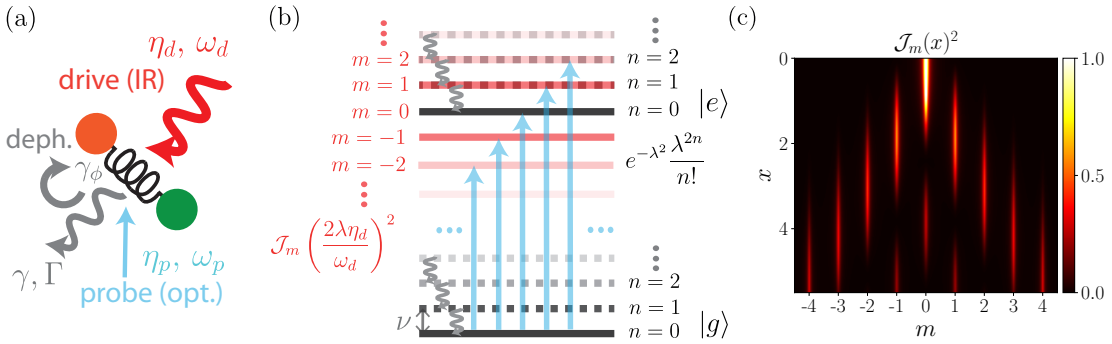


Figure 4.1: *Floquet quasienergies & transitions.* (a) An infrared-active nuclear coordinate that can be imagined as the vibration of a diatomic molecule is driven with amplitude $\eta_d$ and frequency $\omega_d$. Simultaneously, the optical transition is probed by a weak field with amplitude $\eta_p$ and frequency $\omega_p$. The molecule is embedded in a dephasive environment leading to a temperature-dependent broadening with rate $\gamma_\phi$. Additional losses are radiative emission ($\gamma$) and vibrational relaxation ($\Gamma$). (b) Quasienergy scheme of an infrared-dressed molecule in the case of $\omega_d = \nu$. Additionally to the usual vibronic sidebands (grey dashed lines) with transition strengths given by a Poissonian distribution $e^{-\lambda^2}\lambda^{2n}/n!$, one obtains a set of driving-induced quasienergies at $\omega_0 + m\omega_d$ with transition strengths proportional to Bessel functions squared $\mathcal{J}_m\left(2\lambda\eta_d/\omega_d\right)^2$. Vibrational relaxation is indicated by wavy lines. (c) Bessel functions $\mathcal{J}_m(x)^2$ determining the intensities of the driving-induced sidebands.

becomes

$$\tilde{\mathcal{H}}_d = \eta_d \cos(\omega_d t)(b^\dagger + b + 2\lambda\sigma^\dagger\sigma). \tag{4.3}$$

Therefore, the effect on the electronic transition is a periodic modulation of the excited state energy with $\tilde{\omega}_0(t) = \omega_0 + 2\lambda\eta_d\cos(\omega_d t)$. Let us now additionally perform a transformation into an interaction picture with the following unitary operator

$$\mathcal{U}_{\text{int}} = e^{i\sigma^\dagger\sigma\int_0^t \mathrm{d}t'\,\tilde{\omega}_0(t') + i\nu b^\dagger b t}. \tag{4.4}$$

Moreover, we also expand the displacement operator $\mathcal{D}^\dagger$ in terms of annihilation and creation operators by means of the Baker–Campbell–Hausdorff identity in order to reveal the fundamental processes involved in the absorption and emission of optical photons. We also introduce $\mathcal{J}_m(x)$ as Bessel functions of the first kind and the probe beam detuning $\Delta_p = \omega_p - \omega_0$. We can then find the following expression for the probe Hamiltonian in the displaced interaction picture

$$\tilde{\mathcal{H}}_p^{\text{int}} = i\eta_p e^{-\lambda^2/2}\left(\sigma^\dagger\sum_{k,\ell=0}^{\infty}\frac{(-\lambda)^k\lambda^\ell}{\ell!\,k!}\left(b^\dagger e^{i\nu t}\right)^k\left(be^{-i\nu t}\right)^\ell\sum_{m=-\infty}^{\infty}\mathcal{J}_m\left(\frac{2\lambda\eta_d}{\omega_d}\right)e^{im\omega_d t}e^{-i\Delta_p t} - \text{h.c.}\right). \tag{4.5}$$

Additionally, one is still left with a transformed term $\tilde{\mathcal{H}}_d^{\text{int}} = \eta_d\cos(\omega_d t)(b^\dagger e^{i\nu t} + be^{-i\nu t})$ which can drive transitions between vibrational states and becomes very important for $\omega_d \approx \nu$. Let us first un-

derstand the above expression on the simplified case of $\eta_d = 0$ where we expect the usual selection rules for Franck-Condon physics. In this case, only the term with $m = 0$ contributes and operator combinations of the kind $\sigma^\dagger (b^\dagger)^k b^\ell$ have time dependence $e^{-i[\Delta_p - (k-\ell)\nu]t}$. Imposing resonance allows to find the transition strength for different processes. For example, the transition from $|g,0\rangle$ to $|e,n\rangle$ can only be achieved by $k = n$ and $\ell = 0$. The resonance condition then asks that the laser frequency is $\omega_p = \omega_0 + n\nu$ and the strength is proportional to $e^{-\lambda^2/2}\lambda^n/\sqrt{n!}$ as expected.
For $\eta_d \neq 0$, the driving induces a set of additional resonances at $\omega_p = \omega_0 + m\omega_d$ where $m = 0, \pm 1, \pm 2, \ldots$. In the vicinity of these resonances, the Hamiltonian in Eq. (4.5) can be transformed back into a time-independent frame for a given $m$

$$\tilde{\mathcal{H}}_m = -(\Delta_p - m\omega_d)\sigma^\dagger\sigma + \nu b^\dagger b + i\eta_p \left( \sigma^\dagger \mathcal{D}^\dagger \mathcal{J}_m \left( \frac{2\lambda\eta_d}{\omega_d} \right) - \text{h.c.} \right), \tag{4.6}$$

where the driving-induced Floquet quasienergies of the electronic excited state are at $\omega_0 + m\omega_d$. In the Jablonski scheme in Fig 4.1(b) we illustrate the energy levels and corresponding transitions for resonant driving $\omega_d = \nu$. In this case, some of the Floquet states $|e,m\rangle$ become degenerate to the vibrational states $|e,n\rangle$ ($m \geq 0$). The selection rules for the transition probabilities $P_{\text{abs}}(n)$ from ground to excited state are then given by $\ell = 0, n = k + m$ and the transition probability can be summed up to

$$P_{\text{abs}}(n) = e^{-\lambda^2} \sum_{m=-\infty}^{n} \frac{\lambda^{2(n-m)}}{(n-m)!} \mathcal{J}_m \left( \frac{2\lambda\eta_d}{\omega_d} \right)^2. \tag{4.7}$$

In the Floquet picture, each of the above terms corresponds to the absorption of a photon from the ground state $|g,0\rangle$ to $|e,n-m\rangle$ ($m \in [-\infty, n]$) in combination with the simultaneous dressing by $|m|$ infrared photons. The term corresponding to $n = m$ in the above sum with probability $e^{-\lambda^2}\mathcal{J}_n(2\lambda\eta_d/\omega_d)^2$ describes a transition on the zero-phonon line (or 'zero-vibron line') in combination with the absorption of $n$ infrared photons. In the following sections we will show that this term can become dominant and can be used to modify the vibronic linewidths and coherences since the zero-phonon line is not affected by vibrational relaxation $\Gamma$.

## 4.3 Langevin equations of motion

In a frame rotating at the probe frequency $\omega_p$, under the assumption of weak probe fields $\eta_p \ll \gamma$ and therefore $\langle \sigma^\dagger\sigma \rangle \ll 1$, the simplified quantum Langevin equations of motion for the mechanical

degrees of freedom $\{q, p\}$ as well as for the polaron operator $\tilde{\sigma}$ are given by

$$\dot{q} = \nu p, \tag{4.8a}$$

$$\dot{p} = -2\Gamma p - \nu q - \sqrt{2}\eta_d \cos(\omega_d t) + \xi, \tag{4.8b}$$

$$\dot{\tilde{\sigma}} = -(\tilde{\gamma} - i\Delta_p)\tilde{\sigma} - 2i\lambda\eta_d \cos(\omega_d t)\tilde{\sigma} + \tilde{\Sigma}_{\text{in}}, \tag{4.8c}$$

where $\tilde{\gamma} = \gamma + \gamma_\phi$. Here, we defined the input affecting the electronic transition as

$$\tilde{\Sigma}_{\text{in}} = \left[\eta_p + \sqrt{2\gamma}\sigma_{\text{in}} + \sqrt{2\gamma_\phi}\left((\sigma^\dagger\sigma)_{\text{in}}\sigma - \sigma(\sigma^\dagger\sigma)_{\text{in}}\right)\right]\mathcal{D}^\dagger, \tag{4.9}$$

with correlations of the zero-average electronic noise operators given by $\langle\sigma_{\text{in}}(t)\sigma^\dagger_{\text{in}}(t')\rangle = \delta(t-t')$ and $\langle(\sigma^\dagger\sigma)_{\text{in}}(t)(\sigma^\dagger\sigma)_{\text{in}}(t')\rangle = \delta(t-t')$ for the noise associated with the dephasing. From Eq. (4.8c) one can see that, as previously discussed, the driving of the vibrational mode also leads to an effective modulation of the electronic transition frequency $\tilde{\omega}_0 = \omega_0 + 2\lambda\eta_d\cos(\omega_d t)$. Eqs. (4.8) can simply be seen as an extension of the scenario discussed in section 3.1. Again, similarly to section 3.1, one can proceed with a formal integration of Eq. (4.8c), to obtain a solution for the bare electronic coherence $\langle\sigma(t)\rangle$ and subsequently for the excited state population $\langle\sigma^\dagger\sigma\rangle$, corresponding to the absorption spectrum.

We start by describing how the driving of the vibrations modifies the molecular absorption spectrum. Driving close to resonance $\omega_d \approx \nu$ will steer the vibrational mode into a coherent state and will lead to a non-zero steady state occupation of the vibrational mode $|\beta|^2 := \langle b^\dagger b\rangle = (\eta_d/2)^2/\left(\Gamma^2 + \Delta_d^2\right)$ with the detuning $\Delta_d = \omega_d - \nu$ and $\beta = (\eta_d/2)/(\Gamma - i\Delta_d)$. For the calculation of the absorption spectrum, one again has to evaluate the displacement correlation function $\langle\mathcal{D}(t)\mathcal{D}^\dagger(t')\rangle$ which is now however non-stationary due to the driving of the vibrational mode. The calculation of $\langle\mathcal{D}(t)\mathcal{D}^\dagger(t')\rangle$ requires the momentum correlation function $\langle p(t)p(t')\rangle$ whose stationary part for a given time ordering $t \geq t'$ equates to (see Appendix C for full expression)

$$\langle p(t)p(t')\rangle_{\text{st}} = \frac{1}{2}e^{-(\Gamma+i\nu)(t-t')} + |\beta|^2\cos(\omega_d(t-t')). \tag{4.10}$$

Here, the first part describes the free evolution of the vibrational mode and the second part describes the modification due to the driving. The displacement correlation function (see Appendix C for derivation) can then be evaluated as

$$\langle\mathcal{D}(t)\mathcal{D}^\dagger(t')\rangle = e^{-\lambda^2}e^{\lambda^2\exp[-(\Gamma+i\nu)(t-t')]}e^{-i\sqrt{2}\lambda\langle p(t)-p(t')\rangle}, \tag{4.11}$$

with $\langle p(t)\rangle = \left(\beta^* e^{i\omega_d t} + \beta e^{-i\omega_d t}\right)/\sqrt{2}$ the time-dependent momentum expectation value.

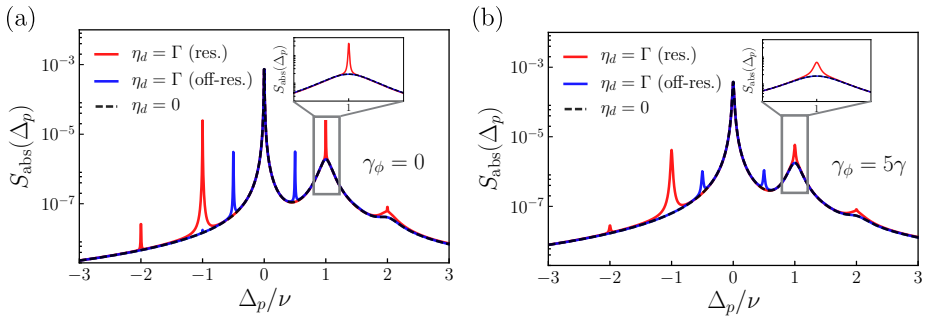


Figure 4.2: *Absorption spectrum & sideband control.* (a) Modification of molecular absorption spectrum (logarithmic scale) by means of off-resonant driving (blue, $\omega_d = 0.5\nu$, $|\beta|^2 \approx 0$), and resonant driving (red, $\omega_d = \nu$, $|\beta|^2 = 1/4$) in the low-temperature (zero dephasing) regime for $\lambda = 0.2$. The inset shows a zoom-in on the first vibronic sideband at $\Delta_p = \nu$. Other parameters: $\Gamma = 0.1\nu = 50\gamma$, $\gamma = 5 \cdot 10^{-3}\nu$, $\eta_p = 10^{-2}\gamma$. (b) Absorption spectrum for the same parameters as in (a) but with additional dephasing $\gamma_\phi = 5\gamma$.

## 4.4 Sideband control via Floquet engineering

While the ground-excited coherence $\langle\sigma(t)\rangle$ is generally not stationary, under the assumption of $\gamma \ll \omega_d$, the excited state population (i.e., the absorption spectrum) $\langle\sigma^\dagger\sigma\rangle = S_{\rm abs}(\Delta_p)$ becomes time independent and expresses as (see Appendix C)

$$S_{\rm abs}(\Delta_p) = \frac{\eta_p^2}{\gamma} \sum_{\substack{n=0 \\ m,\ell=-\infty}}^{\infty} \frac{s_n^\lambda(\tilde{\gamma}+n\Gamma)\mathcal{J}_m\left(\frac{2\lambda\eta_d}{\omega_d}\right)^2 \mathcal{J}_\ell\left(2\lambda|\beta|\right)^2}{(\tilde{\gamma}+n\Gamma)^2 + (\Delta_p - n\nu - (m+\ell)\omega_d)^2}, \tag{4.12}$$

In addition to the usual vibronic sidebands weighted by a Poissonian distribution $s_n^\lambda = e^{-\lambda^2}\lambda^{2n}/n!$ at frequencies $n\nu$ ($n \in \mathbb{N}_0$) and linewidths $\tilde{\gamma} + n\Gamma$, the driving induces a series of Lorentzian sidebands weighted by Bessel functions of the first kind $\mathcal{J}_m\left(2\lambda\eta_d/\omega_d\right)^2$ at multiples of the driving frequency $m\omega_d$ ($m \in \mathbb{Z}$) and a series of sidebands weighted by Bessel functions $\mathcal{J}_\ell(2\lambda|\beta|)^2$, also at multiples of the driving frequency $\ell\omega_d$ ($\ell \in \mathbb{Z}$). While the former stems, as previously discussed, from the shaking of the electronic transition and is discussed in more detail below, the latter accounts for the finite occupation of the vibrational mode and comes into play in case of resonant driving of the vibrational mode, i.e., if $\omega_d \approx \nu$. We also note that the result in Eq. (4.12) fulfills the standard Thomas-Reiche-Kuhn sum rule for optical transitions, i.e., the oscillator strengths of all possible transitions sum up to unity [152]

$$e^{-\lambda^2}\sum_{n=0}^{\infty}\frac{\lambda^{2n}}{n!}\sum_{m,\ell=-\infty}^{\infty}\mathcal{J}_m\left(\frac{2\lambda\eta_d}{\omega_d}\right)^2\mathcal{J}_\ell\left(2\lambda|\beta|\right)^2 = 1. \tag{4.13}$$

In Fig. 4.2(a) we plot the absorption spectrum $S_{\rm abs}(\Delta_p)$ in the limit of $\tilde{\gamma} \ll \Gamma$ and zero dephasing for both resonant and off-resonant driving of the vibron, revealing a set of narrow additional sidebands

which can increase the absorption of the molecule by orders of magnitude. The narrow sidebands stem from transitions on the zero-phonon line in combination with the simultaneous absorption of infrared photons, either via a driving-induced Floquet state or through the absorption of a vibrational quantum (see Figs. 4.3(a) and (b) for possible processes contributing to first vibronic sideband). Dephasing of the zero-phonon line transition (see Fig. 4.2(b)) increases the width and reduces the height of these driving-induced sidebands. For $\tilde{\gamma} \ll \Gamma$, the intensity of the zero-phonon line ($S_{\text{abs}}(\Delta_p = 0)$) can be approximated by ($n = m = \ell = 0$, assuming all other combinations $n\nu + (\ell + m)\omega_d = 0$ to be much smaller)

$$I_{\text{ZPL}} = \frac{\eta_p^2}{\gamma\tilde{\gamma}} e^{-\lambda^2} \mathcal{J}_0\left(\frac{2\lambda\eta_d}{\omega_d}\right)^2 \mathcal{J}_0\left(2\lambda|\beta|\right)^2 . \tag{4.14}$$

For small arguments of the Bessel functions, the effective Franck-Condon factor describing the oscillator strength of the zero-phonon line can be approximated by $\exp\left[-\lambda^2(1 + 2|\beta|^2 + 2\eta_d^2/\omega_d^2)\right]$. Assuming a narrow zero-phonon linewidth $\tilde{\gamma} \ll \Gamma$, the main contribution of the infrared drive in Eq. (4.12) stems from $n = 0$ and the intensity of the driving-induced sideband $I_d$ at e.g. $\Delta_p = \nu$ (normalized by the intensity of the bare vibronic sideband $I_b$) can be approximated by $I_d/I_b \approx \eta_d^2/(4\tilde{\gamma}\Gamma)$ ($\mathcal{J}_1(x)^2 \approx (x/2)^2$ for $x \ll 1$), i.e., it increases with the driving amplitude $\eta_d$ and is mitigated by dephasing $\gamma_\phi$ and vibrational relaxation $\Gamma$.

An interesting special case is given if one considers off-resonant driving of the vibration (e.g., $\omega_d < \nu$) and consequently $|\beta|^2 \approx 0$. The vibrational mode of the molecule then essentially undergoes free evolution $\dot{p} = -2\Gamma p - \nu q + \xi$, and the displacement correlation function becomes identical to Equation (3.11). In this case, the only effect of the drive is the modulation of the electronic transition

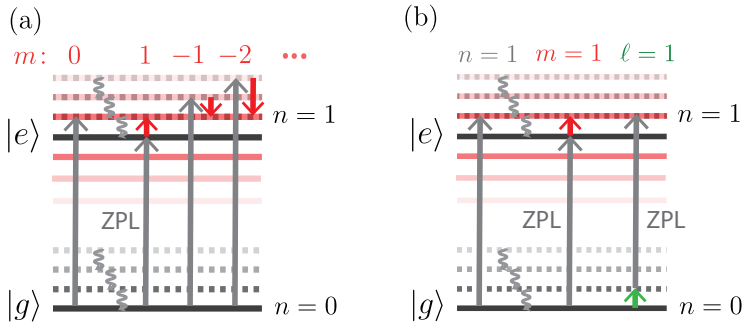


Figure 4.3: *Contributions to first sideband.* (a) Floquet contributions to first vibronic sideband $\Delta_p = \nu$ in the case of resonant driving $\omega_d = \nu$: pure vibronic transition (left arrow, $m = 0$) and transitions due to dressing with infrared field ($m \neq 0$). For $\lambda^2 \ll 1$, the transitions with negative $m$ and $n \geq 2$ are extremely unlikely due to small Franck-Condon overlap. Additional transitions can stem from non-zero vibrational occupation ($\ell \neq 0$). (b) All processes contributing to the generation of coherence in the first vibronic sideband: direct transition (grey), transition via electronic Floquet state (red) and transition due to absorption of a vibrational quantum (green).

frequency $\tilde{\omega}_0 = \omega_0 + 2\lambda\eta_d \cos(\omega_d t)$ and the absorption spectrum simplifies to

$$S_{\text{abs}}(\Delta_p) = \frac{\eta_p^2}{\gamma} \sum_{\substack{n=0 \\ m=-\infty}}^{\infty} \frac{s_n^{\lambda}(\tilde{\gamma}+n\Gamma)\mathcal{J}_m\left(\frac{2\lambda\eta_d}{\omega_d}\right)^2}{(\tilde{\gamma}+n\Gamma)^2 + (\Delta_p - n\nu - m\omega_d)^2}. \tag{4.15}$$

The intensities of the driving-induced sidebands are now only determined by the vibronic coupling strength $\lambda$ as well as by the ratio between driving amplitude and driving frequency $\eta_d/\omega_d$. Similar terms appear for frequency-modulated pure two-level systems such as atoms or superconducting qubits [153, 154]. Interestingly, the Bessel functions become zero at some values (e.g., $\mathcal{J}_0(z)^2 \approx 0$ for $z \approx 2.41$, see Fig. 4.1(c)) which can be used to decouple specific sidebands completely from the driving field. The corresponding Floquet states $|e, m\rangle$ are then dark, a phenomenon also known as coherent destruction of tunneling (CDT) [155].

## 4.5 Purcell-induced suppression of sidebands

Let us now turn to the situation depicted in Fig. 4.4(a) and consider a molecule coupled to a confined quantized electromagnetic mode in the infrared. The molecule is only indirectly coupled to a laser drive that feeds the cavity field with an amplitude $\eta_d^c = \sqrt{2\mathcal{P}\kappa/(\hbar\omega_d)}$ and frequency $\omega_d$. The coupling to the quantized cavity mode with photon annihilation and creation operators $a$ and $a^\dagger$ is described by the Hamiltonian

$$\mathcal{H}_{\text{cav}}^{\text{IR}} = g(a^\dagger + a)(b^\dagger + b). \tag{4.16}$$

The coupling is given by $g = \mathbf{e}_c \cdot \mathbf{e}_m \mathcal{E}_0 (\partial \langle d \rangle / \partial q)_0 q_{\text{zpm}}$. Here, the unit vectors $\mathbf{e}_c$ and $\mathbf{e}_m$ account for the polarizations of cavity field and molecular dipole, respectively. The quantum Langevin equations for mechanical and optical degrees of freedom as well as for the polaron operator $\tilde{\sigma}$ then read

$$\dot{q} = \nu p, \tag{4.17a}$$

$$\dot{p} = -2\Gamma p - \nu q - \sqrt{2}g(a^\dagger + a) + \xi(t), \tag{4.17b}$$

$$\dot{a} = -(\kappa + i\omega_c)a - i\sqrt{2}gq + \sqrt{2\kappa}a_{\text{in}} + \eta_d^c \cos(\omega_d t), \tag{4.17c}$$

$$\dot{\tilde{\sigma}} = -(\tilde{\gamma} - i\Delta_p)\tilde{\sigma} - 2i\lambda g(a^\dagger + a)\tilde{\sigma} + \tilde{\Sigma}_{\text{in}}. \tag{4.17d}$$

Assuming resonant driving $\omega_c = \omega_d$, we can identify a first advantage of using the cavity as an increase in the driving strength brought on by the cavity finesse. This can be seen by an elimination of the cavity field to find an effective equation for the polaron operator similar to Eq. (4.8) but with a modified drive strength. The coupling to the cavity leads to a periodic modulation of the electronic transition

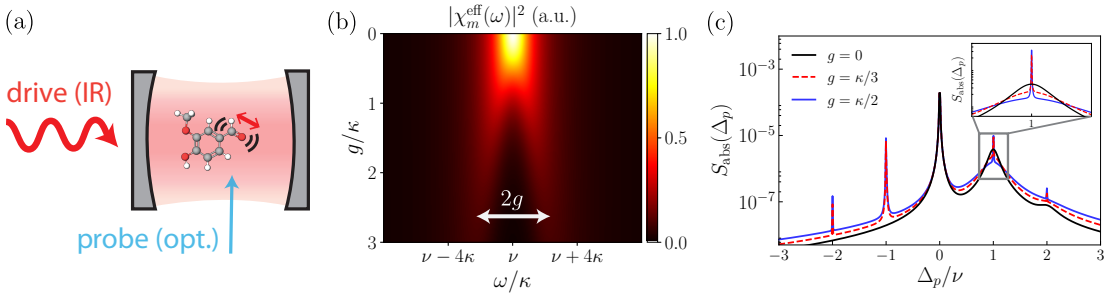


Figure 4.4: *Cavity-modified absorption*. (a) Schematics of an infrared-active molecule which is dressed by the interaction with a quantized, driven infrared cavity field. An external probe field detects the changes of the vibronic dynamics. (b) Effective, cavity-modified mechanical susceptibility $|\chi_m^{\rm eff}(\omega)|^2$ as a function of $g$ and $\omega$ for $\Gamma = \kappa$. For $g > \kappa$, the susceptibility shows a mode splitting of approximately $2g$. (b) Cavity-modified optical absorption spectrum for different values of $g$ in the weak coupling regime. Parameters: $\lambda = 0.2, \Gamma = 10^2\gamma, \kappa = 6\cdot 10^2\gamma = 6\Gamma, \gamma_\phi = 0, \eta_d^c = 0.8\kappa, \eta_p = 0.1\gamma$.

frequency with $\tilde{\omega}_0 = \omega_0 + 2\lambda g\eta_d^c\cos(\omega_d t)/\kappa$, leading to sidebands proportional to $\mathcal{J}_m\left(\frac{2\lambda g\eta_d^c}{\kappa\omega_d}\right)^2$. However, at a difference to the direct driving case, the free space coupling $\eta_d$ has now been replaced by a cavity enhanced strength $g\eta_d^c/\kappa$. To estimate the gain in this approach, let us assume a free space propagating infrared laser beam with transverse area $\mathcal{S}$ and amplitude $\mathcal{E}$ such that $\mathcal{P} = \varepsilon_0 c\mathcal{E}^2\mathcal{S}/2$. If the molecule were to be under direct laser illumination, the free space Rabi frequency could be written as $\eta_d = d\mathcal{E}/\hbar$. In the cavity, using $\kappa = \pi c/(L\mathcal{F})$ ($\mathcal{F}$ is the cavity finesse and $L$ the cavity length) and $g = d/\hbar\sqrt{\hbar\omega_c/(\varepsilon_0 L\mathcal{S})}$ we can then estimate the ratio $(g\eta_d^c/\kappa)/\eta_d = \sqrt{\mathcal{F}/\pi}$. A first advantage of using a cavity is therefore insured when employing a high-finesse resonator, providing an enhancement proportional to $\sqrt{\mathcal{F}}$ of all previously discussed effects.

The second advantage presented by the cavity is an effective Purcell increase of the vibrational relaxation rate when large cooperativities $C_{\rm IR} = g^2/(\kappa\Gamma) > 1$ are employed. To illustrate this effect, we follow a standard optomechanical approach [156, 157], where we incorporate the effect of the infrared field onto the vibrations as an additional cooling bath. This can be seen in frequency space as an additional force $p(\omega) = \chi_m(\omega)[\xi(\omega) + F_{\rm IR}(\omega)]$, with

$$F_{\rm IR}(\omega) = -\sqrt{2}g[a^\dagger(\omega) + a(\omega)], \tag{4.18}$$

added to the intrinsic Brownian noise term $\xi(\omega)$. The bare susceptibility term $\chi_m(\omega) = i\omega/(\omega^2 + 2i\Gamma\omega - \nu^2)$ describes the response of the vibrational mode to the surrounding bath of oscillators. The additional effect of the infrared bath is to give rise to a modified mechanical susceptibility

$$(\chi_m^{\rm eff})^{-1}(\omega) = \left[\chi_m^{-1} + 2g^2\frac{\nu}{\omega}\left(\chi_c(\omega) - \chi_c^*(-\omega)\right)\right], \tag{4.19}$$

by introducing the effect of the cavity via its susceptibility $\chi_c(\omega) = 1/[i(\omega_c - \omega) + \kappa]$. This is the standard picture of optomechanical sideband cooling where an effective damping rate can be com-

puted (evaluated at $\omega = \nu$)

$$\Gamma_{\mathrm{IR}} = \frac{g^2\kappa}{\kappa^2 + (\omega_d - \nu)^2} - \frac{g^2\kappa}{\kappa^2 + (\omega_d + \nu)^2}. \tag{4.20}$$

The resolved sideband condition requiring $\omega_d = \nu$ and $\kappa \ll \nu$ gives rise to a simple expression for the cavity- induced cooling rate $\Gamma_{\mathrm{IR}} = g^2/\kappa$. Adding this expression to the bare vibrational damping rate we obtain $\tilde{\Gamma} = \Gamma + \Gamma_{\mathrm{IR}} = \Gamma(1 + C_{\mathrm{IR}})$. This reveals this effect as stemming from a Purcell modification of the damping rate owing to coupling to a lossy cavity.

Going towards the strong coupling regime, Fig. 4.4(b) illustrates the effective mechanical susceptibility as a function of $g$, revealing a mode splitting at the onset of strong coupling $g > \kappa$. To calculate the cavity-modified absorption spectrum, one then has to again evaluate the momentum correlation function $\langle p(t)p(t')\rangle$ which can be obtained similarly to the free space case by calculating the correlations in frequency domain and then transforming back to the time domain. The stationary part of the momentum correlation function in the weak coupling regime is given by

$$\langle p(t)p(t')\rangle_{\mathrm{st}} = \frac{1}{2}e^{-(\tilde{\Gamma}+i\nu)(t-t')} + |\beta_c|^2\cos(\omega_d(t-t')), \tag{4.21}$$

with the cavity-induced vibrational occupation $|\beta_c|^2 = g^2(\eta_d^c)^2|\chi_m^{\mathrm{eff}}(\omega_d)|^2|\chi_c(\omega_d)^2|$. After integrating calculating $\langle\sigma(t)\rangle$ similarly to the free space case, the absorption spectrum (assuming weak coupling $g < \kappa$) for $\gamma \ll \omega_d$ can be expressed as

$$S_{\mathrm{abs}}(\Delta_p) = \frac{\eta_p^2}{\gamma}\sum_{\substack{n=0\\ m,\ell=-\infty}}^{\infty} \frac{s_n^{\lambda}(\tilde{\gamma} + n\tilde{\Gamma})\mathcal{J}_m(z)^2\mathcal{J}_\ell\left(2\lambda|\beta_c|\right)^2}{(\tilde{\gamma} + n\tilde{\Gamma})^2 + (\Delta_p - n\nu - (m+\ell)\omega_d)^2}. \tag{4.22}$$

with $z = 2\lambda g\eta_d^c/(\kappa\omega_d)$. In the case of complete resonance $\omega_d = \omega_c = \nu$, one can approximate $|\beta_c|^2 \approx [g\eta_d^c/(2\kappa\Gamma)]^2$. The previously discussed Purcell effect is clearly illustrated in the optical spectrum in Fig. 4.4(c) which shows a a leveling of the floor around the driven vibrational sideband at $\Delta_p = \nu$. For increasing values of the cooperativity the amplitude of the sidebands is increasing (owing to the increase in $g$) while at the same time, absorption outside this narrow interval is strongly suppressed.

Let us finally remark that, while our treatment here is restricted to the harmonic case, it would be interesting to extend this to the anharmonic case which becomes relevant for higher vibrational occupations and where nonlinear vibrational effects play a role [158].

# 5

# Molecules in phononic host environments

In quantum optics experiments at the single- or few-particle level, molecules are typically trapped in crystalline host matrices. A commonly used platform is e.g. DBT molecules in anthracene crystalline matrices [see illustration in Fig. 5.1(a)] which has been shown to exhibit lifetime-limited linewidths and high radiative yields at cryogenic temperatures [8, 18, 159].

When molecules couple to a condensed-matter environment, the mechanical modes of the localized intramolecular vibrations (vibrons) are augmented by collective delocalized vibrational excitations of the host material (phonons), leading to vibron-phonon and electron-phonon couplings. In practice, coupling to a large number of phonon modes makes the study of molecular vibrations in the solid state notoriously challenging. Some of the challenges can be tamed under cryogenic conditions where experiments manage to reduce phonon coupling on the ZPL transition between $|g, n_\nu = 0\rangle$ and $|e, n_\nu = 0\rangle$ sufficiently to reach its natural linewidth limit. This can be verified in ensemble measurements, e.g., via hole burning, or in single-molecule spectroscopy [160]. However, even if vibrational spectroscopy at the single-molecule level is readily accessible in the laboratory [89, 161, 162], a quantitative understanding of the couplings between the molecular vibrational modes and their internal and external degrees of freedom and, in particular, a detailed study of decoherence sources is largely missing.

Our open-system approach can shed light onto a few aspects of coherent and incoherent molecular dynamics and onto the light-matter interactions in the presence of vibrons, phonons and cavity-localized photon modes. We note that very similar effects, especially regarding the coupling between electrons and phonons, also occur in related solid-state emitters such as quantum dots or vacancy centers in diamond whose coupling to photonic nanostructures has been studied quite extensively over the last years [121, 123, 163–168].

We start by introducing our model describing the mutual coupling between electrons, vibrons and phonons in section 5.1. While we have simply assumed a Brownian noise dissipation model for the vibrational modes previously, we derive this explicitly in section 5.2 and show that the dynamics can either be Markovian (i.e., exponential) or non-Markovian (i.e., non-exponential), depending on the maximum frequency of the phonon bath. For two molecules immersed in the same phonon bath, the same formalism allows for the derivation of collective relaxation dynamics exhibiting effects similar to super- and subradiance in dense quantum emitter systems. Classical light driving is included in

section 5.4 by extending the previously developed quantum Langevin approach to electron-phonon coupling and calculating absorption spectra for coherently driven molecules under the influence of thermal effects. We discuss dephasing in section 5.5 and show that in a linear coupling model the zero-phonon line is mainly lifetime-limited. Finally, for molecular polaritonic systems in a cavity setting, we derive the transmission function of the cavity field, showing the reduction of the vacuum Rabi splitting with increasing vibronic and phononic coupling, as well as phononic signatures in the Purcell regime in section 5.6. The effect of temperature on the asymmetry of cavity polaritons is quantified by deriving effective rate equations for the polariton cross-talk in section 5.7.

## 5.1 Model and Hamiltonian formulation

We develop here a model of a guest molecule (the dopant) embedded in a host crystal where all interactions between light, electronic transitions, vibrons and phonons are taken into account and are treated on equal footing for finite temperatures. We will then be in the position to derive general expressions for the light scattered by a molecular system embedded in a solid-state environment outside or inside an optical cavity. As schematically illustrated in Fig. 5.1(c) the light (mode $a$) couples to electronic transitions ($\sigma$) via a Jaynes-Cummings Hamiltonian. These are in turn affected by the vibronic coupling to one or more molecular vibrations which leads to the red-shifted Stokes lines in emission [cf. Fig. 5.1(b)]. We focus here on a single molecular vibrational mode with relative motion coordinate $Q$ for the sake of simplicity. The solid-state matrix supports a multitude of bosonic phonon modes with displacements $q_k$ ($k$ from 1 to $N$) which directly modify the electronic transition leading to the occurrence of phonon wings in the emission and absorption spectra. In addition, molecular vibrons can deposit energy into phonons as a displacement-displacement interaction, leading to the irreversible process of vibrational relaxation.

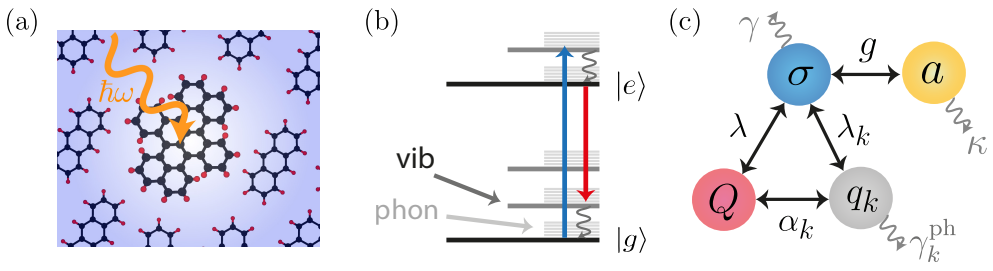


Figure 5.1: *Schematics of molecule-host coupling.* (a) Sketch of a DBT impurity molecule in an anthracene host crystal interacting with light. (b) Jablonski scheme of a molecule in a solid-state environment showing vibrational and phononic sublevels of both electronic excited $|e\rangle$ and ground $|g\rangle$ state. Absorption/emission is indicated by blue/red arrows. Excitation of the molecule is followed by quick vibrational relaxation (wavy lines). (c) Illustration of the relevant couplings between electronic ($\sigma$), localized vibrational ($Q$), phononic ($q_k$) and optical ($a$) degrees of freedom as well as decay processes indicated by wavy lines (spontaneous emission rate $\gamma$, cavity decay rate $\kappa$, and phonon decay rate $\gamma_k^{\mathrm{ph}}$).

We consider one molecule embedded in a bulk medium comprised of $N$ unit cells. Our perturbational assumption is that, since the bulk is large, the dopant does not significantly change the overall modes of the bulk. The molecule itself is described by a standard Holstein Hamiltonian with electron-vibron coupling

$$\mathcal{H}_{\text{el-vib}} = -\lambda\nu\sqrt{2}\sigma^\dagger\sigma Q, \tag{5.1}$$

where $Q = (b + b^\dagger)/\sqrt{2}$. In addition to the coupling to internal vibrations of its nuclei, the electronic transition is also modified through coupling to the delocalized phonon modes of the crystal. We describe the bulk modes as a bath of independent harmonic oscillators with bosonic operators $c_k$ and $c_k^\dagger$ and frequencies $\omega_k$. The electron-phonon coupling (see Appendix D for derivations) can then be cast in the same Holstein form as for the vibron

$$\mathcal{H}_{\text{el-phon}} = -\sum_k \lambda_k\omega_k\sqrt{2}\sigma^\dagger\sigma q_k, \tag{5.2}$$

where the displacement operators refer to each individual collective phonon mode $q_k = (c_k + c_k^\dagger)/\sqrt{2}$ (the momentum operator is given by $p_k = i(c_k^\dagger - c_k)/\sqrt{2}$). The coupling factors $\lambda_k$ depend on the specifics of the molecule and the bulk crystal and are derived for a molecule coupling to a 1D bath of acoustic phonons in Appendix D. Similarly to the vibronic case, the electron-phonon interaction can be diagonalized by means of a polaron transformation $\mathcal{U}_{\text{el-phon}} = |g\rangle\langle g| + \mathcal{B}^\dagger|e\rangle\langle e|$, whereby

$$\mathcal{B}^\dagger = \prod_k \mathcal{B}_k^\dagger = e^{\sum_k i\sqrt{2}\lambda_k p_k} \tag{5.3}$$

is the product of all phonon bath mode displacements, signifying a collective transformation for all phonon modes. We assume that the bulk is kept at a constant temperature and is always in thermal equilibrium. The coupling to the phonons gives rise to a multitude of sidebands in the absorption and emission spectra which coalesce into a phonon wing that becomes especially important at elevated temperatures. We will then follow the temporal dynamics of a collective "double" polaron operator $\tilde{\sigma} = \mathcal{D}^\dagger\mathcal{B}^\dagger\sigma$ which includes both vibronic and electron-phonon couplings.

Phonons also affect the dynamics of the vibrational mode. Modifications of the bond length associated with the molecular vibration leads to a force on the surrounding crystal (and vice versa), giving rise to a displacement-displacement coupling,

$$\mathcal{H}_{\text{vib-phon}} = -\sum_k \alpha_k q_k Q\,. \tag{5.4}$$

The coupling coefficients $\alpha_k$ are explicitly derived for a 1D geometry in Appendix D. In the limit of large bulk media, this Hamiltonian can lead to an effective irreversible dynamics, i.e. a vibrational relaxation effect. By eliminating the phonon modes and derving a Brownian motion model, we are then

in a position to identify the Markovian versus non-Markovian regimes of vibrational relaxation conditioned on the phonon spectrum, namely on the maximum phonon frequency $\omega_{\max}$ of the system. We can additionally account for a finite phonon lifetime by including a decay rate $\gamma_k^{\mathrm{ph}}$ for each phonon mode. Finally, by adding the coupling of a confined optical mode at frequency $\omega_c$ to the electronic transition via a Jaynes-Cummings interaction

$$\mathcal{H}_{\mathrm{JC}} = g(a\sigma^\dagger + \sigma a^\dagger), \tag{5.5}$$

will allow us to treat the dynamics of the hybrid light-matter platform in section 5.6.

## 5.2 Vibrational relaxation

A decay path for the molecular vibration stems from its coupling to the bath of phonon modes supported by the bulk. While it is generally agreed that nonlinear vibron-phonon couplings contribute to the vibrational relaxation process, especially in the higher temperature regime, and furthermore also anharmonic couplings among different intramolecular vibrational modes play a role [169, 170], we restrict our treatment to a coupling in the bilinear form of Eq. (5.4). Formal elimination of the phonon modes leads to an effective Brownian motion equation for the momentum of the vibrational mode

$$\dot{P} = -\tilde{\nu}Q - \Gamma * P + \xi, \tag{5.6}$$

while the displacement follows the unmodified equation $\dot{Q} = \nu P$. The effect of the phonon bath is twofold: (i) it can shift the vibrational frequency to $\tilde{\nu} = \nu - \nu_s$ and (ii) it leads to a generally non-Markovian decay kernel expressed as a convolution $\Gamma * P = \int_0^\infty \mathrm{d}t'\, \Gamma(t-t')P(t')$. For the particular case considered in the Appendix, the crystal-induced frequency shift is expressed as

$$\nu_s = \nu \frac{(\Delta k)^2}{2k_0 k_{\mathrm{M}}}, \tag{5.7}$$

where $k_0$ denotes the spring constant of the host crystal, $k_{\mathrm{M}}$ represents the spring constant of the vibron, and $\Delta k$ is a measure for the coupling of the molecule's relative motion to the bulk. For a discrete system, the expression for the damping kernel $\Gamma(t) = \sum_k \alpha_k^2 \nu/\omega_k \cos(\omega_k t)\theta(t)$ involves a sum over all phonon modes which can be turned into the following expression in the continuum limit ($N \to \infty$)

$$\Gamma(t-t') = \Gamma_{\mathrm{m}} \frac{J_1(\omega_{\max}|t-t'|)}{|t-t'|}\theta(t-t'). \tag{5.8}$$

Here, $J_n(x)$ denotes the $n$-th order Bessel function of the first kind and $\Gamma_{\mathrm{m}} = 2\nu\nu_s/\omega_{\max}$ is the decay rate in the Markovian limit. A similar expression is known from the Rubin model [171], where one considers the damping of a single mass defect in a 1D harmonic crystal. The zero-average Langevin

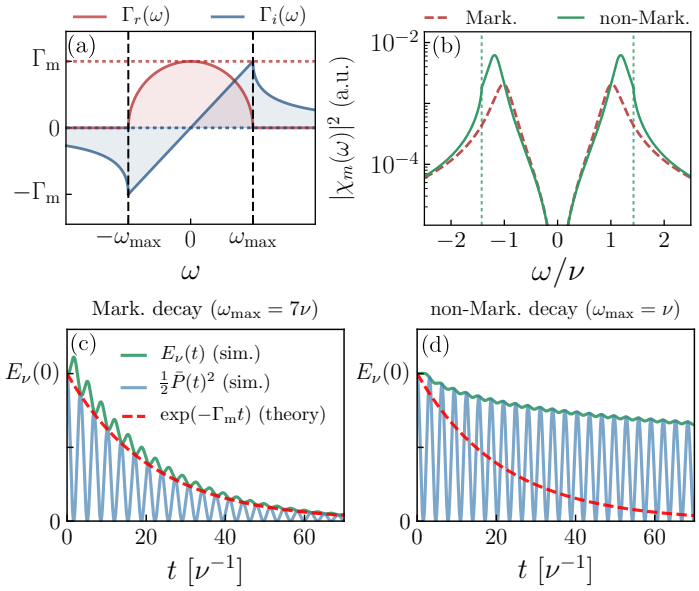


Figure 5.2: *Markovian vs. non-Markovian vibrational relaxation.* (a) Real and imaginary part of the frequency-dependent non-Markovian response function $\Gamma(\omega)$. The dotted horizontal lines $\Gamma_r(\omega) = \Gamma_m$ and $\Gamma_i(\omega) = 0$ show the Markovian limit $\omega_{max} \to \infty$. (b) Logarithmic plot of the mechanical susceptibility $|\chi_m(\omega)|^2$ in the Markovian regime $\omega_{max} \gg \nu$ (dashed curve) and for a finite cutoff $\omega_{max} = 1.4\nu$ (solid curve). In the latter case, the cutoff at $\pm\omega_{max}$ is indicated by the vertical dotted lines. (c) Relaxation of molecular vibrational energy $E_\nu(t)$ due to coupling to $N = 500$ phonon modes (simulation of classical equations of motion) in the Markovian limit $\omega_{max} = 7\nu$ for $\Gamma_m = \nu/20$ and comparison with Brownian motion theory (red dashed curve). (d) Vibrational relaxation for identical $\Gamma_m$ but in the non-Markovian regime $\omega_{max} = \nu$. Exponential decay with $\Gamma_m$ (dashed red curve) then fails to predict the behavior. In both cases we assumed a finite phonon lifetime with constant $Q$-factor $Q = \omega_k/\gamma_k^{ph} = 50$.

noise term $\xi$ is determined by the initial conditions of the phonon bath and can be expressed in discrete form as $\xi(t) = \sum_k \alpha_k \left(q_k(0)\cos(\omega_k t) + p_k(0)\sin(\omega_k t)\right)$. We can treat Eq. (5.6) more easily in the Fourier space where the convolution becomes a product

$$-i\omega P(\omega) = -\tilde{\nu} Q(\omega) - \Gamma(\omega) P(\omega) + \xi(\omega), \tag{5.9}$$

and the Fourier transform of the non-Markovian decay kernel $\Gamma(\omega)$ generally contains a real and imaginary part $\Gamma(\omega) = \Gamma_r(\omega) + i\Gamma_i(\omega)$. Figure 5.2(a) shows a plot of $\Gamma_r(\omega)$ and $\Gamma_i(\omega)$ where we can interpret the imaginary part as a frequency shift which is largest around $\omega = \pm\omega_{max}$. Together with the transformed equation for the position quadrature $-i\omega Q(\omega) = \nu P(\omega)$ we then obtain an algebraic set of equations which allows us to calculate any kind of correlations for the molecular vibration, both in time and frequency domains. This will be needed later on for computing the optical response of the molecule.

The Markovian limit is achieved when the vibrational frequency lies well within the phonon spectrum $\omega_{max} \gg \nu$ and $\Gamma(\omega)$ becomes flat in frequency space: $\Gamma(\omega) = \Gamma_m$. In this case the memory

kernel tends to a $\delta$-function: $\Gamma(t) = 2\Gamma_{\mathrm{m}}\delta(t)\theta(t)$.[1] In the continuum limit, the correlations at different times are

$$\langle \xi(t)\xi(t')\rangle = \frac{1}{2\pi}\int_{-\infty}^{\infty} \mathrm{d}\omega\, e^{-i\omega(t-t')} S_{\mathrm{th}}(\omega), \tag{5.10}$$

where the noise spectrum is expressed similarly to the case of a standard thermal spectrum for a harmonic oscillator in thermal equilibrium $S_{\mathrm{th}}(\omega) = \Gamma_r(\omega)\omega/\nu[\coth(\beta\omega/2)+1]$. The difference lies in the frequency-dependence of the real part of the decay rate function

$$\Gamma_r(\omega) = \Gamma_{\mathrm{m}}\frac{\sqrt{\omega_{\mathrm{max}}^2-\omega^2}}{\omega_{\mathrm{max}}}\theta(\omega_{\mathrm{max}}-\omega)\theta(\omega_{\mathrm{max}}+\omega), \tag{5.11}$$

where the Heaviside functions provide a natural cutoff of the spectrum at $\pm\omega_{\mathrm{max}}$. While in the time domain, the noise is only delta-correlated at high temperatures and $\omega_{\mathrm{max}} \to \infty$, the noise is always delta-correlated (yet colored) in the frequency domain $\langle \xi(\omega)\xi(\omega')\rangle = S_{\mathrm{th}}(\omega)\delta(\omega+\omega')$. This property is helpful for analytical estimation of the molecular absorption and emission in the presence of non-Markovian vibrational relaxation. The response of the vibron to the input noise of the phonons is characterized by the mechanical susceptibility $\chi_m(\omega) = -i\omega\left[\nu^2-\omega^2-i\Gamma(\omega)\omega\right]^{-1}$ defined by $P(\omega) = \chi_m(\omega)\xi(\omega)$.[2] The two-time correlations required for the calculation of the spectra can then be computed from the thermal spectrum convoluted with the mechanical susceptibility in Fourier domain

$$\langle P(t)P(t')\rangle = \frac{1}{2\pi}\int_{-\infty}^{\infty} \mathrm{d}\omega\, e^{-i\omega(t-t')}|\chi_m(\omega)|^2 S_{\mathrm{th}}(\omega). \tag{5.12}$$

In Fig. 5.2(b), we plot $|\chi_m(\omega)|^2$ for the two cases $\omega_{\mathrm{max}} \gg \nu$ (Markovian limit) and $\omega_{\mathrm{max}} \approx \nu$ (non-Markovian regime) for identical $\Gamma_{\mathrm{m}}$. While in the Markovian regime, the susceptibility has two approximately Lorentzian sidebands with linewidth $\Gamma_{\mathrm{m}}$ centered around $\pm\nu$, the finite frequency cutoff in the non-Markovian case leads to an unconventional lineshape with reduced linewidth and slight frequency shift. In the time domain, we can simulate the microscopic classical equations of motion for a large number of phonon modes and compare the results to the standard Markovian limit obtained from Brownian motion theory. This is illustrated in Figs. 5.2(c) and (d) where we simulate the average energy of the vibron mode $E_\nu(t) = \left(\bar{P}(t)^2+\bar{Q}(t)^2\right)/2$ for classical observables $\{\bar{P},\bar{Q}\}$ interacting with $N = 500$ phonon modes in the Markovian and non-Markovian regimes, respectively. While one obtains an exponential decay with $\Gamma_{\mathrm{m}}$ in the Markovian regime [Fig. 5.2(c)], in the non-Markovian case [Fig. 5.2(d)] one finds a slower nonexponential decay (for identical $\Gamma_{\mathrm{m}}$) which does not reach zero for long times.

[1] With convention $\theta(0) = 1/2$.

[2] For simplicity, we assumed $\tilde{\nu} \approx \nu$.

## 5.3 Collective vibrational relaxation

A collection of impurity molecules sitting close to each other within the same crystal will see the same phonon bath and can, therefore, undergo a collective vibrational relaxation process. This is similar to the phenomenon of subradiance/superradiance of quantum emitters commonly coupled to an electromagnetic environment discussed in section 2.4.b, where the rate of photon emission from the whole system can be smaller or larger than that of an individual isolated emitter. In order to elucidate this aspect, we follow the approach sketched above, i.e., we eliminate the phonon modes to obtain a set of coupled Langevin equations for two molecules situated $2j$ sites apart from each other (see Fig. 5.3(a)):

$$\dot{P}_1 = -\tilde{\nu}_1 Q_1 - \Omega Q_2 - \Gamma_1 * P_1 - \Gamma_{12} * P_2 + \xi_1, \tag{5.13a}$$

$$\dot{P}_2 = -\tilde{\nu}_2 Q_2 - \Omega Q_1 - \Gamma_2 * P_2 - \Gamma_{21} * P_1 + \xi_2. \tag{5.13b}$$

The mutually induced (small) energy shift $\Omega = \sum_k \alpha_{k,1}\alpha_{k,2}/\omega_k$ and the mutual damping kernels

$$\Gamma_{12} = \nu_2 \sum_k \alpha_{k,1}\alpha_{k,2}/\omega_k \cos(\omega_k t)\theta(t), \qquad \Gamma_{21} = \nu_1 \sum_k \alpha_{k,1}\alpha_{k,2}/\omega_k \cos(\omega_k t)\theta(t), \tag{5.14}$$

are strongly dependent on the intermolecular separation $2j$ whereas the individual decay terms $\Gamma_1$ and $\Gamma_2$ are given by the expressions derived previously. Importantly, now also the noise terms $\xi_1$ and $\xi_2$ are not independent of each other but correlated. In the continuum limit $N \to \infty$, the collective interaction kernels can be approximated with the aid of higher-order Bessel functions (assuming molecules with identical vibrational frequency $\nu_1 = \nu_2$ and consequently $\Gamma_{12}(t) = \Gamma_{21}(t)$):

$$\Gamma_{12}(t - t') = \Gamma_{\mathrm{m}} \frac{4jJ_{4j}(\omega_{\max}|t - t'|)}{|t - t'|}\theta(t - t'). \tag{5.15}$$

In Fig. 5.3(b), we plot the collective decay kernel as a function of time and intermolecular separations $2j$. The collective effects do not occur instantaneously but in a highly time-delayed fashion [cf. Fig 4.2(c)]. We can interpret the collective interaction as an exchange of phonon wavepackets between the two molecules, where the wavepackets are traveling with the group velocity $v_g = \partial\omega/\partial q$ of the crystal (lattice constant $a$) at a maximum speed $v_g^{\max} \approx a\omega_{\max}/2$ (the high frequency components towards the band edge are slower). This leads to an approximate time of $\tau = 4j\omega_{\max}^{-1}$ for the wavepacket to propagate from one molecule to the other.

The collective interaction will also lead to a modification of the vibrational lifetimes of the molecules which we want to describe in the following. To this end, one can again proceed with a Fourier analysis

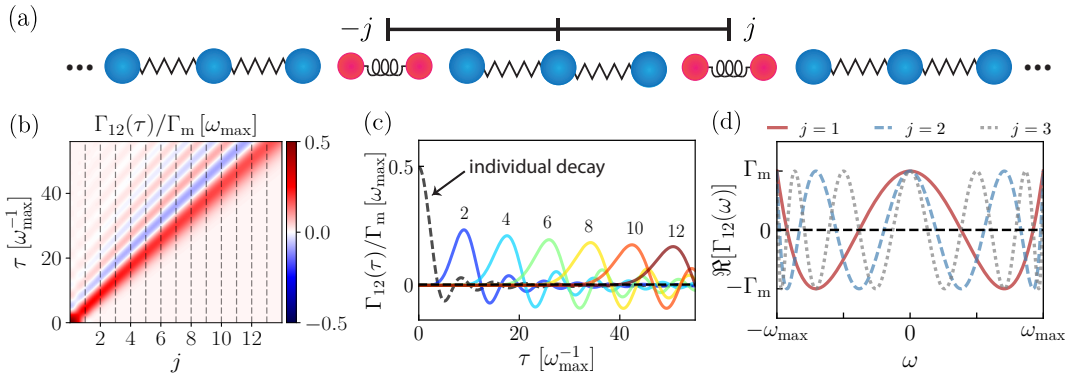


Figure 5.3: *Collective vibrational effects.* (a) Two molecular impurities are embedded in a host crystal with separation $2j$. (b) Collective interaction kernel $\Gamma_{12}(\tau) = \Gamma_{21}(\tau)$ as a function of time delay $\tau$ and separation $j$. In the crystal, only integer values of $j$ are permitted (dashed vertical lines). (c) Comparison between individual decay (dashed curve, assuming two identical molecules $\Gamma_1(\tau) = \Gamma_2(\tau)$) and collective interaction for increasing distance $j$ (as indicated by the numbers above the curves). (d) Real part of $\Gamma_{12}(\omega)$ between $-\omega_{\max}$ and $+\omega_{\max}$ for $j = 1$ (solid), 2 (dashed), and 3 (dotted).

of Eqs. (5.13). The expression for the non-Markovian collective interaction kernel in frequency space (between $-\omega_{\max}$ and $+\omega_{\max}$) reads

$$\Gamma_{12}(\omega) = i\Gamma_{\mathrm{m}} U_{4j-1}\left(\frac{\omega}{\omega_{\max}}\right)\frac{\sqrt{\omega_{\max}^2-\omega^2}}{\omega_{\max}} + \Gamma_{\mathrm{m}} T_{4j}\left(\frac{\omega}{\omega_{\max}}\right), \tag{5.16}$$

where we introduced the Chebychev polynomials of first ($T_n$) and second kind ($U_n$). We are interested in the real part of the above expression which will give rise to a collectively-induced modification of the vibrational lifetime while the imaginary part corresponds again to a frequency shift. In Figs. 5.3(d) we plot the real part of $\Gamma_{12}(\omega)$ for small distances $j$, respectively.

In the Markovian limit $\omega_{\max} \gg \nu$ everything becomes flat in frequency space and one can approximate $\Gamma_{12}(\omega) = \Gamma_{12}(0) = \Gamma_{\mathrm{m}}$ and consequently $(\Gamma_{12} * P_i) \approx \Gamma_{\mathrm{m}} P_i$ with $i = \{1, 2\}$. A diagonalization can be performed by moving into collective quadratures $P_+ = P_1 + P_2$ and $P_- = P_1 - P_2$ (and identically for the positions) for which the equations of motion decouple

$$\dot{P}_+ \approx -(\tilde{\nu} + \Omega)Q_+ - 2\Gamma_{\mathrm{m}} P_+ + \xi_1 + \xi_2, \tag{5.17a}$$

$$\dot{P}_- \approx -(\tilde{\nu} - \Omega)Q_- + \xi_1 - \xi_2. \tag{5.17b}$$

While one of the collective modes undergoes relaxation at an increased rate $2\Gamma_{\mathrm{m}}$, the orthogonal collective mode can be eventually decoupled from the phononic environment. Of course, as the derivation we have performed is a very simplified model restricted to one-dimensional crystals, it would be interesting to explore this effect in three dimensional scenarios where both longitudinal and transverse phonon modes have to be considered with effects stemming from the molecular orientation as well as the influence of anharmonic potentials. A recent theoretical work also discusses phonon-bath me-

diated interactions between two molecular impurities immersed in nanodroplets with respect to the rotational degrees of freedom of the molecules [172].

## 5.4 Phonon wing

For the calculation of the absorption spectrum, we follow the time dynamics of the collective polaron operator $\tilde{\sigma} = \mathcal{D}^\dagger \mathcal{B}^\dagger \sigma$ (assuming Markovian relaxation for the vibrational mode). Making the same assumptions as in section 3.1, we obtain the polaron Langevin equation

$$\dot{\tilde{\sigma}} = -\left[\gamma - i\left(\omega_\ell - \tilde{\omega}_0\right)\right]\tilde{\sigma} + \eta_\ell \mathcal{D}^\dagger \mathcal{B}^\dagger + \sqrt{2\gamma}\tilde{\sigma}_{\text{in}}, \tag{5.18}$$

where we used that $\dot{\tilde{\sigma}} = \dot{\mathcal{D}}^\dagger \mathcal{B}^\dagger \sigma + \mathcal{D}^\dagger \dot{\mathcal{B}}^\dagger \sigma + \mathcal{D}^\dagger \mathcal{B}^\dagger \dot{\sigma}$. The coupling to the phonons additionally leads to a renormalization of the electronic transition frequency $\tilde{\omega}_0 = \omega_0 - \sum_k \lambda_k^2 \omega_k$. The expectation value of the dipole operator at large times can then be derived as

$$\langle \sigma \rangle = \eta_\ell \int_{-\infty}^{t} \mathrm{d}t'\, e^{-[\gamma - i(\omega_\ell - \tilde{\omega}_0)](t-t')} \langle \mathcal{B}(t)\mathcal{B}^\dagger(t')\rangle \, \langle \mathcal{D}(t)\mathcal{D}^\dagger(t')\rangle \,. \tag{5.19}$$

The expression in Eq. (5.19) now jointly contains all of the effects: electron-phonon coupling, electron-vibron coupling and vibrational relaxation (through the correlation function $\langle \mathcal{D}(t)\mathcal{D}^\dagger(t')\rangle$). Since we consider phonon modes to be independent of each other, their displacement correlation function can be factorized $\langle \mathcal{B}(t)\mathcal{B}^\dagger(t')\rangle = \prod_k \langle \mathcal{B}_k(t)\mathcal{B}_k^\dagger(t')\rangle$. When replacing the sum over $k$ with an integral over $\omega$ in the continuum limit, this yields the phonon bath displacement correlation function [3]

$$\langle \mathcal{B}(t)\mathcal{B}^\dagger(t')\rangle = \exp\left\{ \int_0^\infty \mathrm{d}\omega\, \frac{J(\omega)}{\omega^2} \left[ \coth\left(\frac{\beta\omega}{2}\right)\left(\cos\left(\omega\tau\right) - 1\right) - i\sin\left(\omega\tau\right)\right]\right\}. \tag{5.20}$$

Here, we have introduced the spectral density $J(\omega) = \sum_k |\lambda_k \omega_k|^2 \delta(\omega - \omega_k) = n(\omega)\lambda(\omega)^2\omega^2$ of the electron-phonon coupling where $n(\omega)$ denotes the density of states. In the one-dimensional derivation considered here we obtain for the spectral density (see Appendix D)

$$J^{\text{1D}}(\omega) = \lambda_{\text{e-ph}}^{\text{1D}} \cdot \omega \frac{\sqrt{\omega_{\max}^2 - \omega^2}}{\omega_{\max}} \theta(\omega_{\max} - \omega). \tag{5.21}$$

with the electron-phonon coupling constant $\lambda_{\text{e-ph}}^{\text{1D}}$. The coupling constant is derived explicitly in Appendix D and depends, among other things, on the coupling of the dopant to the neighboring crystal atoms as well as on the displacement of the neighboring atoms upon excitation of the molecule. The cutoff at $\omega_{\max}$ arises naturally from the dispersion of the crystal. In the continuum limit considered here, this spectral density leads to a divergence of the integral in Eq. (5.20) due to the high density of

[3] Neglecting the finite phonon lifetime.

low-frequency phonons, which is a well known problem for 1D crystals [173, 174]. This issue can for example be resolved by considering only a finite-sized 1D crystal with a minimum phonon frequency cutoff $\omega_{\text{min}} > 0$. However, one can instead also consider a spectral density stemming from a 3D density of states:

$$J^{\text{3D}}(\omega) = \lambda^{\text{3D}}_{\text{e-ph}} \cdot \omega^3 \frac{\sqrt{\omega^2_{\text{max}} - \omega^2}}{\omega_{\text{max}}} \theta(\omega_{\text{max}} - \omega), \tag{5.22}$$

where the 3D electron-phonon coupling constant $\lambda^{\text{3D}}_{\text{e-ph}}$ has units $[\text{s}^2]$ and is explicitly stated in Appendix D . In Figs. 5.4(a) and (b) we plot the resulting absorption spectrum of the ZPL for 1D and 3D densities of states, whereby the exact shape of the phonon wing is determined by the spectral density function $J(\omega)$. While analytical expressions for the integral in Eq. (5.20) are difficult to obtain in the continuum case, we can express the absorption spectrum of the ZPL including phonon sideband in terms of discrete lines as

$$S^{\text{phon}}_{\text{abs}}(\Delta_\ell) = \eta^2_\ell \sum_{\{n_k\}}^{\infty} \sum_{\{l_k\}}^{\{n_k\}} \frac{\prod_{k=1}^{N} L_k(n_k) B_k(n_k, l_k)}{\gamma^2 + \left[\omega_\ell - \tilde{\omega}_0 - \sum_{k=1}^{N} (n_k - 2l_k)\omega_k\right]^2}. \tag{5.23}$$

Here the sum runs over all $\{n_k\} = n_1, \ldots, n_N$ and $\{l_k\} = l_1, \ldots, l_N$. This can be seen as a generalization of the result in Eq. (3.24) for many modes where the $N$ phonon modes are indexed by $k$ and the function $L_k(n_k)$ accounts for the displacement of the excited state while the distribution $B_k(n_k, l_k)$ accounts for the thermal occupation of each mode. As one can see in Figs. 5.4(a) and (b), thermal occupation of the phonons leads to red-shifted phonon sidebands in absorption and eventually to a symmetric absorption spectrum around the zero-phonon line in the limit of large temperatures. Note that here we did not explicitly include phonon decay $\gamma^{\text{ph}}_k$ as it does not influence the absorption spectra in the continuum limit (the phonon peaks overlap and are not resolved). However, one can easily account for a finite phonon lifetime by including it in the momentum correlation function

$$\langle p_k(t) p_k(t') \rangle = \frac{1}{2}[(1 + 2\bar{n}_k)\cos(\omega_k \tau) - i \sin(\omega_k \tau)] e^{-\gamma^{\text{ph}}_k |\tau|}. \tag{5.24}$$

Similarly to the Franck-Condon factor for vibrons, one defines the Debye-Waller factor

$$f_{\text{DW}} = \langle \mathcal{B}^\dagger \rangle^2 = \exp\left[ - \int_0^\infty \text{d}\omega \, J(\omega) \omega^{-2} \coth(\beta\omega/2) \right], \tag{5.25}$$

which quantifies the reduction of the ZPL intensity due to the scattering of light into phonons. In Fig. 5.4(c) we show the behavior of the $f_{\text{DW}}$ in the 3D case for different coupling strengths at low temperatures, revealing a stronger temperature-dependence for larger couplings. The total reduction of the ZPL intensity as compared to the two-level system case is then given by the product $f_{\text{FC}} \cdot f_{\text{DW}}$.

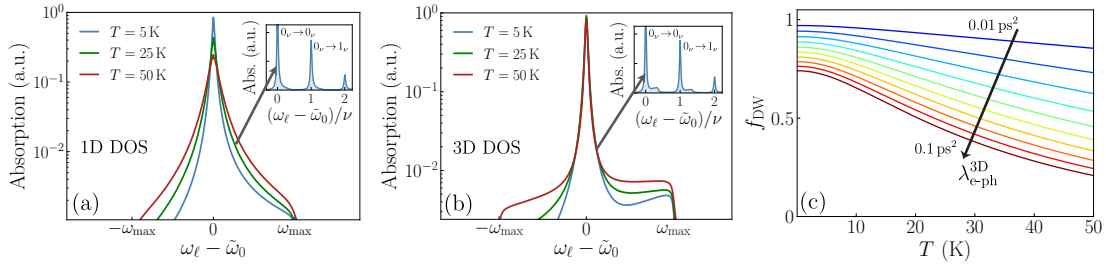


Figure 5.4: *Phonon imprint on absorption.* Absorption spectra (logarithmic scale) of zero-phonon line including phonon wing at different temperatures for (a) 1D density of states and $\lambda^{1\mathrm{D}}_{\text{e-ph}} = 0.03$ and (b) 3D density of states and $\lambda^{3\mathrm{D}}_{\text{e-ph}} = 0.02\,\mathrm{ps}^2$ with $\omega_{\max} = 3\,\mathrm{THz}$ in both cases. Insets show schematic of total molecular absorption spectrum with vibrational sidebands accompanied by phonon wings. (c) Debye-Waller factor $f_{\mathrm{DW}}$ for a 3D density of states as a function of temperature with increasing coupling strength $\lambda^{3\mathrm{D}}_{\text{e-ph}}$ (as indicated by arrow) in equidistant steps from $\lambda^{3\mathrm{D}}_{\text{e-ph}} = 0.01\,\mathrm{ps}^2$ to $\lambda^{3\mathrm{D}}_{\text{e-ph}} = 0.1\,\mathrm{ps}^2$ and cutoff frequency of $\omega_{\max} = 3\,\mathrm{THz}$.

## 5.5 Dephasing

Within the model we consider, where all interactions stem from a harmonic treatment of both intramolecular vibrations and crystal motion, the zero-phonon linewidth of the electronic transitions is largely independent of temperature. In reality, to account for higher temperature effects one needs contributions quadratic in the phononic displacements which has been theoretically pointed out and experimentally observed [124, 151, 175]. However, even in the linear regime, the fact that vibronic and electron-phonon couplings do not lead to significant dephasing is a non-trivial result. One could e.g. expect that the Holstein-Hamiltonian for electron-phonon coupling which sees a stochastic shift of the excited electronic level $\mathcal{H}_{\mathrm{Hol}} = [\omega_0 - \sum_k \sqrt{2}\lambda_k\omega_k q_k]\sigma^\dagger\sigma + \sum_k \omega_k c_k^\dagger c_k$ should lead to a dephasing of the ground-excited coherence $\langle\sigma\rangle$. One reason is the similarity to the pure dephasing of a two-level transition subjected to a noisy laser undergoing evolution with the Hamiltonian $[\omega_0 + \dot{\varphi}(t)]\sigma^\dagger\sigma$ where the frequency is continuously shaken by a white noise stochastic term of zero average and obeying $\langle\dot{\varphi}(t)\dot{\varphi}(t')\rangle = \gamma_{\mathrm{deph}}\delta(t-t')$. It is straightfoward to show that the time evolution of the coherence in this case becomes $\langle\sigma(t)\rangle = \langle\sigma(0)\rangle\, e^{-i\omega_0 t}e^{-\gamma_{\mathrm{deph}}t}$ such that the correlations of the noise indicate the increase in the linewidth of the transition. Similarly, one could expect that the zero-averaged quantum noise stemming from the shaking of the electronic transition in the Holstein-Hamiltonian would lead to the same kind of effect. However, computing the exact time evolution of the coherence in the interaction picture [with Hamiltonian $\tilde{\mathcal{H}}_{\mathrm{Hol}}(t)$] one obtains:

$$\begin{aligned}\langle\sigma(t)\rangle &= \langle\sigma(0)\rangle\, \mathcal{T}\{e^{-i\int_0^t \mathrm{d}t'\tilde{\mathcal{H}}_{\mathrm{Hol}}(t')}\}e^{-\gamma t} \\ &= \langle\sigma(0)\rangle\, e^{-(\gamma+i\tilde{\omega}_0)t}\,\langle\mathcal{B}(t)\mathcal{B}^\dagger(0)\rangle\,,\end{aligned} \tag{5.26}$$

where the time-ordered integral can be resolved by a second-order Magnus expansion [176], confirming the result already known from the polaron picture. The correlation $\langle\mathcal{B}(t)\mathcal{B}^\dagger(0)\rangle = e^{-\lambda_k^2(2\bar{n}_k+1)}e^{\phi(t)}$

with $\phi(t) = \lambda_k^2 \left[(2\bar{n}_k + 1)\cos(\omega_k t) - i\sin(\omega_k t)\right]$ (for a single mode $\omega_k$) shows a cosine-term similar to the dephasing but which does not continuously increase in time. For small times $t \ll \omega_k^{-1}$, the cosine-term can be expanded and the dephasing rate can be approximated by $\gamma_{\text{deph}} = \lambda_k^2(\bar{n}_k + 1/2)\omega_k^2 t$ while for larger times the rate goes to zero. In the continuum limit, the time-dependent dephasing rate $\gamma_{\text{deph}}(t) = -\Re[\dot{\phi}(t)]$ expresses as

$$\gamma_{\text{deph}}(t) = \int_0^\infty \mathrm{d}\omega \, \frac{J(\omega)}{\omega} \coth\left(\frac{\beta\omega}{2}\right) \sin(\omega t). \tag{5.27}$$

In accordance with Figs. 5.4(a),(b) we can see that linear Holstein coupling can consequently lead to a temperature-dependence of the zero-phonon line if there is a large density of low frequency (long wavelength) phonon modes with $\omega_k < \gamma$ which is the case in 1D but not in higher dimensions. This peculiarity of dephasing in 1D has already been discussed in the literature [173, 174, 177]. It is however also well established within the literature that the major contribution of the experimentally observed temperature-dependent broadening of the zero-phonon line is caused by a higher-order electron-phonon interaction of the form [151, 177–179]

$$\mathcal{H}_{\text{el-phon}}^{\text{quad}} = \sum_{k,k'} \beta_{kk'} q_k q_{k'} \sigma^\dagger \sigma, \tag{5.28}$$

with the coupling constant of the quadratic interaction $\beta_{kk'}$. This form of the interaction can stem either, within the harmonic assumption, from a difference in curvatures between the ground and excited state potential surfaces or from anharmonic potentials.

## 5.6 Cavity-molecule spectroscopy

We now consider coupling to a cavity mode which is driven with amplitude $\eta_c$ and start with a set of coupled Langevin equations for the electric field operator $a$ as well as the polaron operator $\tilde{\sigma} = \mathcal{D}^\dagger \mathcal{B}^\dagger \sigma$ in a frame rotating at the laser frequency $\omega_\ell$:

$$\dot{a} = -[\kappa - i(\omega_\ell - \omega_c)]a - ig\sigma + \sqrt{2\kappa}A_{\text{in}}, \tag{5.29a}$$

$$\dot{\tilde{\sigma}} = -(\gamma + i\tilde{\omega}_0)\tilde{\sigma} - ig\mathcal{D}^\dagger\mathcal{B}^\dagger a + \sqrt{2\gamma}\mathcal{D}^\dagger\mathcal{B}^\dagger\sigma_{\text{in}}, \tag{5.29b}$$

where we defined the effective cavity input $A_{\text{in}} = \eta_c/\sqrt{2\kappa} + a_{\text{in}}$ with zero-average input noise $a_{\text{in}}$. We can formally integrate Eq. (5.29b) and substitute it in Eq. (5.29a):

$$\begin{aligned} \langle \dot{a} \rangle = &- \left[\kappa - i(\omega_\ell - \omega_c)\right] \langle a \rangle \\ &- g^2 \int_{-\infty}^{\infty} \mathrm{d}t' e^{-(\gamma + i\tilde{\omega}_0)(t-t')} \theta(t-t') \left\langle \mathcal{D}(t)\mathcal{D}^\dagger(t') \right\rangle \left\langle \mathcal{B}(t)\mathcal{B}^\dagger(t') \right\rangle \left\langle a(t') \right\rangle + \eta_c \,, \end{aligned} \tag{5.30}$$

where we took the averages and assume factorizability between optical and vibronic/phononic degrees of freedom which is valid assumption if the timescales of vibrational relaxation and cavity decay are separated, e.g., $\Gamma_{\mathrm{m}} \ll \kappa$.[4] We notice that the second term in Eq. (5.31) represents a convolution since the correlation functions $\langle \mathcal{D}(t)\mathcal{D}^{\dagger}(t')\rangle$ and $\langle \mathcal{B}(t)\mathcal{B}^{\dagger}(t')\rangle$ only depend on the time difference $|t - t'|$. Denoting $R(t-t') = e^{-(\gamma+i\tilde{\omega}_0)(t-t')}\theta(t-t') \langle \mathcal{D}(t)\mathcal{D}^{\dagger}(t')\rangle \langle \mathcal{B}(t)\mathcal{B}^{\dagger}(t')\rangle$, the normalized cavity transmission amplitude $t_c$ can be derived from the input-output relation in frequency space as

$$t_c(\omega) = \frac{\kappa}{g^2 R(\omega) - i\omega + [\kappa - i(\omega_\ell - \omega_c)]}, \tag{5.31}$$

where $R(\omega)$ is the Fourier transform of $R(t)$ and describes the bare absorption spectrum of the molecule including electron-phonon, electron-vibron and vibron-phonon coupling. If we neglect electron-phonon interactions ($\lambda_{\text{e-ph}} = 0$) and assume Markovian decay for the vibrational mode, $R(\omega)$ acquires the form

$$R(\omega) = \sum_{n=0}^{\infty}\sum_{l=0}^{n} \frac{L(n)B(n,l)}{(\gamma + n\frac{\Gamma_{\mathrm{m}}}{2}) - i[(\omega-\omega_0) - (n-2l)\nu]}. \tag{5.32}$$

Again, the above expression indicates a series of sidebands with strength determined by the Huang-Rhys factor $\lambda^2$ and dependent on the thermal occupation $\bar{n}$. In the case of large vibrational relaxation $\Gamma_{\mathrm{m}} \gg \gamma$, however, those sidebands are suppressed and the cavity will mostly couple to the ZPL transition. We can then define an effective Rabi frequency for the ZPL

$$g_{\text{eff}} = g \langle \mathcal{D}^{\dagger}\rangle \langle \mathcal{B}^{\dagger}\rangle = g\sqrt{f_{\text{FC}} \cdot f_{\text{DW}}}\,, \tag{5.33}$$

which describes the reduction of oscillator strength due to Franck-Condon and Debye-Waller factors. In Figs. 5.5(a) and (b) we plot the cavity transmission at resonance $\omega_c = \omega_\ell$ for increasing thermal occupation with and without the influence of phonons and find that the splitting of the polariton modes is well described by Eq. (5.33). This also manifests itself in the transmission signal in the Purcell regime characterized by weak coupling $g < |\kappa - \gamma|/2$, but large cooperativity $C = g^2/(\kappa\gamma) \gg 1$. In Figure 5.5(c) we compare the transmission of a pure two-level system (obtained by setting $\lambda = 0$, $\lambda_{\text{e-ph}} = 0$) with a molecule in a solid-state environment. Here the ZPL appears as a dip in the transmission profile with an increase in width $\tilde{\gamma} = \gamma(1 + C_{\text{eff}})$ proportional to the effective cooperativity $C_{\text{eff}} = g_{\text{eff}}^2/(\kappa\gamma)$. As compared to the two-level system case, the coupling to vibrons and phonons leads to a reduction in both width and depth of the antiresonance. If the cavity bandwidth is comparable to the maximum phonon frequency $\omega_{\text{max}}$, the imprint of the phonon wing can also be detected in the transmission signal of the cavity, which is relevant for coupling to plasmonic modes characterized by large bandwidths [22] [see Fig. 5.5(c)]. The sidebands of vibrons typically lie at frequencies

[4] This might not always be fulfilled as the timescales can be comparable (GHz) in experiments.

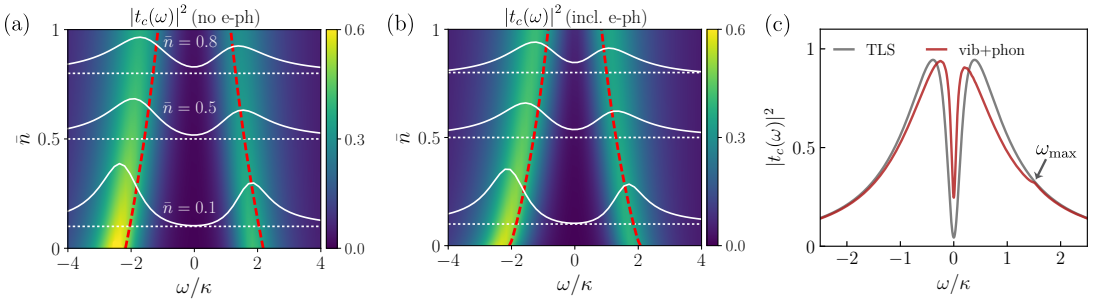


Figure 5.5: *Cavity-molecule spectroscopy*. Normalized cavity transmission $|t_c(\omega)|^2$ at resonance $\omega_c = \omega_\ell$ in strong coupling as a function of frequency and thermal occupation $\bar{n}$ for (a) neglecting electron-phonon coupling and (b) including electron-phonon coupling (using a 3D density of states) for $\lambda = 0.8$, $\lambda^{\text{3D}}_{\text{e-ph}} = 0.03\,\text{ps}^2$. The white lines show cross sections of the transmission profile for different thermal occupations $\bar{n}$. The dashed red lines show the effective Rabi splitting $2g_{\text{eff}}$. Other parameters: $\nu = 6\,\text{THz}$, $\omega_{\max} = 3\,\text{THz}$, $g = \nu/2, \Gamma_{\text{m}} = 0.08\nu$, $\kappa = 1\,\text{THz}$. (c) Comparison of transmission in the Purcell regime between a pure two-level system (TLS) and a molecule subject to electron-vibron and electron-phonon coupling for $\lambda = 0.8$, $\lambda^{\text{3D}}_{\text{e-ph}} = 0.2\,\text{ps}^2$ (exaggerated) at a temperature of $T = 10\,\text{K}$. Other parameters: $\omega_{\max} = 3\,\text{THz} = 1.5\kappa$, $\nu = 6\,\text{THz} = 3\kappa$, $g = 0.35\kappa$.

outside the bandwidth of the cavity $\nu \gg \kappa$ and are consequently unmodified.

## 5.7 Polariton cross-talk and transfer

As shown in the previous sections, vibronic and electron-phonon couplings reduce the oscillator strength of the molecule and lead to decoherence and are consequently considered as detrimental. However such couplings can also lead to new phenomena as they introduce couplings between the polaritonic states which are orthogonal without the presence of vibrations. At low temperatures, this leads to a fast, unidirectional relaxation of the upper polariton into the lower polariton, resulting in dominant emission from the lower polariton (see Figs. 5.5(a),(b)). We derive here an expression for the population transfer between polaritons, showing that for finite thermal occupations of the vibrational mode $\bar{n}$ also a transfer from lower to upper polariton can be activated. Diagonalizing the Jaynes-Cummings part of the Hamiltonian at resonance $\omega_c = \omega_0$ by introducing annihilation operators for upper and lower polariton, $U = (a + \sigma)/\sqrt{2}$ and $L = (a - \sigma)/\sqrt{2}$, the Holstein-Jaynes-Cummings Hamiltonian for a single vibrational mode expresses as

$$\mathcal{H}^{\text{UL}} = \left(\omega_0 + g + \frac{\lambda^2\nu}{2}\right) U^\dagger U + \left(\omega_0 - g + \frac{\lambda^2\nu}{2}\right) L^\dagger L + \nu b^\dagger b - \frac{\lambda\nu}{2}(b^\dagger + b)\left(U^\dagger U + L^\dagger L\right) \tag{5.34}$$
$$+ \frac{\lambda\nu}{2}(U^\dagger L + L^\dagger U)(b^\dagger + b).$$

We can interpret this as two vibrationally-dressed polaritons where the last term describes a coupling between upper and lower polariton. To remove the contributions proportional to $b^\dagger + b$ for the

polaritonic energies, we can perform a polaron transform for both upper and lower polaritonic state

$$\mathcal{U}_{\mathrm{pol,U}} = |g\rangle\langle g| + \mathcal{D}^{\dagger}_{\mathrm{pol}}|U\rangle\langle U|, \qquad \mathcal{U}_{\mathrm{pol,L}} = |g\rangle\langle g| + \mathcal{D}^{\dagger}_{\mathrm{pol}}|L\rangle\langle L|, \tag{5.35}$$

with the the displacement operator $\mathcal{D}^{\dagger}_{\mathrm{pol}} = e^{-\frac{\lambda}{2}(b^{\dagger}-b)}$. Using that $\mathcal{U}_{\mathrm{pol,U}} b \mathcal{U}^{\dagger}_{\mathrm{pol,U}} = b + \frac{\lambda}{2}U^{\dagger}U$ (and similarly for $\mathcal{U}_{\mathrm{pol,L}}$), this gives the transformed Hamiltonian

$$\mathcal{H}^{\mathrm{UL}}_{\mathrm{pol}} = \tilde{\omega}_{+}U^{\dagger}U + \tilde{\omega}_{-}L^{\dagger}L + \nu b^{\dagger}b + \frac{\lambda\nu}{2}(U^{\dagger}L + L^{\dagger}U)(b^{\dagger}+b) + \frac{\lambda^2\nu}{2}(U^{\dagger}L + L^{\dagger}U), \tag{5.36}$$

with $\tilde{\omega}_{\pm} = \omega_0 \pm g + \lambda^2\nu/4$. We notice the additional last term which describes a direct polariton-polariton coupling, which is however negligible in the case of large Rabi splitting $2g \gg \lambda^2\nu$. The interaction between upper and lower polariton is therefore described by

$$\mathcal{H}^{\mathrm{UL}}_{\mathrm{int}} = \frac{\lambda\nu}{2}(U^{\dagger}L + L^{\dagger}U)(b^{\dagger}+b). \tag{5.37}$$

This can be interpreted as an exchange interaction between the polaritons which is mediated by either the destruction or creation of a vibrational quantum. From this one can derive Langevin equations of motion for the polariton operators

$$\frac{\mathrm{d}U}{\mathrm{d}t} = -(\Gamma_{+} + i\tilde{\omega}_{+})U - i\frac{\lambda\nu}{2}L(b^{\dagger}+b) + \sqrt{\kappa}a_{\mathrm{in}} + \sqrt{\gamma}\sigma_{\mathrm{in}}, \tag{5.38a}$$

$$\frac{\mathrm{d}L}{\mathrm{d}t} = -(\Gamma_{-} + i\tilde{\omega}_{-})L - i\frac{\lambda\nu}{2}U(b^{\dagger}+b) + \sqrt{\kappa}a_{\mathrm{in}} - \sqrt{\gamma}\sigma_{\mathrm{in}}, \tag{5.38b}$$

as well as for the populations of upper and lower polaritonic states:

$$\dot{\mathcal{P}}_U = -2\Gamma_{+}\mathcal{P}_U + \lambda\nu\Im\langle U^{\dagger}L(b^{\dagger}+b)\rangle, \tag{5.39a}$$

$$\dot{\mathcal{P}}_L = -2\Gamma_{-}\mathcal{P}_L + \lambda\nu\Im\langle L^{\dagger}U(b^{\dagger}+b)\rangle, \tag{5.39b}$$

with the hybridized decay rates of upper and lower polaritonic state $\Gamma_{\pm} = (\kappa+\gamma)/2$ and one can see that the term $\Im\langle U^{\dagger}L(b^{\dagger}+b)\rangle$ is the one responsible for population transfer between the polaritons. This corresponds to an excitation exchange between the polaritons which is mediated by the creation or destruction of a quantum of the common vibrational mode. After a formal integration of Eqs. (5.38), in the limit of fast vibrational relaxation $\Gamma_{\mathrm{m}} \gg \kappa$ this can be turned into a set of rate equations with an effective excitatation transfer from the upper polariton to the lower polariton $\kappa_{+}$ and a transfer from the lower polariton to the upper polariton $\kappa_{-}$

$$\dot{\mathcal{P}}_U = -(2\Gamma_{+} + \kappa_{+})\mathcal{P}_U + \kappa_{-}\mathcal{P}_L, \tag{5.40a}$$

$$\dot{\mathcal{P}}_L = -(2\Gamma_{-} + \kappa_{-})\mathcal{P}_L + \kappa_{+}\mathcal{P}_U. \tag{5.40b}$$

Under the assumption of weak vibronic coupling as compared to the splitting between upper and lower polaritonic state $\lambda\nu \ll 2g$, the rates can be calculated to first order as (again we assume Markovian decay for the vibration for that sake of simplicity):

$$\kappa_+ = \frac{\lambda^2\nu^2}{2}\Gamma_\mathrm{m}\left[\frac{\bar{n}+1}{\Gamma_\mathrm{m}^2+(\omega_+-\omega_--\nu)^2}+\frac{\bar{n}}{\Gamma_\mathrm{m}^2+(\omega_+-\omega_-+\nu)^2}\right], \tag{5.41a}$$

$$\kappa_- = \frac{\lambda^2\nu^2}{2}\Gamma_\mathrm{m}\left[\frac{\bar{n}+1}{\Gamma_\mathrm{m}^2+(\omega_+-\omega_-+\nu)^2}+\frac{\bar{n}}{\Gamma_\mathrm{m}^2+(\omega_+-\omega_--\nu)^2}\right]. \tag{5.41b}$$

Since the splitting between the polaritons is given by $\omega_+-\omega_- \approx 2g$, one of the terms in the equations above is always off-resonant. Energy transfer between the polaritons occurs if the Rabi splitting is roughly equal to the vibrational frequency $2g \approx \nu$. From Eqs. (5.41) one is then left with two terms, a term from upper to lower polariton proportional to $\bar{n}+1$ and a thermally-activated term proportional to $\bar{n}$ from lower to upper polariton. The ratio between the polaritons is given by $\kappa_-/\kappa_+ = \bar{n}/(\bar{n}+1)$ and tends to unity in the limit $\bar{n} \gg 1$. This ratio can be inferred directly from the polariton heights since for normalized Lorentzians, the height and width are connected. While for single molecules the condition $\omega_+ - \omega_- \approx \nu$ is difficult to achieve for vibrational modes in the THz range, this can be achieved in the collective strong coupling regime for many molecules where the coupling grows as $g\sqrt{\mathcal{N}}$ or for single molecules with phononic modes in the GHz regime. For many molecules coupled to a common cavity mode, however also the energy exchanges between the polaritonic states and the reservoir of dark states becomes important (see chapter 7). We also note that, in a similar fashion to the linear coupling, also quadratic electron-phonon and vibronic coupling gives rise to a vibrationally-mediated polariton cross-talk with coupling $\mathcal{H}_\mathrm{int}^\mathrm{quad} = \beta(U^\dagger L + L^\dagger U)Q^2/2$ (for a single vibrational mode). To this end, one could again derive effective rate equations for the quadratically-mediated population transfer between the polaritons in a similar fashion as for the linear coupling case.

# 6

# Molecular nanorings

Structured subwavelength arrays of quantum emitters allow for the coherent hopping of excitations via the near-field coupling of neighboring dipoles. In addition, they exhibit correlated spontaneous emission and support super- and subradiant collective modes which can be exploited to control the interaction with impinging light. Possible applications range from the design of highly reflective quantum metasurfaces [180], the engineering of platforms showing robust transport of excitation in topological quantum optics [181, 182], to high-fidelity photon storage devices for quantum information processing [99, 183]. Moreover, quantum emitter rings have been proposed to act as coherent light sources on the nanoscale [100].
While subwavelength separations are not easily achieved in standard quantum optics setups, molecular aggregates can feature deeply subwavelength separations on the nanometer scale while retaining the electronic structure of the individual dipole transitions [184]. They can be artificially synthesized in a wide variety of forms such as 1D chains and 2D films and can moreover also be found in nature, in the photosynthetic light-harvesting complexes of plants and bacteria [101, 185]. The downside is the introduction of the inherent vibronic coupling which is typically considered as detrimental. While it is well established that the strong coherent near-field interactions gives rise to delocalized exciton states in molecular aggregates [186, 187], the characterization of the accompanying collective dissipation is usually not considered in such systems as vibronic effects and dephasing are considered to dominate, especially at larger temperatures. It is therefore interesting to treat cooperative dissipative effects to identify the interplay between super- and subradiance and vibrational effects and to derive scaling laws for super- and subradiance in the presence of vibrations.

We consider a ring configuration of identical emitters, as already introduced in section 2.5.b, however now additionally with coupling of the electronic transitions to a single nuclear coordinate (see Fig. 6.1(b)). The total Hamiltonian of the ring is therefore given by

$$\mathcal{H}_{\text{ring}} = \sum_j \left[ (\omega_0 + \lambda^2 \nu)\sigma_j^\dagger \sigma_j + \nu b_j^\dagger b_j - \lambda\nu (b_j^\dagger + b_j)\sigma_j^\dagger \sigma_j \right] + \sum_{j \neq j'} \Omega_{jj'} \sigma_j^\dagger \sigma_{j'}. \tag{6.1}$$

In a first step, we aim to elucidate the influence of vibronic couplings onto the scaling of collective

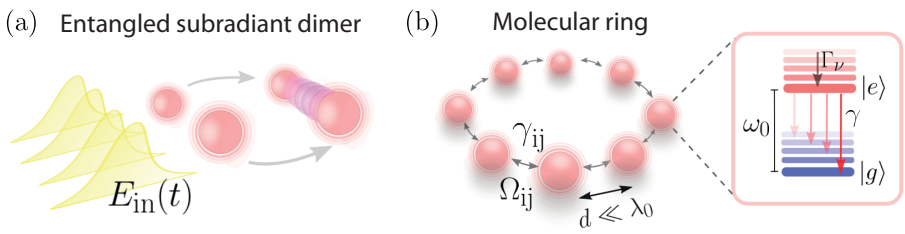


Figure 6.1: *Schematics.* (a) Preparation of an entangled subradiant molecular dimer with subwavelength separation $d \ll \lambda_0$ via an impinging short laser pulse. (b) Schematics of a molecular ring with mutual dipole-dipole interactions at rates $\Omega_{ij}$ as well as collective decay at rates $\gamma_{ij}$. The inset shows branching of electronic transitions between the manifolds of vibrational levels.

emission rates. Results are derived in section 6.1 by averaging over the vibrations in the polaron basis and subsequent transformation to the collective basis of bright (symmetric), typically superradiant and dark (antisymmetric), typically subradiant states, as already introduced in section 2.5.b. We are then in the position to discuss the dispersion relations of excitations propagating along the ring in section 6.2. While averaging over the vibrations in the polaron basis provides a first understanding of how standard radiative properties are modified in the presence of vibronic coupling, another approach consists in moving into a collective basis also for the vibrational degrees of freedom. In such a basis, one can then understand how collective vibrational modes couple between collective electronic states, leading to a coupling between electronic symmetric and antisymmetric states as well as a coupling among antisymmetric states. In section 6.3 we show, first for a molecular dimer and then for a ring, that this leads to a unidirectional flow of population from driven symmetric states to long-lived, entangled antisymmetric dark states, via a process similar to the polariton cross-talk discussed in chapter 5 (schematically illustrated in Fig. 6.1(a)).

## 6.1 Collective effects under vibronic coupling

In a first step, we can apply the polaron transformation $\mathcal{U}_{\rm pol}^\dagger = \prod_j \mathcal{U}_{{\rm pol},j}^\dagger$ to the Hamiltonian Eq. (6.1) such as to diagonalize the whole vibronic Hamiltonian. We are however left with the transformed dipole-dipole interaction as well as the polaron-transformed Lindblad term for spontaneous emission, which now describes dissipation via polaron collapse operators

$$\tilde{\mathcal{L}}_e[\rho] = \sum_{j,j'} \gamma_{jj'} \left[ 2\sigma_j \mathcal{D}_j \rho \mathcal{D}_{j'}^\dagger \sigma_{j'}^\dagger - \{\mathcal{D}_j^\dagger \sigma_j^\dagger \sigma_{j'} \mathcal{D}_{j'}, \rho\} \right]. \tag{6.2}$$

We can now make the assumption that the vibrations are in a thermal state and that the electronic and vibrational states factorize. This leads to a renormalization of the dipole-dipole interaction $\Omega_{jj'}^\lambda = \Omega_{jj'} e^{-\lambda^2(1+2\bar{n})}$ as well as renormalized off-diagonal (or mutual) decay rates as evident from the polaron

transformed Lindblad term

$$\tilde{\mathcal{L}}_e[\rho] = \sum_{jj'} e^{-\lambda^2(1+2\bar{n})(1-\delta_{jj'})}\gamma_{jj'}\left[2\sigma_j\rho\sigma_{j'}^\dagger - \{\sigma_j^\dagger\sigma_{j'},\rho\}\right], \tag{6.3}$$

yielding a reduction by the Franck-Condon factor for a two-molecule term and no changes for single molecule terms. For large $\lambda$ or large thermal occupancies, the off-diagonal elements of the Lindblad term above (corresponding to cooperative emission) vanish, leading to the disappearance of any subradiant or superradiant behavior and the recovery of the independent decay behavior.

The total Hamiltonian can now be diagonalized in terms of the symmetric/antisymmetric operators introduced in section 2.5.b: $\tilde{\mathcal{H}}_{\text{ring}} = \omega_{\mathcal{S}}^\lambda \mathcal{S}^\dagger\mathcal{S} + \sum_{k=1}^{\mathcal{N}-1}\omega_k^\lambda \mathcal{A}_k^\dagger\mathcal{A}_k$. The modified eigenenergies are now given by $\omega_{\mathcal{S}}^\lambda = \omega_0 + \sum_{j=2}^{\mathcal{N}}\Omega_{1j}^\lambda$, for the symmetric states and $\omega_k^\lambda = \omega_0 + \sum_{j=2}^{\mathcal{N}}\Omega_{1j}^\lambda e^{2\pi i(j-1)k/\mathcal{N}}$ for the set of antisymmetric combinations.
Also, the thermally averaged Lindblad term from Eq. (6.3) can now be split into $\mathcal{N}$ decay channels: a symmetric one with loss rate $\gamma_{\mathcal{S}}^\lambda(d)$ and $\mathcal{N}-1$ channels with rates $\gamma_k^\lambda(d)$. These can be expressed as

$$\gamma_{\mathcal{S},k}^\lambda(d) = \gamma\left[1 - e^{-\lambda^2(1+2\bar{n})}\right] + \gamma_{\mathcal{S},k}^{\lambda=0}(d)e^{-\lambda^2(1+2\bar{n})}, \tag{6.4}$$

in terms of the bare rates for zero vibronic coupling

$$\gamma_k^{\lambda=0}(d) = \sum_{j=1}^{\mathcal{N}}\gamma_{1j}(d)e^{i2\pi(j-1)k/\mathcal{N}} \tag{6.5}$$

and $\gamma_{\mathcal{S}}^{\lambda=0}(d) = \sum_{j=1}^{\mathcal{N}}\gamma_{1j}(d)$. Notice that for zero distance and no vibronic couplings, the Dicke superradiance effect with rate $\mathcal{N}\gamma$ is recovered. For larger distances this is effect is reduced; additional reduction appears for nonzero vibronic coupling and temperature. Finally, for large $\lambda$ or $\bar{n}$, a complete washout of superradiance occurs and the first term in the expression above indicates the independent rate $\gamma$ for both symmetric and antisymmetric states.
For a better understanding of the coupling between states of different symmetries, we now perform an analysis in the full Hilbert space, i.e. without tracing over the thermal bath. Instead, intuitive understanding is offered by an additional transformation to a collective basis for the vibrational degrees of freedom as well, introduced via

$$Q_k = \frac{1}{\sqrt{\mathcal{N}}}\sum_{j=1}^{\mathcal{N}} e^{2\pi ijk/\mathcal{N}}(b_j + b_j^\dagger), \tag{6.6}$$

where $k \in \{1,...,\mathcal{N}\}$ (with $k = \mathcal{N}$ corresponding to the symmetric vibrational mode) and with the momentum quadratures satisfying $[Q_k, P_{k'}] = 2i\delta_{kk'}$.[1] The ring Hamiltonian in this collective basis

[1]Note that here we chose a different normalization of the collective quadratures as in section 2.6.

expresses as

$$\mathcal{H}_{\text{ring}}^{\text{coll}} = \omega_{\mathcal{S}}(Q_{\mathcal{N}})\mathcal{S}^{\dagger}\mathcal{S} + \sum_{k=1}^{\mathcal{N}-1} \omega_k(Q_{\mathcal{N}})\mathcal{A}_k^{\dagger}\mathcal{A}_k - \frac{\lambda\nu}{\sqrt{\mathcal{N}}}\sum_{k=1}^{\mathcal{N}-1}(Q_k\mathcal{S}^{\dagger}\mathcal{A}_k + \text{h.c.}) \tag{6.7}$$
$$- \frac{\lambda\nu}{\sqrt{\mathcal{N}}}\sum_{k\neq k'}^{\mathcal{N}-1}(Q_{k-k'}\mathcal{A}_k^{\dagger}\mathcal{A}_{k'} + \text{h.c.}) + \nu\sum_{k=1}^{\mathcal{N}} b_k^{\dagger}b_k,$$

where the energies of the collective states are shifted by the contribution of the symmetric vibrational mode (for $k = 1, \ldots, \mathcal{N}$)

$$\omega_k(Q_{\mathcal{N}}) = \omega_0 + \lambda^2\nu + \Omega_k - \lambda\nu Q_{\mathcal{N}}/\sqrt{\mathcal{N}}. \tag{6.8}$$

The $Q_{\mathcal{N}}$-dependent energy shifts can be removed by a polaron transformation in the collective basis

$$\mathcal{U}_{\text{pol,coll}}^{\dagger} = \prod_{k=1}^{\mathcal{N}}\mathcal{U}_{\mathcal{A}_k}^{\dagger} = \prod_{k=1}^{\mathcal{N}} e^{i\lambda P_{\mathcal{N}}\mathcal{A}_k^{\dagger}\mathcal{A}_k/\sqrt{\mathcal{N}}}, \tag{6.9}$$

which transforms the symmetric vibrational mode as

$$\mathcal{U}_{\text{pol,coll}}^{\dagger} Q_{\mathcal{N}} \mathcal{U}_{\text{pol,coll}} = Q_{\mathcal{N}} + \sum_{k=1}^{\mathcal{N}} \frac{2}{\sqrt{\mathcal{N}}}\mathcal{A}_k^{\dagger}\mathcal{A}_k \tag{6.10}$$

and leads to a renormalization of the collective state energies as $\tilde{\omega}_k = \omega_0 + \lambda^2\nu/2 + \Omega_k$. The crucial terms in Eq. (6.7) are however the interaction term coupling the symmetric states with the antisymmetric states as well as the introduction of a coupling among the antisymmetric states themselves. In the mesoscopic limit where a very large number of such states exist, the existence of many channels of energy loss from the symmetric subspace to all other subspaces orthogonal to it, then allows to derive an effective unidirectional Markovian loss dynamics for the symmetric operator, as we show in chapter 7 for a mesoscopic disordered ensemble inside a cavity, where similar interactions between collective states occur.

## 6.2 Dispersion relation

We now consider a single excitation hopping along the molecular ring. The single excitation subspace is especially relevant for the case of mesoscopic systems of quantum emitters which are weakly driven. Dipole-dipole interactions induce tunneling behavior between neighboring emitters, allowing the understanding of the system's properties in terms of the band structure or dispersion relations for the propagation of collective excitations. Non-Hermitian, dissipative effects such as superradiance and

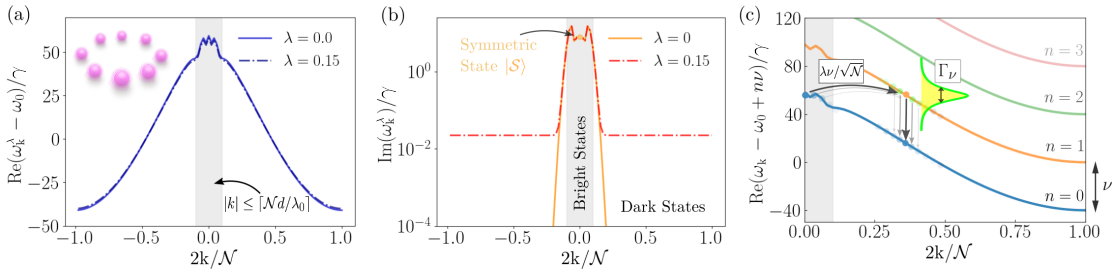


Figure 6.2: *Dispersion relation of molecular nanoring.* (a) Single-excitation dispersion relation in the first Brillouin zone for a ring of $\mathcal{N} = 100$ molecules at zero temperature with nearest-neighbour separation $d = 0.05\lambda_0$ (dipole orientation transverse to ring). Bright states enclosed by the shaded region are characterized by a mode number $|k| \leq \lceil \mathcal{N}d/\lambda_0 \rceil$ whereas the region beyond is occupied by dark states. (b) Bright states feature a finite decay rate with the symmetric state located at $k = 0$. For $d \ll \lambda_0$ the dark state decay rates are approximately given by $\gamma_k^\lambda \sim (1-\exp[-\lambda^2])\gamma$ whereas the bright state decay rate approaches $\gamma_\mathcal{S}^\lambda \sim \gamma + \exp[-\lambda^2](\mathcal{N}-1)\gamma$ . (c) Dispersion relation in the full vibrational Hilbert space: states with $n$ vibrational energy quanta are shifted by $n\nu$ with respect to the zero-vibrational states. Vibrations lead to coherent population transfer between bright states and dark states with a coupling strength $\lambda\nu/\sqrt{\mathcal{N}}$ for $\mathcal{N}$ molecules which is followed by a non-radiative vibrational relaxation into the dark state with zero vibrations at a rate $\Gamma \gg \gamma$.

subradiance of such linear systems can also be understood in terms of the localization of collective states within or outside a light cone.

Restricting the Hilbert space to a single excitation, one can recast the polaron-averaged Hamiltonian and Lindbladian into the following non-Hermitian form by disregarding the recycling term in the Lindbladian

$$\mathcal{H}_{\text{ring}} = \omega_0 \sum_j^{\mathcal{N}} \sigma_j^\dagger \sigma_j + \sum_{jj'}^{\mathcal{N}} \left[\Omega_{jj'}^\lambda(d) - i\gamma_{jj'}^\lambda(d)\right] \sigma_j^\dagger \sigma_{j'}. \tag{6.11}$$

As mentioned in the previous section, the collective basis offers a diagonalization of the dynamics. In the single excitation subspace, one can proceed with diagonalization of both coherent and incoherent parts by writing $\tilde{\mathcal{H}}_{\text{ring}} = \sum_{k=1}^{\mathcal{N}} \bar{\omega}_k^\lambda \mathcal{A}_k^\dagger \mathcal{A}_k$ where by definition the symmetric state operator corresponds to the case $\mathcal{S} = \mathcal{A}_{k=\mathcal{N}}$. The eigenenergies and the decay rates are given by the real and imaginary part of the complex eigenvalues

$$\bar{\omega}_k^\lambda = \omega_0 + \Omega_k^\lambda(d) - i\gamma_k^\lambda(d). \tag{6.12}$$

The excitations can be understood in terms of the quasimomentum along the ring $q = 2\pi k/(\mathcal{N}d)$ where due to the periodicity we can define the first Brillouin zone as running from $k = 0, \pm 1, \ldots \pm \lceil (N-1)/2 \rceil$ with $\lceil x \rceil$ the ceiling function. Note that the center of the Brillouin zone $k = 0$ corresponds now to the symmetric mode and the edges at $k_\pm = \pm\lceil (\mathcal{N}-1)/2 \rceil$ to the most subradiant modes with degenerate eigenvalues $\omega_{k_\pm}$. This can be understood from the wave equation $q^2 + q_\perp^2 = (2\pi/\lambda_0)^2$ which asks that for modes with $|q| \geq 2\pi/\lambda_0$, the radial electric field compo-

nents are evanescent, i.e., exponentially decaying, and the excitation is guided along the ring. Modes inside the region $|q| \leq 2\pi/\lambda_0$ on the other hand have electric field components transverse to the ring and are therefore radiating energy away into the vacuum.

In Fig. 6.2(a) the dispersion relation for a ring of $\mathcal{N} = 100$ molecules is shown for the cases with and without vibronic coupling $\lambda$. The region defined by the integer number $|k| \geq \lceil \mathcal{N} d/\lambda_0 \rceil$ is occupied by dark states as shown in Fig. 6.2(b) whose decay rates are decreasing exponentially with the number of emitters for $\lambda = 0$ as $\gamma_k^{\lambda=0}/\gamma \sim e^{-\mathcal{N}}$. For molecules with a non-zero vibronic coupling $\lambda$ the exponential scaling gets strongly modified and the decay rates for eigenstates with mode number $k$ are approximately given by $\gamma_k^{\lambda}/\gamma \sim (1 - e^{-\lambda^2})$.

While Figs. 6.2(a) and (b) show the real and imaginary parts of the dispersion relation using the reduced, polaron-averaged Hamiltonian, one can also discuss the dispersion relation in the collective basis including vibrations unsing the Hamiltonian (6.7). The coupling term between symmetric and antisymmetric states illuminates the fact that the presence of vibrations causes a coherent transfer of population between the symmetric mode $\mathcal{S}$ and the dark modes $\mathcal{A}_k$. The coupling strength between the symmetric mode in the vibrational ground state and a dark mode with one vibrational excitation is given by $\lambda\nu/\sqrt{\mathcal{N}}$ which is illustrated in Fig. 4.2(c). Since the vibrational relaxation rate $\Gamma$ is fast compared on the timescale $1/\gamma$ of the electronic decay rate, the population relaxes quickly to the dark state with no vibrational quanta. In general the coupling strength between $\mathcal{S}$ with $n$ vibrations and mode $\mathcal{A}_k$ with $n+1$ vibrations is given by $\langle \mathcal{S}, n_k | \mathcal{H} | \mathcal{A}_k, n_k + 1 \rangle = \sqrt{(n_k+1)/\mathcal{N}}\lambda\nu$ where the Hamiltonian includes the vibrational degrees of freedom and in particular the terms in the Hamiltonian (6.7) which mediate the coherent transfer. The transfer rate for a ring geometry is derived in section 6.3 and generally the large vibrational linewidth $\Gamma \gg \gamma$ will create resonances between multiple modes thereby enhancing the population transfer to the dark state manifold.

## 6.3 Subradiant state preparation

Let us now revisit the vibronic dimer from section 2.6. We show that the coupling between symmetric (bright) and antisymmetric (dark) collective states, combined with the vibrational relaxation can lead to an efficient preparation of long-lived quantum entangled states of the two chromophores. The mechanism is similar to the polariton cross-talk discussed in section 5.7 and also reminiscent of the FRET process between donor and acceptor molecules discussed in section 3.4, where coherent energy exchanges followed by quick vibrational relaxation can lead to a unidirectional flow of energy.

The dimer Hamiltonian of electronic and vibrational degrees of freedom in the collective basis expresses as

$$\mathcal{H}_{\text{dim}} = \omega_{\mathcal{S}}(Q_+)\mathcal{S}^\dagger\mathcal{S} + \omega_{\mathcal{A}}(Q_+)\mathcal{A}^\dagger\mathcal{A} + \frac{\nu}{4}\sum_{k=\pm}(Q_k^2 + P_k^2) - \frac{\lambda\nu}{\sqrt{2}}Q_-(\mathcal{S}^\dagger\mathcal{A} + \mathcal{A}^\dagger\mathcal{S}), \quad (6.13)$$

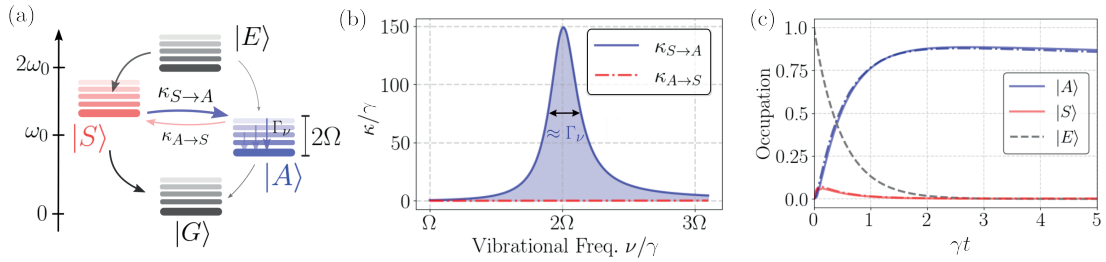


Figure 6.3: *Transfer to subradiant state.* (a) Energy diagram showing population transfer between symmetric (superradiant) and antisymmetric (subradiant) collective states via their mutual coupling to the vibrational bath. (b) Energy transfer rates between the symmetric and antisymmetric dimer state as a function of the vibrational frequency. (c) Time evolution of a fully inverted molecular dimer. The fully excited state decays exponentially via the symmetric state which transfers energy to the antisymmetric state. The analytical results in dashed-dotted lines show a good agreement. Parameters are $\nu = 2\Omega, d = \lambda_0/40, \Gamma = 30\gamma, \lambda = 0.1, \Omega(d) \approx 191.1\gamma$ and the dipole orientation is chosen perpendicular to the dimer axis.

where the collective states frequencies become now operators including the symmetric vibrational coordinate $\omega_\mathcal{S} = \tilde{\omega}_0 + \Omega - \lambda\nu Q_+/\sqrt{2}$ and $\omega_\mathcal{A} = \tilde{\omega}_0 - \Omega - \lambda\nu Q_+/\sqrt{2}$. While the symmetric and antisymmetric states are orthogonal without vibrations, this is not true anymore in the presence of vibrations. The last term in Eq. (6.13) can mediate transfer of excitation between the bright and dark state through the annihilation or creation of a vibrational quantum of the relative motion coordinate. The equations of motion for the populations of the collective states can be obtained as

$$\partial_t \langle \mathcal{S}^\dagger \mathcal{S} \rangle = -2\gamma_\mathcal{S} \langle \mathcal{S}^\dagger \mathcal{S} \rangle - \sqrt{2}\lambda\nu \Im \langle \mathcal{S}^\dagger \mathcal{A} Q_- \rangle \,, \tag{6.14a}$$

$$\partial_t \langle \mathcal{A}^\dagger \mathcal{A} \rangle = -2\gamma_\mathcal{A} \langle \mathcal{A}^\dagger \mathcal{A} \rangle - \sqrt{2}\lambda\nu \Im \langle \mathcal{A}^\dagger \mathcal{S} Q_- \rangle \,. \tag{6.14b}$$

Under the assumption that the vibrational relaxation is fast as compared to the coherent coupling $\Gamma \gg \lambda\nu$ as well as all other decay rates, a perturbative set of rate equations for the populations $\mathcal{P}_\mathcal{S} = \langle \mathcal{S}^\dagger \mathcal{S} \rangle$ and $\mathcal{P}_\mathcal{A} = \langle \mathcal{A}^\dagger \mathcal{A} \rangle$ can be obtained [2]

$$\dot{\mathcal{P}}_\mathcal{S} = -(2\gamma_\mathcal{S} + \kappa_{\mathcal{S}\to\mathcal{A}})\mathcal{P}_\mathcal{S} + \kappa_{\mathcal{A}\to\mathcal{S}} p_\mathcal{A}, \tag{6.15a}$$

$$\dot{\mathcal{P}}_\mathcal{A} = -(2\gamma_\mathcal{A} + \kappa_{\mathcal{A}\to\mathcal{S}})\mathcal{P}_\mathcal{A} + \kappa_{\mathcal{S}\to\mathcal{A}} p_\mathcal{S}, \tag{6.15b}$$

with transfer rate from the symmetric to antisymmetric state

$$\kappa_{\mathcal{S}\to\mathcal{A}} = \frac{\lambda^2\nu^2\Gamma}{\Gamma^2 + (2\Omega - \nu)^2}. \tag{6.16}$$

The transfer from the antisymmetric to symmetric state $\kappa_{\mathcal{A}\to\mathcal{S}}$ has a similar expression, however with a term $(2\Omega + \nu)$ present in the denominator. For $\Omega > 0$ the resonance condition is given by $2\Omega = \nu$ leading to unidirectional transfer from the symmetric to the antisymmetric state while the back trans-

[2] The calculation is similar to the calculation of the polariton cross-talk in section 5.7.

fer is off-resonant and therefore suppressed (see Fig. 6.3(b)). In Fig. 6.3(c), we plot the time dynamics of a dimer initialized in the fully excited state $|E\rangle$ under this resonance condition. Initial decay to the symmetric state is followed immediately by a rapid transfer to the antisymmetric state, causing only a small temporary population in the symmetric state and a large accumulation of population in the antisymmetric state. Remarkably, this can lead to a near-unity population in the antisymmetric state even for moderate vibronic coupling strengths $\lambda$. Since vibrational frequencies are on the order of $\nu/2\pi \sim 10$ THz and the spontaneous emission rate is on the order of $\gamma/2\pi \sim 10$ MHz, this requires dipole-dipole shifts on the order of $\sim 10^6\,\gamma$ which can be achieved by dimers with nm separations.

The dark state preparation scheme presented for the dimer can be extended to configurations of many molecules. To this end, we have performed numerical simulations showing the drive of collective states which are not accessible via direct illumination but are populated via the incoherent, vibrationally mediated transfer. Therefore, we consider a laser drive modeled by a pulsed excitation with electric field amplitude

$$E_{\text{in}}(t) = \Omega_\ell(t) \sum_{j=1}^{\mathcal{N}} \left( e^{i\mathbf{k}_\ell \cdot \mathbf{R}_j} e^{-i\omega_\ell t} \sigma_j^\dagger + e^{-i\mathbf{k}_\ell \cdot \mathbf{R}_j} e^{i\omega_\ell t} \sigma_j \right). \tag{6.17}$$

The laser pulse is considered to be impinging from the ring plane with a linear polarization $\mathbf{e}_z$ coinciding with the dipole orientation of the molecules. The time dependence is a Gaussian envelope of the form $\Omega_\ell(t) = \eta \exp[-(t-t_0)^2/\tau^2]$, with maximum amplitude $\eta$, duration $\tau$ and the wave vector of the laser is assumed to be $\mathbf{k}_\ell = k_0 \mathbf{e}_x$. In Fig. 6.4(a), the enhanced absorption profile for a ring of $\mathcal{N} = 7$ molecules signals the transfer of population from the symmetric, laser accessible collective state to a number of initially dark states. The increase in the linewidth is simply given by the sum of

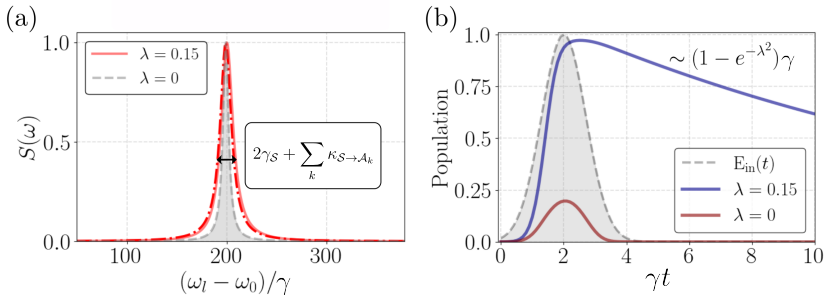


Figure 6.4: *Absorption spectrum of molecular nanoring.* (a) Absorption spectrum in steady state for a ring with $\mathcal{N} = 7$ molecules with the linewidth of the symmetric state broadened by the sum of the energy transfer rates to the dark state manifold. The dashed-dotted line is a Lorentzian with linewidth given by $2\gamma_S + \sum_k \kappa_{S\to A_k}$ and maximum at $\omega_\ell = \omega_0 + \Omega_S^{\lambda=0}$. (b) Laser pulse with a Gaussian time profile as in Eq. (6.17) with $\eta = 2.5\,\gamma, t_0 = 2/\gamma, \tau = 1/\gamma$. The laser frequency $\omega_\ell$ is tuned to the superradiant mode $k = 0$. The single excitation manifold is populated almost with unity and decays with a subradiant rate $\sim \gamma(1 - e^{-\lambda^2})$ afterwards. Further parameters for both plots are $d = \lambda_0/30, \Gamma = 100\gamma, \lambda = 0.15, \nu = 120\gamma$.

all transfer rates to the dark state manifold which are obtained as a generalization of the dimer result

$$\sum_k \kappa_{\mathcal{S}\to\mathcal{A}_k} = \sum_k \frac{\lambda^2\nu^2\Gamma}{\Gamma^2 + (\Omega_{\mathcal{S}} - \Omega_{\mathcal{A}_k} - \nu)^2}. \tag{6.18}$$

In Fig. 6.4(b) the total population is shown following a pulsed excitation with the laser frequency tuned to the superradiant mode $\omega_\ell = \omega_{\mathcal{S}}$. For a non-zero vibronic coupling, most of the population is trapped into dark states with a decay rate equal to $\gamma(1 - e^{-\lambda^2})$ as predicted in section 6.2.

# 7

# Cavity QED with mesoscopic disordered molecular ensembles

Many of the intriguing phenomena observed in the field of molecular polaritonics over the last years are a consequence of the collective enhancement of the vacuum Rabi splitting proportional to the square root of the number of molecules $g\sqrt{\mathcal{N}}$. While this scaling results from the hybridization of a single *bright* superposition state with light, there exists a large number of $\mathcal{N}-1$ *dark* states indirectly coupled to light owing to disorder [52, 61, 188–191] which also participate in the dynamics and are thought to have a crucial impact on some observed properties [55, 190, 192]. We take an open system dynamics approach to derive an analytical rate for the irreversible loss of energy from polaritonic states into the dark state manifold accompanied by a degradation of the VRS. Importantly, a natural averaging occurs in our formalism in the mesoscopic limit of $\mathcal{N}\to\infty$, as opposed to previous treatments involving averaging over many disorder realizations [193–196]. We analyze the cavity transmission of a disordered ensemble in section 7.1 and introduce the collective dark-bright basis in section 7.2 which sheds light onto the relevant interactions and which is similar to the symmetric/antisymmetric basis used in the previous chapter. Finally, in section 7.3 we show how this leads to a generally non-Markovian decay of polaritonic states into the dark state manifold and derive scaling laws for the decay rate in the Markovian limit.

## 7.1 Cavity transmission

We consider $\mathcal{N}$ molecules indexed by $j=1,\dots,\mathcal{N}$ with electronic states $|g\rangle_j$ and $|e\rangle_j$ separated by energy splittings $\omega_j$ which are inhomogeneously distributed around a central frequency $\omega_0$ with a distribution function $p(\delta)$ normalized to unity $\int_{-\infty}^{\infty}p(\delta)\mathrm{d}\delta=1$. The inhomogeneous broadening originates from the fact that each molecule sees a slightly different environment, leading to a shift of the electronic transition frequency. We choose a Gaussian distribution for the frequency disorder

$$p(\delta)=\frac{1}{\sqrt{2\pi w^2}}e^{-\delta^2/(2w^2)}. \tag{7.1}$$

We write each molecule's transition frequency as $\omega_0 + \delta_j$ where the average around the central frequency vanishes $\langle \delta_j \rangle_{\mathrm{cl}} = 0$ while the variance is $\langle \delta_j^2 \rangle_{\mathrm{cl}} = w^2$.

We will first show, that the effect of frequency disorder is the occurrence of additional dark state resonances in the linear spectral response of the cavity when driven with an external weak laser source. The pump is modeled via the following Hamiltonian

$$\mathcal{H}_d = i\eta_c(a^\dagger e^{-i\omega_\ell t} - a e^{i\omega_\ell t}), \tag{7.2}$$

where the pump frequency is $\omega_\ell$ and the weak drive amplitude is $\eta_c$. The equations of motion for the averages $\alpha = \langle a \rangle$ and $\beta_j = \langle \sigma_j \rangle$ under Tavis-Cummings evolution then read

$$\dot{\beta}_j = -i(\omega_0 - \omega_\ell + \delta_j - i\gamma)\beta_j - i g_j \alpha, \tag{7.3a}$$

$$\dot{\alpha} = -i(\omega_c - \omega_\ell - i\kappa)\alpha - i\textstyle\sum_j g_j^* \beta_j + \eta_c. \tag{7.3b}$$

In steady state, the equations above lead to the normalized cavity amplitude transmission $t_c = \kappa \langle a \rangle / \eta_c$ expressed as

$$t_c = \kappa \left[ \kappa + i(\omega_c - \omega_\ell) + \sum_{j=1}^{\mathcal{N}} \frac{|g_j|^2}{\gamma + i(\omega_0 - \omega_\ell) + i\delta_j} \right]^{-1}, \tag{7.4}$$

valid also for positioning and orientational disorder with randomized couplings $g_j$. While in the following we will restrict the discussion to identical couplings $g_j = g$, a simple estimate can be made on the influence of orientational disorder, arising from randomly oriented dipole moments with respect to the cavity polarization direction. The effect of this disorder manifest itself in the definition of the bright and dark modes where the bright mode is now given by $\hat{B} = \left(1/\sqrt{\sum_{j=1}^{\mathcal{N}} |g_j|^2}\right) \sum_{j=1}^{\mathcal{N}} g_j^* \sigma_j$ which results in the equation of motion for the cavity field amplitude

$$\dot{\alpha} = -i(\omega_c - \omega_\ell - i\kappa)\alpha - i\tilde{g}_{\mathcal{N}} \mathcal{B} + \eta_c, \tag{7.5}$$

where $\tilde{g}_{\mathcal{N}} = \sqrt{\sum_{j=1}^{\mathcal{N}} |g_j|^2}$. Taking the limit for large numbers of molecules $\mathcal{N}$ where we can describe the random orientation with respect to the electric field of the cavity mode $a$ by $g_j = g\cos(\theta_j)$ where $\theta_j \in [0, \pi]$, we obtain

$$\tilde{g}_{\mathcal{N}}^2 \approx \frac{\mathcal{N} g^2}{\pi} \int_0^\pi \mathrm{d}\theta \, \cos^2(\theta) = \frac{\mathcal{N} g^2}{2}. \tag{7.6}$$

Orientational disorder of the molecular dipoles therefore leads to a trivial renormalization of the coupling from $g\sqrt{\mathcal{N}} \to g\sqrt{\mathcal{N}/2}$. The cavity transmission is illustrated in Figs. 7.1(a) and (b). For a

few molecules and a given realization of disorder, Fig. 7.1(a) shows two polaritonic peaks at $\pm g\sqrt{\mathcal{N}}$ obtained by the hybridization of a symmetric collective state to the cavity field. Non-zero disorder introduces couplings to $\mathcal{N}-1$ orthogonal antisymmetric states visible in the cavity transmission as narrow unequal height peaks between the polaritons. In the mesoscopic limit [Fig. 7.1(b)], a natural averaging occurs which leads to a smoothing out of the additional peaks. However, the height of the polaritons is decreased while the splitting between them is slightly increased. We quantitatively address this in the following in the transformed bright-dark basis.

## 7.2 Dark-bright state dynamics

For zero disorder case $w = 0$, as already discussed in section 2.7, the cavity couples only to a symmetric superposition $\hat{B} = \sum_j \sigma_j/\sqrt{\mathcal{N}}$, i.e., a *bright state*, with a collective coupling strength $g_{\mathcal{N}} = \sqrt{\mathcal{N}}g$. Frequency disorder introduced coupling to $\mathcal{N}-1$ other combinations which define *dark states* and which are generally obtainable by a Gram-Schmidt algorithm that leads to all vectors orthogonal to the bright state one and to each other. However, for the simplest case $g_j = g$ a straightforward choice of coefficients is indicated by a discrete Fourier transform

$$\hat{D}_k = \frac{1}{\sqrt{\mathcal{N}}} \sum_{j=1}^{\mathcal{N}} e^{-i2\pi jk/\mathcal{N}} \sigma_j. \tag{7.7}$$

We index the dark state manifold for $k = 1, \ldots, \mathcal{N}-1$ and for $k = \mathcal{N}$ we recover the bright state $\hat{D}_{\mathcal{N}} = \hat{B}$. The equations of motion for averages $\mathcal{B} = \langle \hat{B} \rangle$, $\mathcal{D} = \langle \hat{D} \rangle$ and $\alpha$ become (in a frame

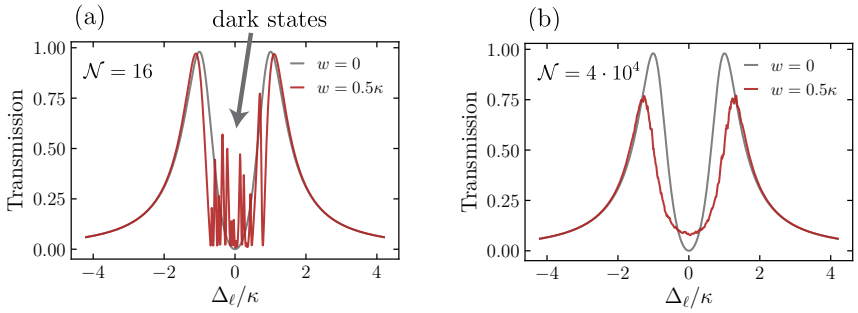


Figure 7.1: *Cavity transmission of a disordered ensemble.* (a) Transmission for $\mathcal{N} = 16$, $g = 0.25$, $\gamma = 10^{-2}$ (in units of $\kappa$) for $w = 0$ and $w = 0.5$ as a function of the laser detuning. The dark states appear as narrow peaks in the middle. (b) In the mesoscopic limit ($\mathcal{N} = 4 \times 10^4$) with $g = 0.005$ (such that $g\sqrt{\mathcal{N}}$ is the same as in (a)), the dark state peaks are smoothed out. However, loss into dark states leads to a reduction of polariton height and increase of splitting (red, $w = 0.5\kappa$) compared to the $w = 0$ case (gray).

rotating at the central emitter frequency $\omega_0$)

$$\dot{\mathcal{D}}_k = -\gamma \mathcal{D}_k - i \sum_{k'=1}^{\mathcal{N}} \Delta_{kk'} \mathcal{D}_{k'} - i g_{\mathcal{N}} \alpha \delta_{k\mathcal{N}}, \tag{7.8a}$$

$$\dot{\alpha} = -(\kappa - i\Delta_c)\alpha - i g_{\mathcal{N}}^* \mathcal{D}_{\mathcal{N}} + \eta_c \tag{7.8b}$$

and the couplings are defined as Fourier transforms of the disorder distribution

$$\Delta_{kk'} = \frac{1}{\mathcal{N}} \sum_{j=1}^{\mathcal{N}} \delta_j e^{-i2\pi j(k-k')/\mathcal{N}}. \tag{7.9}$$

For $k = \mathcal{N}$, the equations above indicate that the bright state is the only one coupled to the cavity mode with the expected collective rate $g_{\mathcal{N}}$. However, disorder induces couplings to the whole manifold of dark states and within the dark manifold as well.
We can more compactly write the equations above as $\partial_t \mathbf{V} = -i\mathbf{M}_{\text{coll}}\mathbf{V}$ where $\mathbf{V} = (\mathcal{D}_1, \ldots, \mathcal{D}_{\mathcal{N}-1}, \mathcal{B}, \alpha)^\top$ and the drift matrix is

$$\mathbf{M}_{\text{coll}} = \begin{pmatrix} (\bar{\delta} - i\gamma) & \Delta_{12} & \ldots & \Delta_{1\mathcal{N}} & 0 \\ \Delta_{21} & (\bar{\delta} - i\gamma) & \ldots & \Delta_{2\mathcal{N}} & 0 \\ \vdots & \vdots & \ddots & \vdots & \vdots \\ \Delta_{\mathcal{N}1} & \Delta_{\mathcal{N}2} & \ldots & (\bar{\delta} - i\gamma) & g_{\mathcal{N}} \\ 0 & 0 & \ldots & g_{\mathcal{N}}^* & -i(\Delta_c + \kappa) \end{pmatrix}, \tag{7.10}$$

where the average of the disorder distribution (expected to vanish in the mesoscopic limit) is $\bar{\delta} = \Delta_{kk} = \sum_{j=1}^{\mathcal{N}} \delta_j/\mathcal{N}$. This matrix can be put in a more convenient form due to the structure of the terms $\Delta_{l\mathcal{N}}$. Considering the relations $\Delta_{\mathcal{N}l} = \Delta_{\mathcal{N}-l\mathcal{N}}$ and $\Delta_{1\mathcal{N}} = \Delta_{\mathcal{N}\mathcal{N}-1}$, we can rewrite the matrix as

$$\mathbf{M}_{\text{coll}} = \begin{pmatrix} \mathbf{M}_{\text{red}} & \mathbf{p} \\ \mathbf{p}^\dagger & (\delta - i\kappa) \end{pmatrix}, \tag{7.11}$$

with $\mathbf{p} = (0, \ldots, 0, g_{\mathcal{N}})^\top$. Notice that here we have separated between the cavity and matter states by introducing the reduced matrix of dimensions $\mathcal{N} \times \mathcal{N}$ referring to the matter part which assumes the following form

$$\mathbf{M}_{\text{red}} = \begin{pmatrix} (\bar{\delta} - i\gamma) & \Delta_{\mathcal{N}-1\mathcal{N}} & \Delta_{\mathcal{N}-2\mathcal{N}} & \ldots & \Delta_{1\mathcal{N}} \\ \Delta_{1\mathcal{N}} & (\bar{\delta} - i\gamma) & \Delta_{\mathcal{N}-1\mathcal{N}} & \ldots & \Delta_{2\mathcal{N}} \\ \Delta_{2\mathcal{N}} & \Delta_{1\mathcal{N}} & (\bar{\delta} - i\gamma) & \ldots & \Delta_{3\mathcal{N}} \\ \vdots & \vdots & \vdots & \ddots & \vdots \\ \Delta_{\mathcal{N}-1\mathcal{N}} & \Delta_{\mathcal{N}-2\mathcal{N}} & \Delta_{\mathcal{N}-3\mathcal{N}} & \ldots & (\bar{\delta} - i\gamma) \end{pmatrix}. \tag{7.12}$$

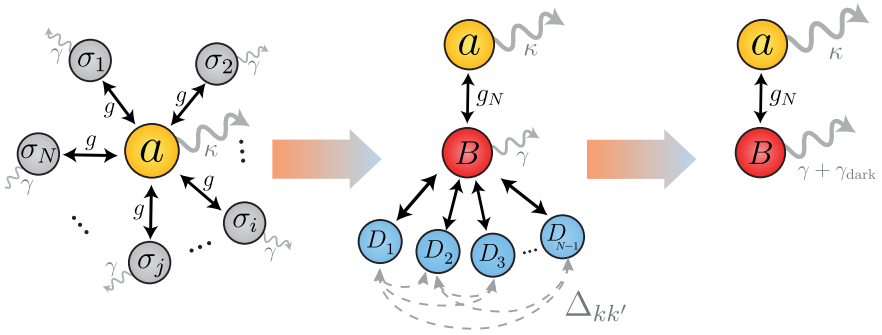


Figure 7.2: *Schematics of the elimination procedure.* To obtain the reduced dynamics for the bright mode only, in a first step, a transformation to the collective basis sees the cavity mode coupled to the bright mode and the bright mode coupled to the dark modes (in addition, the dark modes are also coupled to each other). Elimination of the dark reservoir then gives rise to a renormalized loss rate $\gamma + \gamma_{\text{dark}}$ for the bright mode.

The eigenvectors of the cyclic matrix $\mathbf{M}_{\text{red}}$ are given by

$$\mathbf{v}_j = (1/\sqrt{\mathcal{N}})(1, \xi_j, \xi_j^2, \ldots, \xi_j^{\mathcal{N}-1})^\top, \tag{7.13}$$

for $j \in \{1, \ldots, \mathcal{N}-1\}$ where $\xi_j = \exp(i2\pi j/\mathcal{N})$. The eigenvalues are given by

$$\lambda_j = (\bar{\delta} - i\gamma) + \Delta_{\mathcal{N}-1\mathcal{N}}\xi_j + \cdots + \Delta_{1\mathcal{N}}\xi_j^{\mathcal{N}-1}. \tag{7.14}$$

## 7.3 Elimination of dark reservoir

In the limit of many molecules, the dark states can be seen as a reservoir inducing a dissipative dynamics for the bright mode. We are therefore interested in obtaining the reduced dynamics for the bright mode only. The procedure we perform to this end is illustrated in Fig. 7.2 showing first the identification of a bright state and then the elimination of the dark reservoir resulting in an effective unidirectional loss of energy from the polaritonic states. The elimination of the dark state manifold can be done in an exact way without making a Markovian approximation, which would imply that the dark state reservoir has no memory and therefore it would allow to set all derivatives of $\mathcal{D}_k$ to zero. Instead, one can write the quantum Langevin equations for bright and dark modes and formally integrate the equations for $\mathcal{D}_k$ to obtain (as detailed in Appendix E)

$$\dot{\mathcal{B}}(t) = -(\gamma + i\bar{\delta})\mathcal{B}(t) - \int_{-\infty}^{\infty} \mathrm{d}t' f(t-t')\mathcal{B}(t') - ig_{\mathcal{N}}\alpha, \tag{7.15}$$

with a memory kernel describing a generally non-Markovian loss process. In the mesoscopic limit, one finds (see Appendix E)

$$f(t-t') \approx \theta(t-t')w^2 e^{-i(\bar{\delta}-i\gamma)(t-t')}\,\mathrm{sinc}(2w(t-t')). \tag{7.16}$$

Now one can identify a Markovian limit as a particular case of wide frequency distributions $w \gg \gamma$. The Markovian result is then simply reproduced by seeing that the kernel $f(t-t')$ naturally tends to a delta function. In such a case the treatment can be simplified by setting all derivatives to zero in Eqs. (7.8) to find the dark state amplitudes

$$\mathcal{D}_k = -\sum_{k'} (\boldsymbol{\mathcal{M}}^{-1})_{kk'} \Delta_{k'\mathcal{N}} \mathcal{B}. \tag{7.17}$$

The matrix $\boldsymbol{\mathcal{M}}$ has dimensions $(\mathcal{N}-1)\times(\mathcal{N}-1)$ and represents the part of the matrix $\mathbf{M}_{\rm red}$ referring to the dark states only

$$\boldsymbol{\mathcal{M}} = \begin{pmatrix} (\bar{\delta}-i\gamma) & \Delta_{12} & \dots & \Delta_{1(\mathcal{N}-1)} \\ \Delta_{21} & (\bar{\delta}-i\gamma) & \dots & \Delta_{2(\mathcal{N}-1)} \\ \vdots & \vdots & \ddots & \vdots \\ \Delta_{(\mathcal{N}-1)1} & \Delta_{(\mathcal{N}-1)2} & \dots & (\bar{\delta}-i\gamma) \end{pmatrix}. \tag{7.18}$$

Replacing the eliminated variables into the equation of motion for the bright mode we obtain the effective dissipative dynamics

$$\dot{\mathcal{B}} = -i\left[(\bar{\delta}-\delta_{\rm dark}) - i(\gamma+\gamma_{\rm dark})\right]\mathcal{B} - ig_{\mathcal{N}}\alpha, \tag{7.19}$$

where the effect of the reservoir is to induce an effective frequency shift $\delta_{\rm dark}$ and loss rate $\gamma_{\rm dark}$ obtained as the real and imaginary parts, respectively, of the following expression

$$\begin{aligned} \delta_{\rm dark} + i\gamma_{\rm dark} &= \sum_{k,k'=1}^{\mathcal{N}-1} \Delta_{\mathcal{N}k} (\boldsymbol{\mathcal{M}}^{-1})_{kk'} \Delta_{k'\mathcal{N}} \\ &= \frac{1}{\mathcal{N}^2} \sum_{j,j'=1}^{\mathcal{N}} \sum_{k,k'=1}^{\mathcal{N}-1} \delta_j \delta_{j'} (\boldsymbol{\mathcal{M}}^{-1})_{kk'} e^{-i2\pi(jk-j'k')/\mathcal{N}}. \end{aligned} \tag{7.20}$$

Some more insight can be obtained by evaluating the norm of the coupling vector for the dark states $\mathbf{m} = (\Delta_{1\mathcal{N}}, \dots, \Delta_{\mathcal{N}-1\mathcal{N}})^\top$. Here, we obtain

$$\begin{aligned} \mathbf{m}^\dagger \mathbf{m} &= \sum_{k=1}^{\mathcal{N}-1} |\Delta_{\mathcal{N}k}|^2 = \sum_{k=1}^{\mathcal{N}-1} \frac{1}{\mathcal{N}^2} \left( \sum_{j,j'=1}^{\mathcal{N}} \delta_j \delta_{j'} e^{i2\pi k(j-j')/\mathcal{N}} \right) \\ &= \frac{1}{\mathcal{N}^2} \sum_{j,j'=1}^{\mathcal{N}} \delta_j \delta_{j'} (\mathcal{N}\delta_{jj'} - 1) = \frac{1}{\mathcal{N}} \sum_{j}^{\mathcal{N}} \delta_j^2 - \left( \frac{1}{\mathcal{N}} \sum_{j}^{\mathcal{N}} \delta_j \right)^2 = {\rm Var}(\delta), \end{aligned} \tag{7.21}$$

which is the variance of the frequency distribution. In the case of a Gaussian distribution for the disorder we therefore obtain ${\rm Var}(\delta) = w^2$. We can use this result to rewrite $\mathbf{m} = w\hat{\mathbf{m}}$, where $\hat{\mathbf{m}}$ is

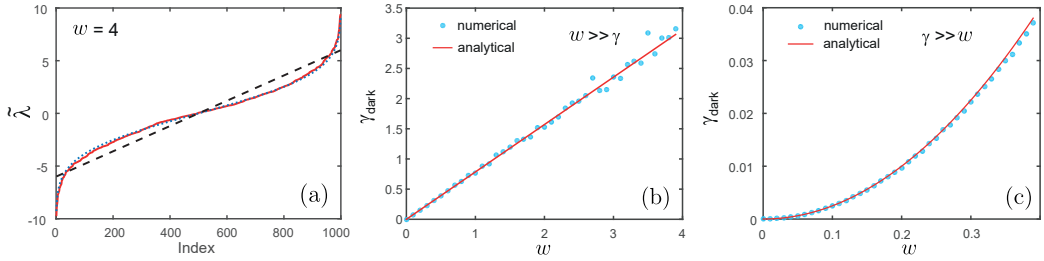


Figure 7.3: *Approximations for the derivation of the loss rate.* (a) Sorted eigenvalue distribution for $\mathcal{N} = 10^3$ and $w = 4$ (in units of $\kappa$). The solid line shows the real part of the eigenvalues $\tilde{\lambda}_{1,\ldots,\mathcal{N}-1}$ of the matrix $\boldsymbol{\mathcal{M}}$ while the dashed line gives the linear eigenvalue distribution fit used in the derivation to determine $\gamma_{\text{dark}}$. The blue dotted line shows the quantile of the corresponding Gaussian distribution. (b) The blue dots give the numerical derivation of $\gamma_{\text{dark}}$ averaged over many disorder realizations (400) for $\mathcal{N} = 100$ as a function of the width (standard deviation) $w$ of the disorder distribution. The solid red line shows the approximation with $\gamma_{\text{dark}} = (\pi/4)w$. We have used $\gamma = 10^{-2}$. (c) In the case that $\gamma \gg w$ we find good agreement of the numerical data blue dots with the relation $\gamma_{\text{dark}} = w^2/\gamma$ given by the red line for $\gamma = 4$.

the normalized vector of $\mathbf{m}$. This allows us to further evaluate the expression in Eq. (7.20) to

$$\delta_{\text{dark}} + i\gamma_{\text{dark}} = \mathbf{m}^\dagger \boldsymbol{\mathcal{M}}^{-1}\mathbf{m} = w^2 \hat{\mathbf{m}}^\dagger \boldsymbol{\mathcal{M}}^{-1}\hat{\mathbf{m}} = w^2 \hat{\mathbf{c}}^\dagger \tilde{\mathbf{D}}^{-1}\hat{\mathbf{c}}, \tag{7.22}$$

where $\boldsymbol{\mathcal{M}} = \mathbf{T}\tilde{\mathbf{D}}\mathbf{T}^\dagger$ with the diagonal matrix $\tilde{\mathbf{D}}$ and $\hat{\mathbf{c}} = \mathbf{T}^\dagger\hat{\mathbf{m}}$. Since $\tilde{\mathbf{D}}^{-1}$ is diagonal, we can find the expression

$$\delta_{\text{dark}} + i\gamma_{\text{dark}} = w^2 \sum_{j=1}^{\mathcal{N}-1} |\hat{c}_j|^2 (\tilde{\mathbf{D}}^{-1})_{jj} \approx w^2 \sum_{j=1}^{\mathcal{N}-1} |\hat{c}_j|^2 \tilde{\lambda}_j^{-1}, \tag{7.23}$$

which is the weighted average over the eigenvalues $\tilde{\lambda}_j^{-1}$ of the matrix $\boldsymbol{\mathcal{M}}^{-1}$ times the variance of the distribution. Since the eigenvalues of $\boldsymbol{\mathcal{M}}$ follow the form $\lambda_{1,\ldots,\mathcal{N}-1} = \bar{\delta} - i\gamma - \tilde{\lambda}_{1,\ldots,\mathcal{N}-1}$, where $\tilde{\lambda}_{1,\ldots,\mathcal{N}-1} \in \mathbb{R}$, we obtain

$$\delta_{\text{dark}} + i\gamma_{\text{dark}} = w^2 \sum_{j=1}^{\mathcal{N}-1} |\hat{c}_j|^2 \frac{1}{\bar{\delta} - i\gamma - \tilde{\lambda}_j}. \tag{7.24}$$

For large $\mathcal{N}$ where $\bar{\delta} \to 0$ we finally obtain the expression

$$\delta_{\text{dark}} + i\gamma_{\text{dark}} = \left( w^2 \sum_{j=1}^{\mathcal{N}-1} |\hat{c}_j|^2 \frac{-\tilde{\lambda}_j}{\tilde{\lambda}_j^2 + \gamma^2} \right) + i \left( w^2 \sum_{j=1}^{\mathcal{N}-1} |\hat{c}_j|^2 \frac{\gamma}{\tilde{\lambda}_j^2 + \gamma^2} \right). \tag{7.25}$$

In the case that $\gamma \gg \tilde{\lambda}_{1,\ldots,\mathcal{N}-1}$ which is given if $\gamma \gg w$, we can obtain a solution for $\gamma_{\text{dark}}$ which is obtained from

$$\delta_{\text{dark}} + i\gamma_{\text{dark}} \approx \left( w^2 \sum_{j=1}^{\mathcal{N}-1} |\hat{c}_j|^2 \frac{-\tilde{\lambda}_j}{\gamma^2} \right) + i \left( \frac{w^2}{\gamma} \sum_{j=1}^{\mathcal{N}-1} |\hat{c}_j|^2 \right) = \left( -\frac{w^2}{\gamma^2} \sum_{j=1}^{\mathcal{N}-1} |\hat{c}_j|^2 \tilde{\lambda}_j \right) + i \left( \frac{w^2}{\gamma} \right), \quad (7.26)$$

since $\sum_{j=1}^{\mathcal{N}-1} |\hat{c}_j|^2 = 1$. Since the eigenvalues $\tilde{\lambda}_{1,\ldots,\mathcal{N}-1}$ are equally distributed around zero as shown in Fig. 7.3(a) and the weights can be roughly approximated by $|\hat{c}_j|^2 \approx 1/(\mathcal{N}-1)$ (due to the fact that $\langle |\hat{c}_j|^2 \rangle = 1/(\mathcal{N}-1)$), the frequency shift becomes $\delta_{\text{dark}} \to 0$ for large $\mathcal{N}$ and $\gamma_{\text{dark}} = w^2/\gamma$.
An approximation can be performed in the case $\tilde{\lambda}_j \gg \gamma$ for most $j \in \{1, \ldots, \mathcal{N}-1\}$. Here we set again $|\hat{c}_j|^2 \approx 1/(\mathcal{N}-1)$ and we obtain

$$\begin{aligned} \delta_{\text{dark}} + i\gamma_{\text{dark}} &\approx \left( \frac{w^2}{\mathcal{N}-1} \sum_{j=1}^{\mathcal{N}-1} \frac{-\tilde{\lambda}_j}{\tilde{\lambda}_j^2 + \gamma^2} \right) + i \left( \frac{w^2}{\mathcal{N}-1} \sum_{j=1}^{\mathcal{N}-1} \frac{\gamma}{\tilde{\lambda}_j^2 + \gamma^2} \right) \\ &\approx -\frac{w}{2q} \int_{-qw}^{qw} \mathrm{d}\tilde{\lambda} \frac{\tilde{\lambda}}{\tilde{\lambda}^2 + \gamma^2} + i \frac{w\gamma}{2q} \int_{-qw}^{qw} \mathrm{d}\tilde{\lambda} \frac{1}{\tilde{\lambda}^2 + \gamma^2} \\ &\approx i \frac{w\gamma}{2q} \left[ \frac{2}{\gamma} \arctan\left( \frac{qw}{\gamma} \right) \right] \approx i \frac{\pi}{2q} w, \end{aligned} \quad (7.27)$$

where we have assumed that the eigenvalues $\tilde{\lambda}_j$ are linearly distributed from $-qw$ to $qw$ where $q$ is an adjustment or fitting parameter. This is a rather rough approximation of the real eigenvalue distribution depicted in Fig. 7.3(a). In reality, the eigenvalue distribution follows $\tilde{\lambda}_j = \sqrt{2\pi} w \, \mathrm{erf}^{-1}(2j/\mathcal{N} - 1)$ for $j \in \{1, \ldots, \mathcal{N}-1\}$ when $\mathcal{N} \to \infty$, which is the so-called quantile function of the Gaussian distribution, expressed in terms of the inverse error function. The best approximation is given for $q = 2$ resulting in $\gamma_{\text{dark}} = (\pi/4)w$ as shown in Fig. 7.3(b) while $\delta_{\text{dark}} = 0$. In total, we therefore obtain the

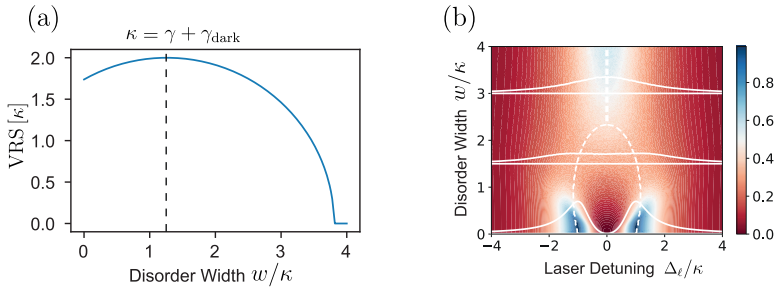


Figure 7.4: *Behavior of the VRS.* (a) VRS with increasing frequency disorder $w$. The maximum of $g_{\mathcal{N}}$ is reached when $\kappa = \gamma + \gamma_{\text{dark}}$. (b) Exact numerical results for the cavity transmission as a function of the width $w$ for $\mathcal{N} = 4 \times 10^4$ and $g = 0.005\kappa$. Dashed line shows the maxima of the transmission under the Markovian approximation.

simple scaling laws for the decay into the dark state manifold

$$\gamma_{\text{dark}} = \begin{cases} w^2/\gamma & \text{for} \quad \gamma \gg w \\ \pi w/4 & \text{for} \quad w \gg \gamma \end{cases}. \tag{7.28}$$

From here we can deduce the dependence of the VRS on disorder which can be obtained by diagonalizing the dynamics in the reduced cavity-bright state subspace to lead to

$$\text{VRS} \approx \Im\left\{2\sqrt{(\gamma + \gamma_{\text{dark}} - \kappa)^2/4 - g_{\mathcal{N}}^2}\right\}. \tag{7.29}$$

The VRS is illustrated in Fig. 7.4(a) as a function of increasing disorder. The initial increase of the polariton splitting occurs in the case $\kappa > \gamma$ as the maximum value of $2g_{\mathcal{N}}$ is reached when $\gamma + \gamma_{\text{dark}} = \kappa$. The complete degradation of the strong coupling condition occurs when the disorder level is of the order of the cavity photon loss. The graphically check the validity of the Markovian approximation for the derivation of the VRS in Fig. 7.4(b) by comparison with exact numerical results. Generally, the Markovian approximation underestimates the effects of disorder a little bit for small degrees of disorder but otherwise we find good agreement.

While we have focused on purely electronic disorder here, let us finally briefly remark how vibronic coupling could be incorporated. In some sense, the action of vibronic coupling is very similar to electronic disorder, since vibronic coupling simply can be seen as a time-dependent shift of the electronic excited state. Considering $\mathcal{N}$ molecules, each coupled to a single nuclear coordinate, in the presence of vibronic coupling the dark-bright couplings from Eq. (7.9) become now Fourier transforms of the vibrational displacements

$$\Delta_{kk'} = -\frac{\lambda\nu}{\mathcal{N}} \sum_{j=1}^{\mathcal{N}} (b_j + b_j^\dagger) e^{-i2\pi j(k-k')/\mathcal{N}}, \tag{7.30}$$

which is identical to the interactions between dark and bright modes analyzed for the free space molecular rings in chapter 6. There, by going into a collective basis also for the vibrational degrees of freedom, we showed how this leads to a unidirectional flow of energy into the dark states. The difference here is that the molecular bright mode is additionally hybridized with the cavity field, giving rise to upper and lower polaritonic states where the latter is typically lower in energy than the dark state reservoir. This would then enable a process mediated by vibrational resonances where the upper polariton decays into the dark state reservoir which then decays into the lower polariton [54]. Depending on the energy scales of the system, this process would compete with the direct polariton-polariton coupling discussed in chapter 5 [54].

Another alternative approach was taken in Ref. [4]. There, for a dense molecular ensemble, we com-

bined the effects of vibronic coupling and near-field dipole-dipole interactions into an effective FRET model describing hopping of excitation between the molecules inside the cavity. This leads to an effective disorder in the decay rates of the molecules which opens up a decay channel into the reservoir of dark states similar to frequency disorder.

# 8

# Discussion and Outlook

In this thesis, we have investigated the open system dynamics of molecules coupled to light and interacting with each other. To this end, in chapter 3, we have developed a stochastic approach based on quantum Langevin equations for the description of coherent and incoherent molecular dynamics. The strengths of the PLE method lie in the inclusion of an arbitrary number of vibrational modes at any temperature and a simple derivation of spectroscopic quantities by a formal integration of the equations of motion. Let us stress here again that, in principle, the method is applicable to all systems where electron-phonon or electron-vibration couplings play a role.
Generally speaking, in the future it would be interesting to go beyond the relatively simple models for molecular dynamics discussed here. This could include considering more realistic potential energy surfaces beyond the harmonic approximation or considering non-adiabatic dynamics such as occuring at conical intersections. It has been shown that non-adiabatic dynamics can also be induced by the collective strong coupling of a molecular ensemble to a cavity mode [197, 198].

In chapter 4 we have applied the PLE method to Floquet engineering of infrared-active molecules and have shown how strong driving of the vibrations modifies the optical absorption and gives rise to a control over the vibronic sidebands. Let us remark that this describes Floquet engineering of a dissipative system which is not widely discussed in the literature as standard Floquet techniques are typically restricted to the Hamiltonian level and extensions to include dissipative dynamics are non-trivial [199, 200]. The strength of the PLE is however that all quantities can be obtained by an integration of the equations of motion and therefore we do not rely on standard Floquet techniques such as e.g. Floquet-Magnus expansion. Our approach could be extended to the level of many molecules and could e.g. find application in controlling the flow of energy by effectively modulating the intermolecular coupling for the hopping of excitation. Similar ideas have already been proposed in the literature [149, 201].

In chapter 5 we have extended the PLE to describe the experimentally relevant scenario of molecules immersed in crystalline host environments and additionally coupled to confined cavity modes. We have shown how electron-vibron and electron-phonon couplings imprint themselves on the optical absorption and cavity output field. The results from our simplified model could be readily compared

to real experimental data or ab-initio calculations obtained from density functional theory [89]. While we have only considered coupling to acoustic bulk phonons, in a next step, the method could be extended to also include coupling to optical phonons. In our first principle derivation, this would imply adding at least a second atom to the unit cell of the host crystal and would result in an additional spectral density for the coupling of electronic transitions to optical phonons. On a different note, we started investigating the dynamics of molecules interacting with polar solvents, with possible applications for the description of chemical reaction kinetics such as electron transfer and proton transfer reactions [202]. Here, similar interactions are occurring between the molecular degrees of freedom and the bath coordinates and we speculate that we can transfer some of the developed formalism.

In chapter 6 we have analyzed the cooperative radiative properties of molecular ensembles in ring configurations. We have found that a collective basis description provides insight into how the symmetric collective state couples to dark, antisymmetric states via collective molecular vibrations. We have shown that this coupling can be exploited to prepare long-lived dark states via dissipative vibrational relaxation processes. In the low excitation regime, we have analyzed the open system band diagram and found the imprint of the vibronic coupling on both energy and loss rate dispersions. Molecular rings supplemented with an additional, incoherently pumped central gain molecule could serve as candidates for the realization of coherent nanoscale light sources [5].

In chapter 7 we have investigated the decay of polaritonic states into the reservoir of dark states for a disordered ensemble of molecules in the Markovian and non-Markovian regime and derived analytical scaling laws for the behavior of the VRS in the Markovian regime. We have used a Tavis-Cummings model which suffices to describe the polariton dynamics but might loose validity as some experiments operate on the brink of the ultrastrong coupling regime where the collective coupling becomes on the order of the transition frequency [203–205] and where the counter-rotating terms which are neglected in the Tavis-Cummings Hamiltonian become important. It would be interesting to investigate the ultrastrong coupling regime which has been shown to lead to interesting new phenomena and open questions from the theoretical side such as e.g. a breakdown of gauge invariance [206, 207].

# A

# Dipole-dipole coupling functions

The expression for the near-field coupling function $F(kR)$ in Eq. (2.44) can be brought into a more convenient form widely used in the literature by expressing the nabla operator in spherical coordinates

$$\nabla_{\mathbf{R}} = \partial_R \mathbf{e}_R + \frac{1}{R}\partial_\theta \mathbf{e}_\theta + \frac{1}{R\sin\theta}\partial_\varphi \mathbf{e}_\varphi. \tag{A.1}$$

Assuming the dipoles to be aligned along the $z$ direction $\mathbf{e_d} = \mathbf{e}_z$ with $\mathbf{e}_z = \cos\theta \mathbf{e}_R - \sin\theta \mathbf{e}_\theta$, we can express

$$\mathbf{e_d} \cdot \nabla_{\mathbf{R}} = \cos\theta\, \partial_R - \frac{\sin\theta}{R}\partial_\theta, \tag{A.2}$$

Calculating the derivatives, one obtains

$$F(kR) = (1-\cos^2\theta)\frac{\sin(kR)}{kR} + (1-3\cos^2\theta)\left[\frac{\cos(kR)}{(kR)^2} - \frac{\sin(kR)}{(kR)^3}\right], \tag{A.3}$$

where $\theta$ is the angle enclosed by the dipole moment of the emitters and the connection vector $\mathbf{R}$. The calculation of $G(kR)$ which characterizes the collective decay involves evaluation of the principal value integral Eq. (2.46). One obtains

$$G(kR) = (1-\cos^2\theta)\frac{\cos(kR)}{kR} - (1-3\cos^2\theta)\left[\frac{\sin(kR)}{(kR)^2} + \frac{\cos(kR)}{(kR)^3}\right]. \tag{A.4}$$

# B

# Derivation of FRET rate

We provide here a derivation of the FRET rate starting from Eqs. (3.26) of the main text. Formal integration of the equation of motion for the acceptor gives

$$\begin{aligned}\sigma_A^\dagger(t) =&\sigma_A(0)e^{-(\gamma_A-i\omega_A)t}\mathcal{D}_A(0)\mathcal{D}_A^\dagger(t) \\ &+\int_0^t \mathrm{d}t' e^{-(\gamma_A-i\omega_A)(t-t')}\left[i\Omega\sigma_D^\dagger(t')+\sqrt{2\gamma}\sigma_{\mathrm{in},A}^\dagger(t')\right]\mathcal{D}_A(t')\mathcal{D}_A^\dagger(t).\end{aligned} \tag{B.1}$$

Due to the quick vibrational relaxation, we can make a great simplification by neglecting the backaction of the acceptor's dipole moment onto the donor and assume free evolution for the donor

$$\dot{\tilde{\sigma}}_D \approx -\left(\gamma_D+i\omega_D\right)\tilde{\sigma}_D+\sqrt{2\gamma}\tilde{\sigma}_{\mathrm{in},D}. \tag{B.2}$$

Integrating this, one can calculate the term $2\Omega\Im\langle\sigma_A^\dagger\sigma_D\rangle$ which requires the four-point correlation function (assuming $t\geq t'\geq 0$ and $t\gg 1/\Gamma_D$)

$$\langle\mathcal{D}_D(0)\mathcal{D}_D^\dagger(t')\mathcal{D}_D(t)\mathcal{D}_D^\dagger(0)\rangle = e^{-\lambda_D^2}e^{\lambda_D^2 e^{-(\Gamma_D-i\nu_D)(t-t')}}e^{-\lambda_D^2 e^{-(\Gamma_D+i\nu_D)t'}}e^{\lambda_D^2 e^{-(\Gamma_D-i\nu_D)t'}}, \tag{B.3}$$

where the four-operator correlation function can be reduced to a two-operator correlation function by commuting $\mathcal{D}_D^\dagger(0)$ with $\mathcal{D}_D(t)$ and $\mathcal{D}_D^\dagger(t')$ and using that $\mathcal{D}_D(0)\mathcal{D}_D^\dagger(0)=\mathbf{1}$. Under the assumption of $\Gamma_D,\Gamma_A\gg\gamma_D,\gamma_A$, one can finally arrive at an expression for the energy transfer rate showing proportionality to the donor population $2\Omega\langle\sigma_A^\dagger\sigma_D\rangle=\kappa_{\mathrm{ET}}\mathcal{P}_D(t)$ (assuming $\gamma_D=\gamma_A$):

$$\kappa_{\mathrm{ET}}=\sum_{n_D,n_A}\frac{2\Omega^2 s_{\lambda_D}^{n_D}s_{\lambda_A}^{n_A}(n_D\Gamma_D+n_A\Gamma_A)}{(n_D\Gamma_D+n_A\Gamma_A)^2+[\Delta-n_D\nu_D-n_A\nu_A]^2}. \tag{B.4}$$

The denominator of the above expression asks that the resonance condition $\omega_D-n_D\nu_D=\omega_A+n_A\nu_A$ is fulfilled, i.e., fluorescence lines of the donor $|e_D,0\rangle\rightarrow|g_D,n_D\rangle$ have to overlap with absorption lines of the acceptor $|g_A,0\rangle\rightarrow|e_A,n_A\rangle$, both of which are weighted by the respective Franck-Condon factors. In the case of many vibrational modes $n_\nu$ for donor and acceptor, we can generalize the result by writing general displacements $\mathcal{D}_A=\prod_{k=1}^{n_\nu}\mathcal{D}_A^k$ and $\mathcal{D}_D=\prod_{k=1}^{n_\nu}\mathcal{D}_D^k$ for all vibrational modes.

The equations of motion can then be expressed in the same form as in Eqs. (3.26)

$$\dot{\tilde{\sigma}}_D = -(\gamma + i\omega_D)\,\tilde{\sigma}_D - i\Omega\tilde{\sigma}_A\mathcal{D}_A\mathcal{D}_D^\dagger + \sqrt{2\gamma}\tilde{\sigma}_{\mathrm{in},D}, \tag{B.5a}$$

$$\dot{\tilde{\sigma}}_A = -(\gamma + i\omega_A)\,\tilde{\sigma}_A - i\Omega\tilde{\sigma}_D\mathcal{D}_D\mathcal{D}_A^\dagger + \sqrt{2\gamma}\tilde{\sigma}_{\mathrm{in},A}, \tag{B.5b}$$

except that now the displacement is produced by all modes. We assume that the two molecules have the same vibrational properties $\langle \mathcal{D}_A^k(t')\mathcal{D}_A^{k,\dagger}(t)\rangle = \langle \mathcal{D}_D^k(t')\mathcal{D}_D^{k,\dagger}(t)\rangle$. This leads to a generalized energy transfer rate

$$\kappa_{\mathrm{ET}} = \sum_{\{m_k=0\}}^{\infty}\sum_{\{l_k=0\}}^{\infty} 2\prod_{k=1}^{n_\nu} e^{-2\lambda_k^2}\frac{\lambda_k^{2(m_k+l_k)}}{m_k!l_k!}\frac{\sum_{k=1}^{n}(m_k+l_k)\Gamma_k\Omega^2}{[\sum_{k=1}^{n}(m_k+l_k)\Gamma_k]^2 + [\Delta - \sum_{k=1}^{n}(m_k+l_k)\nu_k]^2}. \tag{B.6}$$

Here the sums go over all indices $\{m_k\} = m_1, \ldots, m_n$ and $\{l_k\} = l_1, \ldots, l_n$ referring to the possible occupancies of all $n_\nu$ vibrational modes of the two involved molecules.

# C

# Optical response of infrared-dressed molecule

We provide here a brief derivation of the momentum correlation function, displacement correlation function and resulting absorption spectrum for the infrared-dressed molecule discussed in chapter 4.

### Momentum correlation function

For the calculation of the momentum correlation function it is convenient to go to Fourier space, using the definition

$$O(\omega) = \mathcal{F}\{O(t)\} = \frac{1}{\sqrt{2\pi}} \int_{-\infty}^{\infty} \mathrm{d}t\, O(t) e^{i\omega t}. \tag{C.1}$$

In Fourier space, the set of equations (4.8) can be solved for the momentum variable

$$p(\omega) = \chi_m(\omega) \left[\xi(\omega) + \eta_d \sqrt{\pi} \left(\delta(\omega + \omega_d) + \delta(\omega - \omega_d)\right)\right], \tag{C.2}$$

with the mechanical susceptibility $\chi_m(\omega) = i\omega(\omega^2 + 2i\Gamma\omega - \nu^2)^{-1}$. The momentum correlation function can then be obtained from the inverse Fourier transform

$$\langle p(t)p(t')\rangle = \frac{1}{2\pi} \int_{-\infty}^{\infty} \mathrm{d}\omega \int_{-\infty}^{\infty} \mathrm{d}\omega'\, e^{-i\omega t} e^{-i\omega' t'} \langle p(\omega)p(\omega')\rangle, \tag{C.3}$$

which for $\Gamma \ll \nu$ can be estimated as (averages over single noise terms vanish and $\chi_m(-\omega) = \chi_m^*(\omega)$):

$$\langle p(t)p(t')\rangle = \tag{C.4}$$
$$\frac{\eta_d^2}{2} \left[e^{-(\Gamma + i\nu)(t-t')} + 2|\chi_m(\omega_d)|^2 \cos(\omega_d(t-t')) + \chi_m(\omega_d)^2 e^{-i\omega_d(t+t')} + \chi_m^*(\omega_d)^2 e^{i\omega_d(t+t')}\right].$$

Approximating $\chi_m(\omega_d) \approx \frac{1}{2} \frac{1}{\Gamma - i(\omega_d - \nu)}$, this can be expressed as

$$\langle p(t)p(t')\rangle = \frac{1}{2} \left[e^{-(\Gamma + i\nu)(t-t')} + 2|\beta|^2 \cos\left(\omega_d(t-t')\right) + \beta^2 e^{-i\omega_d(t+t')} + (\beta^*)^2 e^{i\omega_d(t+t')}\right]. \tag{C.5}$$

Furthermore, one can easily obtain

$$\langle p(t)\rangle = \frac{1}{\sqrt{2\pi}}\int_{-\infty}^{\infty} \mathrm{d}\omega\, e^{-i\omega t}\,\langle p(\omega)\rangle = \frac{1}{\sqrt{2}}\left(\beta^* e^{i\omega_d t} + \beta e^{-i\omega_d t}\right), \tag{C.6}$$

with $\beta = (\eta_d/2)/\left[\Gamma - i(\omega_d - \nu)\right]$.

### Displacement correlation function and absorption spectrum

In the case of (approximately) resonant driving of the vibrational mode $\omega_d \approx \nu$, the vibrations will be steered into a coherent state with average vibron occupancy given by $\langle b^\dagger b\rangle = |\beta|^2 = \frac{(\eta_d/2)^2}{\Gamma^2+(\omega_d-\nu)^2}$ and $\langle p(t)\rangle \neq 0$. The displacement correlation function then becomes non-stationary and is given by (making use of Isserlis' theorem)

$$\begin{aligned}\langle \mathcal{D}(t)\mathcal{D}^\dagger(t')\rangle &= \langle e^{-i\sqrt{2}\lambda p(t)} e^{i\sqrt{2}\lambda p(t')}\rangle = \langle e^{-i\sqrt{2}\lambda(p(t)-p(t'))}\rangle\, e^{\lambda^2[p(t),p(t')]} \\ &= \langle \sum_m \frac{(-i\sqrt{2}\lambda)^{2m}}{(2m)!}\left(P(t,t') - \langle P(t,t')\rangle\right)^{2m}\rangle\, e^{\lambda^2[p(t),p(t')]} e^{-i\sqrt{2}\lambda\langle P(t,t')\rangle} \\ &= e^{-\lambda^2\langle (P(t,t')-\langle P(t,t')\rangle)^2\rangle} e^{\lambda^2\langle [p(t),p(t')]\rangle} e^{-i\sqrt{2}\lambda\langle P(t,t')\rangle} = e^{-\lambda^2} e^{\lambda^2 e^{-(\Gamma+i\nu)(t-t')}} e^{-i\sqrt{2}\lambda\langle P(t,t')\rangle}.\end{aligned} \tag{C.7}$$

where we denoted $P(t,t') = p(t) - p(t')$ and made use of the fact that the variance of coherent states is identical to vacuum states $\langle p(t)^2\rangle - \langle p(t)\rangle^2 = 1/2$. Around the vibrational resonance this becomes ($\beta \approx \beta^*$)

$$\langle \mathcal{D}(t)\mathcal{D}^\dagger(t')\rangle = e^{-\lambda^2} e^{\lambda^2 e^{-(\Gamma+i\nu)(t-t')}} e^{-2i\lambda|\beta|(\cos(\omega_d t)-\cos(\omega_d t'))}. \tag{C.8}$$

The dipole moment can then be expressed as

$$\langle \sigma(t)\rangle = \eta_p \int_{-\infty}^{t} \mathrm{d}t' e^{-(\tilde{\gamma}-i\Delta_p)(t-t')} e^{-2i\lambda\eta_d[\sin(\omega_d t)-\sin(\omega_d t')]/\omega_d} e^{-\lambda^2} e^{\lambda^2 e^{-(\Gamma+i\nu)(t-t')}} e^{-2i\lambda|\beta|(\cos(\omega_d t)-\cos(\omega_d t'))} \tag{C.9}$$

$$= \eta_p e^{-\lambda^2} \sum_{n=0}^{\infty}\sum_{m,\ell=-\infty}^{\infty} \frac{\lambda^{2n}}{n!} \frac{i^\ell \mathcal{J}_m\left(\frac{2\lambda\eta_d}{\omega_d}\right)\mathcal{J}_\ell\left(2\lambda|\beta|\right) e^{i(m+\ell)\omega_d t}}{(\tilde{\gamma}+n\Gamma) - i(\Delta - n\nu - m\omega_d - \ell\omega_d)} e^{-2i\lambda\eta_d \sin(\omega_d t)/\omega_d} e^{-2i\lambda|\beta|\cos(\omega_d t)}.$$

While the dipole moment is generally not stationary, the steady-state population $\langle\sigma^\dagger\sigma\rangle$ becomes stationary in the limit $\gamma \ll \omega_d$ and can be calculated as

$$\langle\sigma^\dagger\sigma(t)\rangle = \tag{C.10}$$

$$2\eta_p^2 e^{-\lambda^2}\sum_{n=0}^{\infty}\sum_{m,\ell,h,k=0}^{\infty}\frac{\lambda^{2n}}{n!}\frac{e^{i(m+\ell+h-k)\omega_d t}}{2\gamma - i(k-m-\ell-h)\omega_d}\Re\left\{\frac{i^{\ell+h}\mathcal{J}_m\left(\frac{2\lambda\eta_d}{\omega_d}\right)\mathcal{J}_k\left(\frac{2\lambda\eta_d}{\omega_d}\right)\mathcal{J}_\ell\left(2\lambda|\beta|\right)\mathcal{J}_h\left(-2\lambda|\beta|\right)}{(\tilde{\gamma}+n\Gamma)-i(\Delta-n\nu-m\omega_d-\ell\omega_d)}\right\}$$

$$\approx \frac{\eta_p^2}{\gamma}e^{-\lambda^2}\sum_{n=0}^{\infty}\sum_{m,\ell,k=-\infty}^{\infty}\frac{\lambda^{2n}}{n!}\Re\left\{\frac{i^{k-m}\mathcal{J}_m\left(\frac{2\lambda\eta_d}{\omega_d}\right)\mathcal{J}_k\left(\frac{2\lambda\eta_d}{\omega_d}\right)\mathcal{J}_\ell\left(2\lambda|\beta|\right)\mathcal{J}_{k-m-\ell}\left(-2\lambda|\beta|\right)}{(\tilde{\gamma}+n\Gamma)-i(\Delta-n\nu-m\omega_d-\ell\omega_d)}\right\}$$

$$= \frac{\eta_p^2}{\gamma}e^{-\lambda^2}\sum_{n=0}^{\infty}\sum_{m,\ell=-\infty}^{\infty}\frac{\lambda^{2n}}{n!}\frac{(\tilde{\gamma}+n\Gamma)\mathcal{J}_m\left(\frac{2\lambda\eta_d}{\omega_d}\right)^2\mathcal{J}_\ell\left(2\lambda|\beta|\right)^2}{(\tilde{\gamma}+n\Gamma)^2+(\Delta_p-n\nu-(m+\ell)\omega_d)^2},$$

where we used that for $\gamma \ll \omega_d$ one can approximate $\sum_{\ell=-\infty}^{\infty}\frac{e^{i(\ell-m)\omega_d t}}{2\gamma-i(\ell-m)\omega_d}f_\ell \approx (1/2\gamma)f_m$.

# D

# Derivation of molecule-host coupling

We provide here a simple first-principle derivation of electron-phonon and vibron-phonon coupling for a molecule embedded in a host crystal as discussed in chapter 5. To this end, we consider a diatomic molecule with reduced mass $\mu = \frac{m_L m_R}{m_L + m_R}$ which is embedded in a 1D chain with lattice constant $a$ [see Figure D.1] and $2N + 1$ unit cells (we assume the molecule to be at position $N + 1$). Excitation of the molecule will reconfigure the electronic orbitals and bond length of the molecule and will consequently lead to a modified potential between the molecule and the crystal atoms. Therefore, the equilibrium positions of the lattice will depend on the electronic state of the molecule and will be shifted in the excited state by $\Delta x_\ell = x_\ell^e - x_\ell^g$. This interaction can be described by the general Hamiltonian

$$\mathcal{H}_{\text{bulk-mol}} = \sum_\ell \left[ \sigma\sigma^\dagger \left( W_{L\ell}^g + W_{R\ell}^g \right) + \sigma^\dagger\sigma \left( W_{L\ell}^e + W_{R\ell}^e \right) \right], \tag{D.1}$$

where $W_{L\ell}^{g/e}$ and $W_{R\ell}^{g/e}$ are the potentials in ground and excited state between the left and right nuclei of the dopant and a lattice site $\ell$. Assuming harmonic potentials between the guest and host atoms, we can expand around the equilibrium positions in the excited state (assuming that the vibrational frequencies in ground and excited state are identical)

$$W_{L\ell}^e(|x_L - x_\ell|) = \hbar\omega_0 + \frac{1}{2} k_{L\ell} (x_L - x_\ell - \Delta x_{L\ell})^2, \tag{D.2a}$$

$$W_{R\ell}^e(|x_R - x_\ell|) = \hbar\omega_0 + \frac{1}{2} k_{R\ell} (x_R - x_\ell - \Delta x_{R\ell})^2, \tag{D.2b}$$

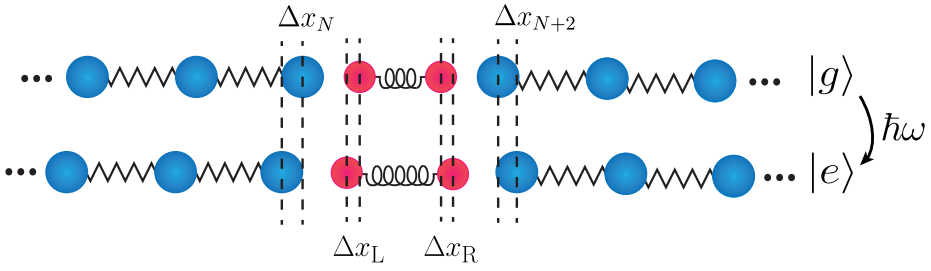


Figure D.1: *Derivation of coupling terms.* Electronic excitation of a diatomic molecule will lead to a modified equilibrium configuration and consequently to a push of the surrounding host crystal.

where $\Delta x_{\mathrm{L}\ell} = \Delta x_{\mathrm{L}} - \Delta x_\ell$ and $\Delta x_{\mathrm{R}\ell} = \Delta x_{\mathrm{R}} - \Delta x_\ell$ account for the displaced equilibrium positions in the excited state and the spring constants $k_{\mathrm{L}\ell}$, $k_{\mathrm{R}\ell}$ are given as the second derivatives of the potentials evaluated at the excited state equilibrium positions. Expressing the potentials in terms of center-of-mass and relative motion coordinates of the molecule gives (defining $W_{\mathrm{L}\ell} = \sigma\sigma^\dagger W^g_{\mathrm{L}\ell} + \sigma^\dagger\sigma W^e_{\mathrm{L}\ell}$, $W_{\mathrm{R}\ell} = \sigma\sigma^\dagger W^g_{\mathrm{R}\ell} + \sigma^\dagger\sigma W^e_{\mathrm{R}\ell}$)

$$W_{\mathrm{L}\ell} = \frac{1}{2}k_{\mathrm{L}\ell}\left(x_{\mathrm{cm}} - \frac{m_{\mathrm{R}}}{M}x_{\mathrm{rm}} - x_\ell\right)^2 - k_{\mathrm{L}\ell}\left(x_{\mathrm{cm}} - \frac{m_{\mathrm{R}}}{M}x_{\mathrm{rm}} - x_\ell\right)\Delta x_{\mathrm{L}\ell}\sigma^\dagger\sigma + \frac{1}{2}k_{\mathrm{L}\ell}\Delta x^2_{\mathrm{L}\ell}\sigma^\dagger\sigma, \tag{D.3a}$$

$$W_{\mathrm{R}\ell} = \frac{1}{2}k_{\mathrm{R}\ell}\left(x_{\mathrm{cm}} + \frac{m_{\mathrm{L}}}{M}x_{\mathrm{rm}} - x_\ell\right)^2 - k_{\mathrm{R}\ell}\left(x_{\mathrm{cm}} + \frac{m_{\mathrm{L}}}{M}x_{\mathrm{rm}} - x_\ell\right)\Delta x_{\mathrm{R}\ell}\sigma^\dagger\sigma + \frac{1}{2}k_{\mathrm{R}\ell}\Delta x^2_{\mathrm{R}\ell}\sigma^\dagger\sigma. \tag{D.3b}$$

We are mostly interested in the coupling between the phonons and the relative motion of the molecule (which will give rise to vibrational relaxation) as well as the coupling between the electronic excitation and the phonons. In the expanded equations above we can see that the first term couples couples the relative motion of the molecule $x_{\mathrm{rm}}$ to the motion of the lattice atoms $x_\ell$, while the second term couples $x_\ell$ to the electronic excitation $\sigma^\dagger\sigma$ and the last term is a constant energy shift. For the left and right atom together, we then arrive at the interaction Hamiltonians

$$\mathcal{H}_{\text{vib-phon}} = -\frac{1}{2}\sum_\ell \left(k_{\mathrm{R}\ell} - k_{\mathrm{L}\ell}\right) x_\ell x_{\mathrm{rm}}, \tag{D.4a}$$

$$\mathcal{H}_{\text{el-phon}} = -\sum_\ell \Delta x_\ell \left(k_{\mathrm{R}\ell} + k_{\mathrm{L}\ell}\right) x_\ell \sigma^\dagger\sigma, \tag{D.4b}$$

where for simplicity we assumed equal masses $m_{\mathrm{L}} = m_{\mathrm{R}}$ and used that for symmetric molecules $\Delta x_{\mathrm{L}} = -\Delta x_{\mathrm{R}}$.

### Bulk solution for acoustic phonons

The contribution of the bulk adds as (just considering nearest-neighbour interactions)

$$\mathcal{H}_{\text{bulk}} = \sum_\ell \left(\frac{p_\ell^2}{2m} + \frac{1}{2}k_0\left(x_\ell - x_{\ell+1}\right)^2\right), \tag{D.5}$$

with the main assumption that the presence of the molecule does not significantly change the bulk modes. Newton's equations of motion for the displacements of the lattice atoms can be arranged in matrix form as

$$\ddot{\mathbf{x}} = -\mathbf{M}\mathbf{x}, \tag{D.6}$$

where $\mathbf{x} = (x_1, \ldots, x_{2N+1})$ and

$$\mathbf{M} = \frac{1}{m} \begin{pmatrix} 2k_0 & -k_0 & & 0 \\ -k_0 & 2k_0 & \ddots & \\ & \ddots & \ddots & -k_0 \\ 0 & & -k_0 & 2k_0 \end{pmatrix}. \tag{D.7}$$

This is a trigonal Toeplitz matrix which can be easily diagonalized ($\mathbf{D} = \mathbf{T}^{-1}\mathbf{M}\mathbf{T}$) where the $k$-th eigenvalue is given by

$$\omega_k^2 = \frac{4k_0}{m} \sin^2\left(\frac{\pi k}{2(2N+2)}\right) = \omega_{\max}^2 \sin^2\left(\frac{\pi k}{2(2N+2)}\right), \tag{D.8}$$

with $k \in [1, 2N+1]$ and the associated normalized eigenvectors read

$$\mathbf{v}_k = \sqrt{\frac{1}{N+1}} \left(\sin\left(\frac{\pi k}{2N+2}\right), \ldots, \sin\left(\frac{(2N+1)\pi k}{2N+2}\right)\right)^\top, \tag{D.9}$$

such that in the diagonal basis ($\mathbf{u} = \mathbf{T}^{-1}\mathbf{x}$) the equation of motion for the $k$th mode is given by

$$\ddot{u}_k = -\omega_k^2 u_k. \tag{D.10}$$

We can now express the couplings from Eqs. (D.4) in terms of the normal modes of the crystal. Further more we will consider only nearest-neighbour coupling for the molecule, i.e. $k_{\mathrm{R}\ell}, k_{\mathrm{L}\ell} = 0$ for $\ell \neq \{N, N+2\}$. We obtain with $x_\ell = \sum_{k=1}^{2N+2} (T_{\ell k})\, u_k$

$$x_N = \sqrt{\frac{1}{N+1}} \sum_k \sin\left(\frac{\pi k N}{2N+2}\right) u_k, \tag{D.11a}$$

$$x_{N+2} = \sqrt{\frac{1}{N+1}} \sum_k \sin\left(\frac{\pi k (N+2)}{2N+2}\right) u_k, \tag{D.11b}$$

and consequently

$$\mathcal{H}_{\text{vib-phon}} = -\frac{1}{2}\Delta k \,(x_{N+2} - x_N)\, x_{\mathrm{rm}} = -\Delta k x_{\mathrm{rm}} \sqrt{\frac{1}{N+1}} \sum_k \cos\left(\frac{\pi k}{2}\right) \sin\left(\frac{\pi k}{2N+2}\right) u_k, \tag{D.12a}$$

$$\begin{aligned} \mathcal{H}_{\text{el-phon}} &= -\Delta x_{N+2} k_{\mathrm{tot}} \,(x_{N+2} - x_N)\, \sigma^\dagger \sigma = \\ &\quad - 2\Delta x_{N+2} k_{\mathrm{tot}} \sqrt{\frac{1}{N+1}} \sum_k \cos\left(\frac{\pi k}{2}\right) \sin\left(\frac{\pi k}{2N+2}\right) u_k \sigma^\dagger \sigma. \end{aligned} \tag{D.12b}$$

where we used that $\Delta x_{N+2} = -\Delta x_N$ and defined $\Delta k = k_{\mathrm{R}(N+2)} - k_{\mathrm{L}(N+2)} = k_{\mathrm{L}N} - k_{\mathrm{R}N}$, $k_{\mathrm{tot}} = k_{\mathrm{R}(N+2)} + k_{\mathrm{L}(N+2)} = k_{\mathrm{R}N} + k_{\mathrm{L}N}$. We now quantize the Hamiltonians by introducing the position operators (and similarly the momentum operators) $x_{\mathrm{rm}} = x_{\mathrm{zpm}}(b^\dagger + b)$, $u_k = u^{(k)}_{\mathrm{zpm}}\left(c_k^\dagger + c_k\right)$ with $x_{\mathrm{zpm}} = \sqrt{1/(2\mu\nu)}$, $u^{(k)}_{\mathrm{zpm}} = \sqrt{1/(2m_0\omega_k)}$. We obtain

$$\mathcal{H}_{\text{vib-phon}} = -\sum_k \alpha_k q_k Q, \tag{D.13a}$$

$$\mathcal{H}_{\text{el-phon}} = -\sum_k \lambda_k \omega_k \sqrt{2} q_k \sigma^\dagger \sigma, \tag{D.13b}$$

where we have introduced the couplings

$$\alpha_k = 2\Delta k \sqrt{\frac{1}{N+1}} \cos\left(\frac{\pi k}{2}\right) \sin\left(\frac{\pi k}{2N+2}\right) u^{(k)}_{\mathrm{zpm}} x_{\mathrm{zpm}}, \tag{D.14a}$$

$$\lambda_k = 2\frac{k_{\mathrm{tot}}}{\omega_k} \sqrt{\frac{1}{N+1}} \cos\left(\frac{\pi k}{2}\right) \sin\left(\frac{\pi k}{2N+2}\right) u^{(k)}_{\mathrm{zpm}} \Delta x_{N+2}. \tag{D.14b}$$

### Spectral densities

The correlation function of the bath displacement ist given by

$$\langle \mathcal{B}(t)\mathcal{B}^\dagger(t')\rangle = e^{\int_0^\infty \mathrm{d}\omega \frac{J(\omega)}{\omega^2}\left[\coth\left(\frac{\beta\omega}{2}\right)(\cos(\omega\tau)-1) - i\sin(\omega\tau)\right]}. \tag{D.15}$$

The spectral density of the electron-phonon coupling is given by $J(\omega) = \sum_k |\lambda_k\omega_k|^2 \delta(\omega - \omega_k) = n(\omega)\lambda(\omega)^2\omega^2$. From Eq. (D.14b) we can derive for the 1D case

$$n^{\mathrm{1D}}(\omega)\lambda(\omega)^2 = \frac{\lambda^{\mathrm{1D}}_{\text{e-ph}}}{\omega} \frac{\sqrt{\omega^2_{\mathrm{max}} - \omega^2}}{\omega_{\mathrm{max}}} \theta(\omega_{\mathrm{max}} - \omega), \tag{D.16}$$

with the dimensionless 1D electron-phonon coupling constant $\lambda^{\mathrm{1D}}_{\text{e-ph}} = \frac{8k^2_{\mathrm{tot}}\Delta x^2_{N+2}}{\pi m_0 \omega^3_{\mathrm{max}}}$. This leads to a divergence of the integral due to the $1/\omega$-term. Considering a 3D density of states instead:

$$n^{\mathrm{3D}}(\omega) = \frac{V}{(2\pi)^3} \frac{4\pi|\mathbf{q}(\omega)|^2}{v_{\mathrm{g}}(\omega)}, \tag{D.17}$$

with $V/(2\pi)^3$ the mode volume in $k$ space and $\mathbf{q}(\omega)$ the inverted dispersion relation in 3D. Making the Debye assumption and assuming a linear dependence between wave vector and frequency, one obtains

$$J^{\mathrm{3D}}(\omega) = \lambda^{\mathrm{3D}}_{\text{e-ph}} \omega^3 \frac{\sqrt{\omega^2_{\mathrm{max}} - \omega^2}}{\omega_{\mathrm{max}}} \theta(\omega_{\mathrm{max}} - \omega), \tag{D.18}$$

where we introduced the 3D electron-phonon coupling constant $\lambda^{3D}_{\text{e-ph}} = \frac{16}{\pi^2}\frac{k^2_{\text{tot}}\Delta x^2_{N+2}}{m_0\omega^5_{\text{max}}}$ which has units $[s^2]$.

# E

# Non-Markovian loss into the dark state reservoir

We outline here a quantum Langevin equations approach for the dynamics of the bright state decay into the dark state reservoir as discussed in chapter 7. This allows for a description of the non-Markovian regime as well. We start with the full equations of motion for dark and bright states given by

$$\dot{\hat{\mathbf{v}}} = -i\boldsymbol{\mathcal{M}}\hat{\mathbf{v}} - i\mathbf{m}\hat{B} + \sqrt{2\gamma}\hat{\mathbf{v}}_{\text{in}}, \tag{E.1a}$$

$$\dot{\hat{B}} = -i(\bar{\delta} - i\gamma)\hat{B} - i\mathbf{m}^{\dagger}\hat{\mathbf{v}} + \sqrt{2\gamma}\hat{B}_{\text{in}}, \tag{E.1b}$$

where we have defined the vector of dark states $\hat{\mathbf{v}} = (\hat{D}_1, \ldots, \hat{D}_{\mathcal{N}-1})^{\top}$. By substituting the steady state solution for the dark modes

$$\hat{\mathbf{v}}(t) = \int_{-\infty}^{t} \mathrm{d}s\, e^{-i\boldsymbol{\mathcal{M}}(t-s)} \left(-i\mathbf{m}\hat{B}(s) + \sqrt{2\gamma}\hat{\mathbf{v}}_{\text{in}}(s)\right), \tag{E.2}$$

into Eq. (E.1b), we obtain the reduced equation of motion for the bright mode

$$\begin{aligned}
\dot{\hat{B}} &= -i(\bar{\delta} - i\gamma)\hat{B} \\
&\quad - \int_{-\infty}^{\infty} \mathrm{d}s\, \theta(t-s)\mathbf{m}^{\dagger}e^{-i\boldsymbol{\mathcal{M}}(t-s)}\mathbf{m}\hat{B}(s) - i\sqrt{2\gamma}\int_{-\infty}^{\infty} \mathrm{d}s\, \theta(t-s)\mathbf{m}^{\dagger}e^{-i\boldsymbol{\mathcal{M}}(t-s)}\hat{\mathbf{v}}_{\text{in}}(s) + \sqrt{2\gamma}\hat{B}_{\text{in}} \\
&= -i(\bar{\delta} - i\gamma)\hat{B} - \int_{-\infty}^{\infty} \mathrm{d}s\, \theta(t-s) \sum_{j=1}^{\mathcal{N}-1} |c_j|^2 e^{-i(\bar{\delta} - i\gamma - \tilde{\lambda}_j)(t-s)}\hat{B}(s) + \hat{\xi}_{\text{dark}} + \sqrt{2\gamma}\hat{B}_{\text{in}},
\end{aligned} \tag{E.3}$$

where we have defined the noise term induced by the dark reservoir

$$\hat{\xi}_{\text{dark}}(t) = -i\sqrt{2\gamma}\int_{-\infty}^{\infty} \mathrm{d}s\, \theta(t-s)\mathbf{m}^{\dagger}e^{-i\boldsymbol{\mathcal{M}}(t-s)}\hat{\mathbf{v}}_{\text{in}}(s). \tag{E.4}$$

Following the same steps as introduced in chapter 7 for the Markovian approach where we approximate $|c_j|^2 \approx w^2/(\mathcal{N}-1)$ and assume $\tilde{\lambda}_j$ to be linearly distributed between $-2w$ and $2w$, we obtain

$$\sum_{j=1}^{\mathcal{N}-1} |c_j|^2 e^{i\tilde{\lambda}_j(t-s)} \approx \frac{w}{4} \int_{-2w}^{2w} \mathrm{d}\tilde{\lambda}\, e^{i\tilde{\lambda}(t-s)} = w^2\, \mathrm{sinc}(2w(t-s)), \tag{E.5}$$

for the convolution kernel which results in the non-Markovian time evolution

$$\dot{\hat{B}} = -i(\bar{\delta}-i\gamma)\hat{B} - w^2 \int_{-\infty}^{\infty} \mathrm{d}s\, \theta(t-s) e^{-i(\bar{\delta}-i\gamma)(t-s)}\, \mathrm{sinc}(2w(t-s))\hat{B}(s) + \hat{\xi}_{\mathrm{dark}} + \sqrt{2\gamma}\hat{B}_{\mathrm{in}}. \tag{E.6}$$

# References


[1] M. Reitz, C. Sommer, and C. Genes, "Langevin approach to quantum optics with molecules," Phys. Rev. Lett. 122, 203602 (2019).

[2] M. Reitz and C. Genes, "Floquet engineering of molecular dynamics via infrared coupling," J. Chem. Phys. 153, 234305 (2020).

[3] M. Reitz, C. Sommer, B. Gurlek, V. Sandoghdar, D. Martin-Cano, and C. Genes, "Molecule-photon interactions in phononic environments," Phys. Rev. Research 2, 033270 (2020).

[4] C. Sommer, M. Reitz, F. Mineo, and C. Genes, "Molecular polaritonics in dense mesoscopic disordered ensembles," Phys. Rev. Research 3, 033141 (2021).

[5] R. Holzinger, S. A. Oh, M. Reitz, H. Ritsch, and C. Genes, "Cooperative subwavelength molecular quantum emitter arrays," arXiv:2203.04998 (2022).

[6] D. Plankensteiner, C. Sommer, M. Reitz, H. Ritsch, and C. Genes, "Enhanced collective Purcell effect of coupled quantum emitter systems," Phys. Rev. A 99, 043843 (2019).

[7] M. Reitz, C. Sommer, and C. Genes, "Cooperative quantum phenomena in light-matter platforms," PRX Quantum 3, 010201 (2022).

[8] C. Toninelli, I. Gerhardt, A. S. Clark, A. Reserbat-Plantey, S. Götzinger, Z. Ristanović, M. Colautti, P. Lombardi, K. D. Major, I. Deperasińska, W. H. Pernice, F. H. L. Koppens, B. Kozankiewicz, A. Gourdon, V. Sandoghdar, and M. Orrit, "Single organic molecules for photonic quantum technologies," Nature Materials (2021).

[9] B. Lounis and W. E. Moerner, "Single photons on demand from a single molecule at room temperature," Nature 407, 491 (2000).

[10] W. E. Moerner, "Single-photon sources based on single molecules in solids," New Journal of Physics 6, 88–88 (2004).

[11] C. Polisseni, K. D. Major, S. Boissier, S. Grandi, A. S. Clark, and E. A. Hinds, "Stable single-photon emitter in a thin organic crystal for application to quantum-photonic devices," Opt. Express 24, 5615–5627 (2016).

[12] A. Maser, B. Gmeiner, T. Utikal, S. Götzinger, and V. Sandoghdar, "Few-photon coherent nonlinear optics with a single molecule," Nature Photonics 10, 450 (2016).

[13] A. Pscherer, M. Meierhofer, D. Wang, H. Kelkar, D. Martín-Cano, T. Utikal, S. Götzinger, and V. Sandoghdar, "Single-molecule vacuum rabi splitting: Four-wave mixing and optical switching at the single-photon level," Phys. Rev. Lett. 127, 133603 (2021).

[14] G. Mazzamuto, A. Tabani, S. Pazzagli, S. Rizvi, A. Reserbat-Plantey, K. Schädler, G. Navickaite, L. Gaudreau, F. S. Cataliotti, F. Koppens, and C. Toninelli, "Single-molecule study for a graphene-based nano-position sensor," New Journal of Physics 16, 113007 (2014).

[15] Y. Tian, P. Navarro, and M. Orrit, "Single molecule as a local acoustic detector for mechanical oscillators," Phys. Rev. Lett. 113, 135505 (2014).

[16] A. Shkarin, D. Rattenbacher, J. Renger, S. Hönl, T. Utikal, P. Seidler, S. Götzinger, and V. Sandoghdar, "Nanoscopic charge fluctuations in a gallium phosphide waveguide measured by single molecules," Phys. Rev. Lett. 126, 133602 (2021).

[17] D. Wang, H. Kelkar, D. Martin-Cano, T. Utikal, S. Götzinger, and V. Sandoghdar, "Coherent coupling of a single molecule to a scanning fabry-perot microcavity," Phys. Rev. X 7, 021014 (2017).

[18] D. Wang, H. Kelkar, D. Martin-Cano, D. Rattenbacher, A. Shkarin, T. Utikal, S. Götzinger, and V. Sandoghdar, "Turning a molecule into a coherent two-level quantum system," Nature Physics 15, 483 (2019).

[19] S. Faez, P. Türschmann, H. R. Haakh, S. Götzinger, and V. Sandoghdar, "Coherent interaction of light and single molecules in a dielectric nanoguide," Phys. Rev. Lett. 113, 213601 (2014).

[20] P. Lombardi, A. P. Ovvyan, S. Pazzagli, G. Mazzamuto, G. Kewes, O. Neitzke, N. Gruhler, O. Benson, W. H. P. Pernice, F. S. Cataliotti, and C. Toninelli, "Photostable molecules on chip: Integrated sources of nonclassical light," ACS Photonics 5, 126–132 (2018).

[21] D. Rattenbacher, A. Shkarin, J. Renger, T. Utikal, S. Götzinger, and V. Sandoghdar, "Coherent coupling of single molecules to on-chip ring resonators," New Journal of Physics 21, 062002 (2019).

[22] R. Chikkaraddy, B. de Nijs, F. Benz, S. J. Barrow, O. A. Scherman, E. Rosta, A. Demetriadou, P. Fox, O. Hess, and J. J. Baumberg, "Single-molecule strong coupling at room temperature in plasmonic nanocavities," Nature 535, 127 (2016).

[23] O. S. Ojambati, R. Chikkaraddy, W. D. Deacon, M. Horton, D. Kos, V. A. Turek, U. F. Keyser, and J. J. Baumberg, "Quantum electrodynamics at room temperature coupling a single vibrating molecule with a plasmonic nanocavity," Nat. Comm. 10, 1049 (2019).

[24] P. Larkin, *Infrared and Raman Spectroscopy: Principles and Spectral Interpretation* (Elsevier Science, 2011).

[25] F. Benz, M. K. Schmidt, A. Dreismann, R. Chikkaraddy, Y. Zhang, A. Demetriadou, C. Carnegie, H. Ohadi, B. de Nijs, R. Esteban, J. Aizpurua, and J. J. Baumberg, "Single-molecule optomechanics in "picocavities"," Science 354, 726 (2016).

[26] P. Roelli, C. Galland, N. Piro, and T. J. Kippenberg, "Molecular cavity optomechanics as a theory of plasmon-enhanced Raman scattering," Nat. Nanotechnol. 11, 164 (2016).

[27] I. Shlesinger, K. G. Cognée, E. Verhagen, and A. F. Koenderink, "Integrated molecular optomechanics with hybrid dielectric–metallic resonators," ACS Photonics 8, 3506–3516 (2021).

[28] W. Chen, P. Roelli, H. Hu, S. Verlekar, S. P. Amirtharaj, A. I. Barreda, T. J. Kippenberg, M. Kovylina, E. Verhagen, A. Martínez, and C. Galland, "Continuous-wave frequency upconversion with a molecular optomechanical nanocavity," Science 374, 1264–1267 (2021).

[29] D. G. Lidzey, D. D. C. Bradley, M. S. Skolnick, T. Virgili, S. Walker, and D. M. Whittaker, "Strong exciton–photon coupling in an organic semiconductor microcavity," Nature 395, 53–55 (1998).

[30] J. A. Hutchison, T. Schwartz, C. Genet, E. Devaux, and T. W. Ebbesen, "Modifying chemical landscapes by coupling to vacuum fields," Angew. Chem. Int. Ed. 51, 1592 (2012).

[31] J. Galego, F. Garcia-Vidal, and J. Feist, "Suppressing photochemical reactions with quantized light fields," Nat. Commun. 7, 13841 (2017).

[32] F. Herrera and F. C. Spano, "Cavity-controlled chemistry in molecular ensembles," Phys. Rev. Lett. 116, 238301 (2016).

[33] L. A. Martinez-Martinez, R. F. Ribeiro, J. Campos-González-Angulo, and J. Yuen-Zhou, "Can ultrastrong coupling change ground-state chemical reactions?" ACS Photonics 5, 167 (2018).

[34] T. Kampschulte and J. H. Denschlag, "Cavity-controlled formation of ultracold molecules," New Journal of Physics 20, 123015 (2018).

[35] E. Orgiu, J. George, J. Hutchison, E. Devaux, J. F. Dayen, B. Doudin, F. F. Stellacci, C. Genet, J. Schachenmayer, C. Genes, G. Pupillo, P. Samori, and T. W. Ebbesen, "Conductivity in organic semiconductors hybridized with the vacuum field," Nat. Mater. 14, 1123 (2015).

[36] J. Schachenmayer, C. Genes, E. Tignone, and G. Pupillo, "Cavity-enhanced transport of excitons," Phys. Rev. Lett. 114, 196403 (2015).

[37] J. Feist and F. J. Garcia-Vidal, "Extraordinary exciton conductance induced by strong coupling," Phys. Rev. Lett. 114, 196402 (2015).

[38] D. Hagenmüller, J. Schachenmayer, S. Schütz, C. Genes, and G. Pupillo, "Cavity-enhanced transport of charge," Phys. Rev. Lett. 119, 223601 (2017).

[39] D. Hagenmüller, S. Schütz, J. Schachenmayer, C. Genes, and G. Pupillo, "Cavity-assisted mesoscopic transport of fermions: Coherent and dissipative dynamics," Phys. Rev. B 97, 205303 (2018).

[40] J. A. Hutchison, A. Liscio, T. Schwartz, A. Canaguier-Durand, C. Genet, V. Palermo, P. Samorì, and T. W. Ebbesen, "Tuning the work-function via strong coupling," Advanced Materials 25, 2481–2485 (2013).

[41] D. Polak, R. Jayaprakash, T. P. Lyons, L. . Martínez-Martínez, A. Leventis, K. J. Fallon, H. Coulthard, D. G. Bossanyi, K. Georgiou, A. J. Petty, II, J. Anthony, H. Bronstein, J. Yuen-Zhou, A. I. Tartakovskii, J. Clark, and A. J. Musser, "Manipulating molecules with strong coupling: harvesting triplet excitons in organic exciton microcavities," Chem. Sci. 11, 343–354 (2020).

[42] L. A. Martínez-Martínez, E. Eizner, S. Kéna-Cohen, and J. Yuen-Zhou, "Triplet harvesting in the polaritonic regime: A variational polaron approach," J. Chem. Phys. 151, 054106 (2019).

[43] M. A. Sentef, M. Ruggenthaler, and A. Rubio, "Cavity quantum-electrodynamical polaritonically enhanced electron-phonon coupling and its influence on superconductivity," Sci. Adv. 4, 6969 (2018).

[44] A. Shalabney, J. George, J. Hutchison, G. Pupillo, C. Genet, and T. W. Ebbesen, "Coherent coupling of molecular resonators with a microcavity mode," Nat. Comm. 6, 5981 (2015).

[45] J. Lather, P. Bhatt, A. Thomas, T. W. Ebbesen, and J. George, "Cavity catalysis by cooperative vibrational strong coupling of reactant and solvent molecules," Angew. Chem. Int. Ed. 58, 10635–10638 (2019).

[46] A. Thomas, A. Jayachandran, L. Lethuillier-Karl, R. M. Vergauwe, K. Nagarajan, E. Devaux, C. Genet, J. Moran, and T. W. Ebbesen, "Ground state chemistry under vibrational strong coupling: dependence of thermodynamic parameters on the Rabi splitting energy," Nanophotonics 9, 249 – 255 (2020).

[47] A. Shalabney, J. George, H. Hiura, J. A. Hutchison, C. Genet, P. Hellwig, and T. W. Ebbesen, "Enhanced Raman scattering from vibro-polariton hybrid states," Angew. Chem. Int. Ed. 54, 7971–7975 (2015).

[48] W. M. Takele, L. Piatkowski, F. Wackenhut, S. Gawinkowski, A. J. Meixner, and J. Waluk, "Scouting for strong light–matter coupling signatures in raman spectra," Phys. Chem. Chem. Phys. 23, 16837–16846 (2021).

[49] N. Wu, J. Feist, and F. J. Garcia-Vidal, "When polarons meet polaritons: Exciton-vibration interactions in organic molecules strongly coupled to confined light fields," Phys. Rev. B 94, 195409 (2016).

[50] M. A. Zeb, P. G. Kirton, and J. Keeling, "Exact states and spectra of vibrationally dressed polaritons," ACS Photonics 5, 249 (2018).

[51] K. S. U. Kansanen, A. Asikainen, J. J. Toppari, G. Groenhof, and T. T. Heikkilä, "Theory for the stationary polariton response in the presence of vibrations," Phys. Rev. B 100, 245426 (2019).

[52] F. Herrera and F. C. Spano, "Dark vibronic polaritons and the spectroscopy of organic microcavities," Phys. Rev. Lett. 118, 223601 (2017).

[53] F. Herrera and F. C. Spano, "Theory of nanoscale organic cavities: The essential role of vibration-photon dressed states," ACS Photonics 5, 65 (2018).

[54] T. Neuman and J. Aizpurua, "Origin of the asymmetric light emission from molecular exciton polaritons," Optica 5, 1247 (2018).

[55] J. Galego, F. J. Garcia-Vidal, and J. Feist, "Cavity-induced modifications of molecular structure in the strong-coupling regime," Phys. Rev. X 5, 041022 (2015).

[56] J. Flick, M. Ruggenthaler, H. Appel, and A. Rubio, "Atoms and molecules in cavities, from weak to strong coupling in quantum-electrodynamics (QED) chemistry," PNAS 114, 3026 (2017).

[57] J. Flick, H. Appel, M. Ruggenthaler, and A. Rubio, "Cavity Born–Oppenheimer approximation for correlated electron–nuclear-photon systems," Journal of Chemical Theory and Computation 13, 1616 (2017).

[58] T. S. Haugland, E. Ronca, E. F. Kjønstad, A. Rubio, and H. Koch, "Coupled cluster theory for molecular polaritons: Changing ground and excited states," Phys. Rev. X 10, 041043 (2020).

[59] H. L. Luk, J. Feist, J. J. Toppari, and G. Groenhof, "Multiscale molecular dynamics simulations of polaritonic chemistry," Journal of Chemical Theory and Computation 13, 4324–4335 (2017).

[60] J. del Pino, F. A. Y. N. Schröder, A. W. Chin, J. Feist, and F. J. Garcia-Vidal, "Tensor network simulation of non-Markovian dynamics in organic polaritons," Phys. Rev. Lett. 121, 227401 (2018).

[61] R. F. Ribeiro, L. A. Martínez-Martínez, M. Du, J. Campos-Gonzalez-Angulo, and J. Yuen-Zhou, "Polariton chemistry: controlling molecular dynamics with optical cavities," Chem. Sci. 9, 6325 (2018).

[62] J. Feist, J. Galego, and F. J. Garcia-Vidal, "Polaritonic chemistry with organic molecules," ACS Photonics 5, 205–216 (2018).

[63] J. Flick, N. Rivera, and P. Narang, "Strong light-matter coupling in quantum chemistry and quantum photonics," Nanophotonics 7, 1479–1501 (2018).

[64] F. Herrera and J. Owrutsky, "Molecular polaritons for controlling chemistry with quantum optics," J. Chem. Phys. 152, 100902 (2020).

[65] J. Fregoni, F. J. Garcia-Vidal, and J. Feist, "Theoretical challenges in polaritonic chemistry," ACS Photonics (2022).

[66] T. E. Li, B. Cui, J. E. Subotnik, and A. Nitzan, "Molecular polaritonics: Chemical dynamics under strong light–matter coupling," Annual Review of Physical Chemistry 73, null (2022).

[67] T. W. Ebbesen, "Hybrid light–matter states in a molecular and material science perspective," Accounts of Chemical Research 49, 2403–2412 (2016).

[68] K. Hirai, J. A. Hutchison, and H. Uji-i, "Recent progress in vibropolaritonic chemistry," ChemPlusChem 85, 1981–1988 (2020).

[69] K. Nagarajan, A. Thomas, and T. W. Ebbesen, "Chemistry under vibrational strong coupling," Journal of the American Chemical Society 143, 16877–16889 (2021).

[70] H. P. Breuer and F. Petruccione, *The theory of open quantum systems* (Oxford University Press, 2002).

[71] U. Weiss, *Quantum Dissipative Systems*, Series in modern condensed matter physics (World Scientific, 1999).

[72] M. Scully and M. Zubairy, *Quantum Optics* (Cambridge University Press, 1997).

[73] C. Gardiner and P. Zoller, *Quantum noise: A handbook of Markovian and non-Markovian quantum stochastic methods with applications to quantum optics*, Vol. 56 (Springer Science & Business Media, 2004).

[74] W. Vogel and D. Welsch, *Quantum Optics* (Wiley, 2006).

[75] D. Walls and G. Milburn, *Quantum Optics*, Springer Study Edition (Springer Berlin Heidelberg, 2012).

[76] R. Loudon, *The Quantum Theory of Light*, Oxford (Clarendon Press, 1973).

[77] C. Cohen-Tannoudji, J. Dupont-Roc, and G. Grynberg, *Photons and Atoms: Introduction to Quantum Electrodynamics* (Wiley, 1989).

[78] V. Rokaj, D. Welakuh, M. Ruggenthaler, and A. Rubio, "Light-matter interaction in the long-wavelength limit: No ground-state without dipole self-energy," Journal of Physics B: Atomic, Molecular and Optical Physics 51 (2018).

[79] P. Hohenberg and W. Kohn, "Inhomogeneous electron gas," Phys. Rev. 136, B864–B871 (1964).

[80] V. Fock, "Näherungsmethode zur Lösung des quantenmechanischen Mehrkörperproblems," Zeitschrift für Physik 61, 126–148 (1930).

[81] M. Born and R. Oppenheimer, "Zur Quantentheorie der Molekeln," Annalen der Physik 389, 457–484 (1927).

[82] G. Drake, *Springer Handbook of Atomic, Molecular, and Optical Physics*, Springer Handbook of Atomic, Molecular, and Optical Physics No. Bd. 1 (Springer, 2006).

[83] M. Born, K. Huang, and M. Lax, "Dynamical theory of crystal lattices," American Journal of Physics 23, 474–474 (1955).

[84] G. A. Worth and L. S. Cederbaum, "Beyond Born-Oppenheimer: Molecular dynamics through a conical intersection," Annual Review of Physical Chemistry 55, 127–158 (2004).

[85] G. Herzberg, "Molecular Spectra and Molecular Structure. I. Spectra of Diatomic Molecules," American Journal of Physics 19, 390–391 (1951).

[86] T. Holstein, "Studies of polaron motion: Part I. The molecular-crystal model," Annals of Physics 8, 325 (1959).

[87] I. G. Lang and Y. A. Firsov, "Kinetic theory of semiconductors with low mobility," J. Exptl. Theoret. Phys. (U.S.S.R.) 43, 1843–1860 (1963).

[88] F. Duschinskiy, "The importance of the electron spectrum in multi atomic molecules. concerning the Franck-Condon principle," Acta Physicochimica 7, 551–566 (1937).

[89] J. Zirkelbach, M. Mirzaei, I. Deperasińska, B. Kozankiewicz, B. Gurlek, A. Shkarin, T. Utikal, S. Götzinger, and V. Sandoghdar, "High-resolution vibronic spectroscopy of a single molecule embedded in a crystal," J. Chem. Phys. 156, 104301 (2022).

[90] M. Asjad, M. Reitz, C. Sommer, and C. Genes, "Nonlinear opto-vibronic in molecular systems," in preparation (2022).

[91] F. Haake, "Statistical treatment of open systems by generalized master equations," in *Springer Tracts in Modern Physics: Ergebnisse der exakten Naturwissenschaftenc; Volume 66*, edited by G. Höhler (Springer Berlin Heidelberg, Berlin, Heidelberg, 1973) p. 98.

[92] R. Lehmberg, "Radiation from an N-atom system. I. General formalism," Phys. Rev. A 2, 883 (1970).

[93] K. Jacobs, *Stochastic Processes for Physicists: Understanding Noisy Systems* (Cambridge University Press, New York, 2010).

[94] C. Genes, D. Vitali, P. Tombesi, S. Gigan, and M. Aspelmeyer, "Ground-state cooling of a micromechanical oscillator: Comparing cold damping and cavity-assisted cooling schemes," Phys. Rev. A 77, 033804 (2008).

[95] A. Caldeira and A. Leggett, "Path integral approach to quantum Brownian motion," Physica A 121, 587 – 616 (1983).

[96] A. Caldeira and A. Leggett, "Influence of dissipation on quantum tunneling in macroscopic systems," Phys. Rev. Lett. 46, 211–214 (1981).

[97] B. L. Hu, J. P. Paz, and Y. Zhang, "Quantum Brownian motion in a general environment: Exact master equation with nonlocal dissipation and colored noise," Phys. Rev. D 45, 2843 (1992).

[98] R. H. Dicke, "Coherence in spontaneous radiation processes," Phys. Rev. 93, 99 (1954).

[99] A. Asenjo-Garcia, M. Moreno-Cardoner, A. Albrecht, H. J. Kimble, and D. E. Chang, "Exponential improvement in photon storage fidelities using subradiance and "selective radiance" in atomic arrays," Phys. Rev. X 7, 031024 (2017).

[100] R. Holzinger, D. Plankensteiner, L. Ostermann, and H. Ritsch, "Nanoscale coherent light source," Phys. Rev. Lett. 124, 253603 (2020).

[101] R. J. Cogdell, A. Gall, and J. Köhler, "The architecture and function of the light-harvesting apparatus of purple bacteria: from single molecules to in vivo membranes," Quarterly Reviews of Biophysics 39, 227 (2006).

[102] S. Bourne Worster, C. Stross, F. M. W. C. Vaughan, N. Linden, and F. R. Manby, "Structure and efficiency in bacterial photosynthetic light harvesting," J. Phys. Chem. Lett. 10, 7383 (2019).

[103] F. Caycedo-Soler, C. A. Schroeder, C. Autenrieth, A. Pick, R. Ghosh, S. F. Huelga, and M. B. Plenio, "Quantum redirection of antenna absorption to photosynthetic reaction centers," J. Phys. Chem. Lett. 8, 6015 (2017).

[104] A. Witkowski and W. Moffitt, "Electronic spectra of dimers: Derivation of the fundamental vibronic equation," J. Chem. Phys. 33, 872–875 (1960).

[105] M. J. Riley and E. R. Krausz, "The symmetric dimer: Effects of second-order vibronic coupling," Chemical Physics 148, 229 (1990).

[106] A. Eisfeld, L. Braun, W. T. Strunz, J. S. Briggs, J. Beck, and V. Engel, "Vibronic energies and spectra of molecular dimers," J. Chem. Phys. 122, 134103 (2005).

[107] F. P. Diehl, C. Roos, A. Duymaz, B. Lunkenheimer, A. Köhn, and T. Basche, "Emergence of coherence through variation of intermolecular distances in a series of molecular dimers," J. Phys. Chem. Lett 5, 262 (2014).

[108] A. Halpin, P. J. M. Johnson, R. Tempelaar, R. S. Murphy, J. Knoester, T. L. C. Jansen, and R. J. D. Miller, "Two-dimensional spectroscopy of a molecular dimer unveils the effects of vibronic coupling on exciton coherences," Nature Chemistry 6, 196–201 (2014).

[109] S. Haroche and D. Kleppner, "Cavity Quantum Electrodynamics," Phys. Today 42, 24 (1989).

[110] P. Berman, *Cavity Quantum Electrodynamics*, Advances in atomic, molecular, and optical physics (Academic Press, 1994).

[111] H. Walther, B. T. Varcoe, B. Englert, and T. Becker, "Cavity Quantum Electrodynamics," Rep. Prog. Phys. 69, 1325 (2006).

[112] S. Haroche and J.-M. Raimond, *Exploring the Quantum: Atoms, Cavities, and Photons* (Oxford University Press, 2013).

[113] M. Tavis and F. W. Cummings, "Exact solution for an N-molecule—radiation-field Hamiltonian," Phys. Rev. 170, 379 (1968).

[114] E. T. Jaynes and F. W. Cummings, "Comparison of quantum and semiclassical radiation theories with application to the beam maser," Proceedings of the IEEE 51, 89 (1963).

[115] E. M. Purcell, "Spontaneous emission probabilities at radio frequencies," Phys. Rev. 69, 681 (1946).

[116] P. Kirton and J. Keeling, "Nonequilibrium model of photon condensation," Phys. Rev. Lett. 111, 100404 (2013).

[117] R. E. F. Silva, J. d. Pino, F. J. García-Vidal, and J. Feist, "Polaritonic molecular clock for all-optical ultrafast imaging of wavepacket dynamics without probe pulses," Nat. Comm. 11, 1423 (2020).

[118] K. S. U. Kansanen, J. J. Toppari, and T. T. Heikkilä, "Polariton response in the presence of Brownian dissipation from molecular vibrations," J. Chem. Phys. 154, 044108 (2021).

[119] P. Rabl, "Photon blockade effect in optomechanical systems," Phys. Rev. Lett. 107, 063601 (2011).

[120] A. Nunnenkamp, K. Børkje, and S. M. Girvin, "Single-photon optomechanics," Phys. Rev. Lett. 107, 063602 (2011).

[121] D. P. S. McCutcheon and A. Nazir, "Quantum dot Rabi rotations beyond the weak exciton–phonon coupling regime," New J. Phys. 12, 113042 (2010).

[122] D. P. S. McCutcheon, N. S. Dattani, E. M. Gauger, B. W. Lovett, and A. Nazir, "A general approach to quantum dynamics using a variational master equation: Application to phonon-damped Rabi rotations in quantum dots," Phys. Rev. B 84, 081305 (2011).

[123] A. J. Brash, J. Iles-Smith, C. L. Phillips, D. P. S. McCutcheon, J. O'Hara, E. Clarke, B. Royall, L. R. Wilson, J. Mørk, M. S. Skolnick, A. M. Fox, and A. Nazir, "Light scattering from solid-state quantum emitters: Beyond the atomic picture," Phys. Rev. Lett. 123, 167403 (2019).

[124] C. Clear, R. C. Schofield, K. D. Major, J. Iles-Smith, A. S. Clark, and D. P. S. McCutcheon, "Phonon-induced optical dephasing in single organic molecules," Phys. Rev. Lett. 124, 153602 (2020).

[125] J. Johansson, P. Nation, and F. Nori, "Qutip 2: A Python framework for the dynamics of open quantum systems," Computer Physics Communications 184, 1234–1240 (2013).

[126] S. Krämer, D. Plankensteiner, L. Ostermann, and H. Ritsch, "Quantumoptics. jl: A Julia framework for simulating open quantum systems," Computer Physics Communications 227, 109–116 (2018).

[127] H. J. Carmichael and D. F. Walls, "Master equation for strongly interacting systems," Journal of Physics A: Mathematical, Nuclear and General 6, 1552–1564 (1973).

[128] D. Hu, S.-Y. Huang, J.-Q. Liao, L. Tian, and H.-S. Goan, "Quantum coherence in ultrastrong optomechanics," Phys. Rev. A 91, 013812 (2015).

[129] M. T. Naseem, A. Xuereb, and O. E. Müstecaplıoğlu, "Thermodynamic consistency of the optomechanical master equation," Phys. Rev. A 98, 052123 (2018).

[130] B. Gurlek, private communication.

[131] R. M. Wilcox, "Exponential Operators and Parameter Differentiation in Quantum Physics," Journal of Mathematical Physics 8, 962–982 (1967).

[132] M. Suzuki, "Quantum analysis—non-commutative differential and integral calculi," Comm. Math. Phys. 183, 339–363 (1997).

[133] K. Huang and A. Rhys, "Theory of light absorption and non-radiative transitions in F-centres," Proc. R. Soc. A 204, 406–423 (1950).

[134] T. Förster, "Zwischenmolekulare Energiewanderung und Fluoreszenz," Ann. Phys. 437, 55 (1948).

[135] R. E. Blankenship, *Molecular Mechanisms of Photosynthesis, 2nd Edition* (John Wiley & Sons, Inc., Hoboken, NJ, 2014).

[136] I. L. Medintz and N. Hildebrandt, *FRET - Förster resonance energy transfer: from theory to applications* (Wiley VCH Verlag, Weinheim, 2014).

[137] V. May and O. Kühn, *Charge and energy transfer dynamics in molecular systems* (Wiley-VCH Verlag GmbH, New York, 2011).

[138] N. Goldman and J. Dalibard, "Periodically Driven Quantum Systems: Effective Hamiltonians and Engineered Gauge Fields," Phys. Rev. X 4, 031027 (2014).

[139] T. Oka and S. Kitamura, "Floquet Engineering of Quantum Materials," Annu. Rev. Condens. Matter. Phys. 10, 387–408 (2019).

[140] H. Y. Chen, E. R. MacQuarrie, and G. D. Fuchs, "Orbital state manipulation of a diamond nitrogen-vacancy center using a mechanical resonator," Phys. Rev. Lett. 120, 167401 (2018).

[141] E. Pomarico, M. Mitrano, H. Bromberger, M. A. Sentef, A. Al-Temimy, C. Coletti, A. Stöhr, S. Link, U. Starke, C. Cacho, R. Chapman, E. Springate, A. Cavalleri, and I. Gierz, "Enhanced electron-phonon coupling in graphene with periodically distorted lattice," Phys. Rev. B 95, 024304 (2017).

[142] M. Buzzi, D. Nicoletti, M. Fechner, N. Tancogne-Dejean, M. A. Sentef, A. Georges, T. Biesner, E. Uykur, M. Dressel, A. Henderson, T. Siegrist, J. A. Schlueter, K. Miyagawa, K. Kanoda, M.-S. Nam, A. Ardavan, J. Coulthard, J. Tindall, F. Schlawin, D. Jaksch, and A. Cavalleri, "Photomolecular High-Temperature Superconductivity," Phys. Rev. X 10, 031028 (2020).

[143] M. Babadi, M. Knap, I. Martin, G. Refael, and E. Demler, "Theory of parametrically amplified electron-phonon superconductivity," Phys. Rev. B 96, 014512 (2017).

[144] Y. Murakami, N. Tsuji, M. Eckstein, and P. Werner, "Nonequilibrium steady states and transient dynamics of conventional superconductors under phonon driving," Phys. Rev. B 96, 045125 (2017).

[145] H. Hübener, U. De Giovannini, and A. Rubio, "Phonon Driven Floquet matter," Nano Letters 18, 1535–1542 (2018).

[146] D. Shin, H. Hübener, U. De Giovannini, H. Jin, A. Rubio, and N. Park, "Phonon-driven spin-Floquet magneto-valleytronics in MoS2," Nat. Comm. 9, 638 (2018).

[147] M. Först, A. D. Caviglia, R. Scherwitzl, R. Mankowsky, P. Zubko, V. Khanna, H. Bromberger, S. B. Wilkins, Y.-D. Chuang, W. S. Lee, W. F. Schlotter, J. J. Turner, G. L. Dakovski, M. P. Minitti, J. Robinson, S. R. Clark, D. Jaksch, J.-M. Triscone, J. P. Hill, S. S. Dhesi, and A. Cavalleri, "Spatially resolved ultrafast magnetic dynamics initiated at a complex oxide heterointerface," Nat. Mat. 14, 883–888 (2015).

[148] T. F. Nova, A. Cartella, A. Cantaluppi, M. Först, D. Bossini, R. V. Mikhaylovskiy, A. V. Kimel, R. Merlin, and A. Cavalleri, "An effective magnetic field from optically driven phonons," Nat. Phys. 13, 132–136 (2017).

[149] K. Schwennicke and J. Yuen-Zhou, "Optical activity from the Exciton Aharonov–Bohm effect: A Floquet engineering approach," J. Phys. Chem. C 124, 4206–4214 (2020).

[150] B. Metzger, E. Muller, J. Nishida, B. Pollard, M. Hentschel, and M. B. Raschke, "Purcell-enhanced spontaneous emission of molecular vibrations," Phys. Rev. Lett. 123, 153001 (2019).

[151] E. A. Muljarov and R. Zimmermann, "Dephasing in quantum dots: Quadratic coupling to acoustic phonons," Phys. Rev. Lett. 93, 237401 (2004).

[152] J. Sakurai and J. Napolitano, *Modern Quantum Mechanics* (Cambridge University Press, 2017).

[153] M. P. Silveri, J. A. Tuorila, E. V. Thuneberg, and G. S. Paraoanu, "Quantum systems under frequency modulation," Rep. Progr. Phys. 80, 056002 (2017).

[154] C. M. Wilson, T. Duty, F. Persson, M. Sandberg, G. Johansson, and P. Delsing, "Coherence times of dressed states of a superconducting qubit under extreme driving," Phys. Rev. Lett. 98, 257003 (2007).

[155] F. Grossmann, T. Dittrich, P. Jung, and P. Hänggi, "Coherent destruction of tunneling," Phys. Rev. Lett. 67, 516–519 (1991).

[156] M. Aspelmeyer, T. J. Kippenberg, and F. Marquardt, "Cavity optomechanics," Rev. Mod. Phys. 86, 1391–1452 (2014).

[157] A. Dantan, C. Genes, D. Vitali, and M. Pinard, "Self-cooling of a movable mirror to the ground state using radiation pressure," Phys. Rev. A 77, 011804 (2008).

[158] F. J. Hernández and F. Herrera, "Multi-level quantum rabi model for anharmonic vibrational polaritons," J. Chem. Phys. 151, 144116 (2019).

[159] K. D. Major, Y.-H. Lien, C. Polisseni, S. Grandi, K. W. Kho, A. S. Clark, J. Hwang, and E. A. Hinds, "Growth of optical-quality anthracene crystals doped with dibenzoterrylene for controlled single photon production," Rev. Sci. Instrum. 86, 083106 (2015).

[160] R. Rigler, M. Orrit, and T. Basche, *Single Molecule Spectroscopy - Nobel Conference Lectures* (Springer Verlag, Berlin, 2001).

[161] A. Makarewicz, I. Deperasinska, E. Karpiuk, J. Nowacki, and B. Kozankiewicz, "Vibronic spectra of single dibenzoterrylene molecules in anthracene and 2,3-dimethylanthracene crystals," Chem. Phys. Lett. 535, 140 – 145 (2012).

[162] I. Deperasinska, E. Karpiuk, M. Banasiewicz, A. Makarewicz, and B. Kozankiewicz, "Single dibenzoterrylene molecules in naphthalene and 2,3-dimethylnaphthalene crystals: vibronic spectra," Phys. Chem. Chem. Phys. 13, 1872 (2011).

[163] J. Iles-Smith, D. P. S. McCutcheon, J. Mørk, and A. Nazir, "Limits to coherent scattering and photon coalescence from solid-state quantum emitters," Phys. Rev. B 95, 201305 (2017).

[164] A. Norambuena, S. A. Reyes, J. Mejía-Lopéz, A. Gali, and J. R. Maze, "Microscopic modeling of the effect of phonons on the optical properties of solid-state emitters," Phys. Rev. B 94, 134305 (2016).

[165] P. Kaer, T. R. Nielsen, P. Lodahl, A.-P. Jauho, and J. Mørk, "Non-Markovian model of photon-assisted dephasing by electron-phonon interactions in a coupled Quantum-Dot–Cavity system," Phys. Rev. Lett. 104, 157401 (2010).

[166] A. Nazir and D. P. S. McCutcheon, "Modelling exciton–phonon interactions in optically driven quantum dots," J. Phys. Condens. Matter 28, 103002 (2016).

[167] P. Lodahl, S. Mahmoodian, and S. Stobbe, "Interfacing single photons and single quantum dots with photonic nanostructures," Rev. Mod. Phys. 87, 347–400 (2015).

[168] D. Englund, B. Shields, K. Rivoire, F. Hatami, J. Vuckovic, H. Park, and M. Lukin, "Deterministic coupling of a single nitrogen vacancy center to a photonic crystal cavity," Nano letters 10, 3922–6 (2010).

[169] A. Nitzan, S. Mukamel, and J. Jortner, "Energy gap law for vibrational relaxation of a molecule in a dense medium," J. Chem. Phys. 63, 200–207 (1975).

[170] P. M. Felker and A. H. Zewail, "Ultrafast dynamics of ivr in molecules and reactions," in *Jet Spectroscopy and Molecular Dynamics*, edited by J. M. Hollas and D. Phillips (Springer Netherlands, Dordrecht, 1995) pp. 222–308.

[171] R. J. Rubin, "Momentum autocorrelation functions and energy transport in harmonic crystals containing isotopic defects," Phys. Rev. 131, 964–989 (1963).

[172] X. Li, E. Yakaboylu, G. Bighin, R. Schmidt, M. Lemeshko, and A. Deuchert, "Intermolecular forces and correlations mediated by a phonon bath," J. Chem. Phys. 152, 164302 (2020).

[173] J. Kikas, A. Suisalu, V. Zazubovich, and P. Vois, "Anomalous impurity spectra in low--temperature glasses," J. Chem. Phys. 104, 4434–4440 (1996).

[174] V. Hizhnyakov, "Zero-phonon lines of systems with different dimensions and unconventional vibronic interactions," J. Phys. Condens. Matter 24, 104011 (2012).

[175] T. Jakubczyk, V. Delmonte, S. Fischbach, D. Wigger, D. E. Reiter, Q. Mermillod, P. Schnauber, A. Kaganskiy, J.-H. Schulze, A. Strittmatter, S. Rodt, W. Langbein, T. Kuhn, S. Reitzenstein, and J. Kasprzak, "Impact of phonons on dephasing of individual excitons in deterministic quantum dot microlenses," ACS Photonics 3, 2461–2466 (2016).

[176] S. Blanes, F. Casas, J. Oteo, and J. Ros, "The magnus expansion and some of its applications," Physics Reports 470, 151–238 (2009).

[177] D. Reichman, R. J. Silbey, and A. Suárez, "On the nonperturbative theory of pure dephasing in condensed phases at low temperatures," J. Chem. Phys. 105, 10500–10506 (1996).

[178] I. Osad'ko and N. Zaitsev, "Dephasing time in solids and homogeneous optical linewidth: are the mechanisms of the electron-phonon coupling the same?" Chem. Phys. Lett. 121, 209 – 213 (1985).

[179] A. Reigue, J. Iles-Smith, F. Lux, L. Monniello, M. Bernard, F. Margaillan, A. Lemaitre, A. Martinez, D. P. S. McCutcheon, J. Mørk, R. Hostein, and V. Voliotis, "Probing electron-phonon interaction through two-photon interference in resonantly driven semiconductor quantum dots," Phys. Rev. Lett. 118, 233602 (2017).

[180] J. Rui, D. Wei, A. Rubio-Abadal, S. Hollerith, J. Zeiher, D. M. Stamper-Kurn, C. Gross, and I. Bloch, "A subradiant optical mirror formed by a single structured atomic layer," Nature 583, 369 (2020).

[181] J. Perczel, J. Borregaard, D. E. Chang, H. Pichler, S. F. Yelin, P. Zoller, and M. D. Lukin, "Topological quantum optics in two-dimensional atomic arrays," Phys. Rev. Lett. 119, 023603 (2017).

[182] R. J. Bettles, J. Minar, C. S. Adams, I. Lesanovsky, and B. Olmos, "Topological properties of a dense atomic lattice gas," Phys. Rev. A 96, 041603 (2017).

[183] P.-O. Guimond, A. Grankin, D. V. Vasilyev, B. Vermersch, and P. Zoller, "Subradiant Bell states in distant atomic arrays," Phys. Rev. Lett. 122, 093601 (2019).

[184] S. K. Saikin, A. Eisfeld, S. Valleau, and A. Aspuru-Guzik, "Photonics meets excitonics: natural and artificial molecular aggregates," Nanophotonics 2, 21–38 (2013).

[185] A. Mattioni, F. Caycedo-Soler, S. F. Huelga, and M. B. Plenio, "Design principles for long-range energy transfer at room temperature," Phys. Rev. X 11, 041003 (2021).

[186] H. DeVoe, "Optical properties of molecular aggregates. I. classical model of electronic absorption and refraction," J. Chem. Phys 41, 393–400 (1964).

[187] G. D. Scholes and G. Rumbles, "Excitons in nanoscale systems," Nature Materials 5, 683–696 (2006).

[188] V. Agranovich, G. La Rocca, and F. Bassani, "Biexcitons and dark states in semiconductor microcavities," J. Lumin. 76-77, 161 (1998).

[189] M. Litinskaya, P. Reineker, and V. Agranovich, "Fast polariton relaxation in strongly coupled organic microcavities," J. Lumin. 110, 364 (2004).

[190] C. Gonzalez-Ballestero, J. Feist, E. Gonzalo Badía, E. Moreno, and F. J. Garcia-Vidal, "Uncoupled dark states can inherit polaritonic properties," Phys. Rev. Lett. 117, 156402 (2016).

[191] T. Botzung, D. Hagenmüller, S. Schütz, J. Dubail, G. Pupillo, and J. Schachenmayer, "Dark state localization of quantum emitters in a cavity," (2020), arXiv:2003.07179 [quant-ph] .

[192] M. Du and J. Yuen-Zhou, "Catalysis by dark states in vibropolaritonic chemistry," Phys. Rev. Lett. 128, 096001 (2022).

[193] R. Houdré, R. P. Stanley, and M. Ilegems, "Vacuum-field Rabi splitting in the presence of inhomogeneous broadening: Resolution of a homogeneous linewidth in an inhomogeneously broadened system," Phys. Rev. A 53, 2711 (1996).

[194] I. Diniz, S. Portolan, R. Ferreira, J. M. Gérard, P. Bertet, and A. Auffèves, "Strongly coupling a cavity to inhomogeneous ensembles of emitters: Potential for long-lived solid-state quantum memories," Phys. Rev. A 84, 063810 (2011).

[195] Z. Kurucz, J. H. Wesenberg, and K. Mølmer, "Spectroscopic properties of inhomogeneously broadened spin ensembles in a cavity," Phys. Rev. A 83, 053852 (2011).

[196] K. Debnath, Y. Zhang, and K. Mølmer, "Collective dynamics of inhomogeneously broadened emitters coupled to an optical cavity with narrow linewidth," Phys. Rev. A 100, 053821 (2019).

[197] O. Vendrell, "Collective Jahn-Teller interactions through light-matter coupling in a cavity," Phys. Rev. Lett. 121, 253001 (2018).

[198] I. S. Ulusoy, J. A. Gomez, and O. Vendrell, "Modifying the nonradiative decay dynamics through conical intersections via collective coupling to a cavity mode," The Journal of Physical Chemistry A 123, 8832–8844 (2019).

[199] T. Shirai, J. Thingna, T. Mori, S. Denisov, P. Hänggi, and S. Miyashita, "Effective Floquet-Gibbs states for dissipative quantum systems," New Journal of Physics 18 (2016).

[200] A. Schnell, A. Eckardt, and S. Denisov, "Is there a Floquet Lindbladian?" Phys. Rev. B 101, 100301 (2020).

[201] N. Thanh Phuc and A. Ishizaki, "Control of excitation energy transfer in condensed phase molecular systems by Floquet engineering," J. Phys. Chem. Lett. 9, 1243–1248 (2018).

[202] D. F. Calef and P. G. Wolynes, "Classical solvent dynamics and electron transfer. 1. continuum theory," J. Phys. Chem. 87, 3387–3400 (1983).

[203] D. G. Lidzey, D. D. C. Bradley, T. Virgili, A. Armitage, M. S. Skolnick, and S. Walker, "Room temperature polariton emission from strongly coupled organic semiconductor microcavities," Phys. Rev. Lett. 82, 3316 (1999).

[204] T. Schwartz, J. A. Hutchison, C. Genet, and T. W. Ebbesen, "Reversible switching of ultrastrong light-molecule coupling," Phys. Rev. Lett. 106, 196405 (2011).

[205] M. Held, A. Graf, Y. Zakharko, P. Chao, L. Tropf, M. C. Gather, and J. Zaumseil, "Ultrastrong coupling of electrically pumped near-infrared exciton-polaritons in high mobility polymers," Adv. Opt. Mater. 6, 1700962 (2018).

[206] D. De Bernardis, P. Pilar, T. Jaako, S. De Liberato, and P. Rabl, "Breakdown of gauge invariance in ultrastrong-coupling cavity QED," Phys. Rev. A 98, 053819 (2018).

[207] A. Frisk Kockum, A. Miranowicz, S. De Liberato, S. Savasta, and F. Nori, "Ultrastrong coupling between light and matter," Nature Reviews Physics 1, 19–40 (2019)

This thesis was typeset using LaTeX, originally developed by Leslie Lamport and based on Donald Knuth's TeX. The body text is set in 11 point Egenolff-Berner Garamond, a revival of Claude Garamont's humanist typeface. A template that can be used to format a PhD thesis with this look and feel has been released under the permissive MIT (XII) license, and can be found online at github.com/suchow/Dissertate or from its author, Jordan Suchow, at suchow@post.harvard.edu. This template was adapted for Friedrich-Alexander Universität Erlangen-Nürnberg (FAU) by Nikolay Harutyunyan. You can get the source code to this template on Overleaf or from him, at nikolay.harutyunyan [at] fau.de.